Charles University in Prague, Faculty of Science
Department of Physical and Macromolecular Chemistry

Synthesis and Properties of Supramolecular Polymers
Ph.D. thesis

Mgr. Tereza Vitvarová
Supervisors: Prof. Jiří Vohlídal, CSc. and Prof. Muriel Hissler

Prague, 2017

THÈSE / UNIVERSITÉ DE RENNES 1
sous le sceau de l'Université Bretagne Loire

En Cotutelle Internationale avec
Charles University in Prague

pour le grade de

DOCTEUR DE L'UNIVERSITÉ DE RENNES 1

Mention : Chimie

Ecole doctorale SDLM

présentée par

Tereza Vitvarová

UMR 6226-CNRS – Sciences Chimiques de Rennes
Institut de Chimie – Université de Rennes 1
U.F.R. « Structure et Propriétés de la matière » (S.P.M.)

Synthesis and Properties of Supramolecular Polymers

**Thèse soutenue à Prag
le 22 Mai 2017**

devant le jury composé de :
Karel PROCHAZKA
Profeseur / *président*
Jindrich JINDRICH
Profeseur / *rapporteur*
Guy ROYAL
Professeur / *rapporteur*
Jiri PFLEGER
Directeur de recherche/ *examinateur*
Petr STEPANEK
Directeur de recherche. / *examinateur*
Jan RODA
Professor / *examinateur*
Muriel HISSLER
Profeseur/ *co-directeur de thèse*
Jiri VOHLIDAL
Profeseur / *co-directeur de thèse*

STATEMENT

I hereby declare that this submission is my own work and that, to the best of my knowledge and belief, it contains neither material previously published or written by another person nor material which to a substantial extent has been accepted for the award of any other degree or diploma of the University or other Institute of higher education, except for the already published results, which are included in the list of references.

Prague,

ACKNOWLEDGEMENT

ABSTRACT

New π-conjugated building blocks (unimers) for metallo-supramolecular polymers (MSPs), whose comprise: *(i)* substituted phosphole ring surrounded by two thiophene rings as the central block, *(ii)* 2,2':6',2"-terpyridine-4'-yl (*tpy*) end-groups as ion-selectors, and *(iii)* different linkers inserted between the central block and *tpy* end-groups, are described. Chemical and physical properties of those unimers were studied with attention on correlation between properties and structure of unimers. For example the unimer without linkers shows the UV/vis absorption maximum red shifted about 60 to 100 nm compared to bis(*tpy*)terthiophenes, which proves that replacing of the thiophene with phosphole unit significantly enhances the delocalization of electrons within the unimer molecule and significant area of absorption spectra can be covered. Introduction of linkers (ethynediyl, ethynediyl-thiophene-2,5-diyl, ethynediyl-1,4-phenylene) has a minor effect on the bandgap energy.

All prepared unimers underwent self-assembling process with various metal ions (Co^{2+}, Cu^{2+}, Fe^{2+}, Ni^{2+} and Zn^{2+}) resulting into metallo-supramolecular polymers. Three stages of the assembly of unimers into related MSPs were observed and characterized by absorption, fluorescence spectroscopy and size exclusion chromatography: *1)* formation of dimer species: **U**-M^{2+}-**U** (**U** stands for unimer); *2)* prolongation of polymer chain to reach the maximum length at equimolar ratio of unimer and metal ions; *3)* end-capping of polymer chains and their partial decomposition at stoichiometric excess of ion couplers. Optoelectronic properties of newly formed metallo-supramolecular polymers were investigated and choice of the metal ions was shown to be of crucial importance.

Keywords:
Metallo-supramolecular polymers, phosphole, terpyridine, complex stability, unimer

ABSTRAKT

V rámci této disertační práce byly připraveny stavební bloky (nazývající se unimery) pro tvorbu konjugovaných metalo-supramolekulárních polymerů (MSPs), které ve své struktuře obsahují: (*i*) substituovaný fosfolový kruh obklopený dvěma thiofenovými cykly jako centrální blok, *(ii)* 2,2':6',2''-terpyridin-4'-yl (*tpy*) jako koncovou skupinu pro navázání iontů, a (*iii*) různé spojky mezi uvedeným centrálním blokem a *tpy* skupinou. Chemické a fyzikální vlastnosti těchto unimerů byly prostudovány s důrazem na korelaci mezi vlastnostmi a strukturou unimeru. Například unimer bez přídavných spojek vykazuje posun UV/vis absorpčního maxima do červené oblasti o 60 až 100 nm v porovnání s bis(*tpy*)terthiofenem, což značí, že nahrazením thiofenu fosfolem se značně zvyšuje delokalizace elektronů v molekule unimeru a může být pokryta značná část spektra. Začlenění spojek (ethynediyl, ethynediyl-thiofen-2,5-diyl, ethynediyl-1,4-fenylen) do struktury unimeru má jen malý vliv na šířku zakázaného pásu, a tedy pozici absorpčního maxima.

Všechny připravené unimery byly podrobeny procesu samo-seskupování s různými kovovými ionty (Co^{2+}, Cu^{2+}, Fe^{2+}, Ni^{2+} a Zn^{2+}) za vzniku organokovových polymerů. Tři stadia provázející proces samo-seskupování byla pozorována pomocí absorpční a fluorescenční spektroskopie a gelové permeační chromatografie (SEC): *1*) tvorba dimerů **U**-**M**$^{2+}$-**U** (**U** = unimer), *2*) prodlužování polymerních řetězců a dosažení maximální délky při ekvimolárním poměru unimeru a kovových iontů, *3*) vazba kovových iontů na koncové terpyridinové skupiny a rozklad polymerního řetězce na kratší při stechiometrickém přebytku kovových iontů. Optické vlastnosti nově připravených organokovových polymerů byly prozkoumány a ukázalo se, že velmi závisí na vybraném kovovém iontu.

Klíčová slova

Metalo-supramolekulární polymery, fosfol, terpyridin, stabilita komplexu, unimer

RESUMÉ

Lors de ces travaux de thèse, des unités monomériques appelées unimères ont été synthétisées et utilisées pour le développement de polymères métallo-supramoléculaires (MSPs). Ces unités se composent (*i*) d'un bloc central: 2,5-dithiénylphosphole, (*ii*) d'un chélate : 2,2':6',2"-terpyridine-4'-yl (*tpy*) et (*iii*) de connecteurs variés assurant la jonction entre le bloc central et le chélate. Les propriétés physico-chimiques de ces unimères ont été mesurées afin d'établir des relations structures/propriétés. Par exemple, l'unimère ne comportant pas de connecteurs entre l'unité central et le chélate présente un maximum d'absorption fortement décalé vers le rouge ($\Delta\lambda$ = 60-100 nm) par rapport à l'unimère bis(*tpy*)terthiophène. Cette observation montre que la délocalisation électronique est accrue dans ces systèmes et permet de couvrir un large domaine spectral. L'introduction de connecteurs (éthynediyle, éthynediyle-thiophène-2,5-diyle, éthynediyle-1,4-phénylène) entre le bloc central et le chélate a un effet mineur sur l'écart HO-BV et sur la position des maxima d'absorption.

Puis tous les unimères synthétisés ont été mis en présence de différents ions métalliques (Co^{2+}, Cu^{2+}, Fe^{2+}, Ni^{2+} et Zn^{2+}) pour former les MSPs correspondants. Ce phénomène de polymérisation a été étudié en détail en utilisant les spectroscopies d'absorption, d'émission et la chromatographie d'exclusion stérique. Ainsi, cette polymérisation présente 3 étapes : (*i*) la formation des dimères **U**-**M**-**U**, (*ii*) la prolongation de chaine de polymères qui atteint un une longueur maximale pour le ratio 1/1 ion métallique/unimère; (*iii*) terminaison réalisée avec des ions métalliques lorsque ces ions sont présent en excès. Les propriétés optiques de ces nouveaux polymères ont également été étudiées montrant qu'elles dépendent fortement de la nature de l'ion métallique utilisé.

Mots de clés :

Polymères métallo-supramoléculaires, phosphole, terpyridine, constante de stabilité, unimères

CONTENT

LIST OF ABBREVIATIONS

ACN	acetonitrile
Aliquat® 336	trioctylmethylammonium chloride
bpy	2,2'-bipyridine
Br-*tpy*	4'-bromo-2,2':6',2"-terpyridine
Bu	butyl
COD	cycloocta-1,5-diene
Cp	cyclopentadiene
DAD	diode array detector
DBU	1,8-diazabicyclo[5.4.0]undec-7-ene
DCM	dichloromethane
dtbpy	4,4'-di-*tert*-butyl-2,2'-dipyridyl
E-*tpy*	4'-ethynyl-2,2':6',2"-terpyridine
Et_2O	diethyl ether
GC	gas chromatography
Hex	hexyl
HOMO	highest occupied molecular orbital
iPr	isopropyl
L	ligand
LUMO	lowest unoccupied molecular orbital
M	metal
MLCT	metal to ligand charge transfer
MSP	metallo-supramolecular polymer
NMR	nuclear magnetic resonance
P-E*tpy*	4'-{[2,5-bis(thiophen-2-yl)phosphol-1-yl]ethynyl}-2,2':6',2"-terpyridine
$Pd(dba)_2$	bis(dibenzylideneacetone)palladium(0)
PEPPSI™-IPr	[1,3-bis(2,6-diisopropylphenyl)imidazol-2-ylidene](3-chloropyridyl)palladium(II) dichloride
SEC	size exclusion chromatography
Terpyridine	2,2':6',2"-terpyridine
THF	tetrahydrofurane
Thio-*tpy*	4'-(thiophen-2-yl)-2,2':6',2"-terpyridine
tht	tetrahydrothiophene
TLC	thin layer chromatography
tpy	2,2':6',2"-terpyridin-4'-yl
U	unimer
UV/vis	ultraviolet-visible

1   INTRODUCTION

1.1 CONJUGATED POLYMERS

Conjugated polymers have attracted much interest in the past few decades as electroactive materials for applications such as batteries, solar cells and light emitting diodes. The research efforts started in 1977 with the discovery of the conductivity of doped polyacetylene by Shirakawa et al.[1] Polyacetylene (Figure 1) is a linear polymer with main chains consisting of a contiguous series of the sp^2 hybridized carbons formally connected by alternating single and double bonds. Overlaps of neighboring formally localized π-orbitals across intervening σ-bonds results in delocalization of π-electrons along the macromolecule backbone, which enables transport of unpaired electrons (radicals) along this backbone. Doping of a conjugated polymer consists in oxidation or reduction of its chains resulting in the formation of mobile charge carriers (holes or electrons, respectively) and simultaneous creation of conducting interconnection of individual neighboring macromolecules, which results in a substantial increase in the conductivity of a doped polymer even up to the level of metals. Therefore, such polymers are often referred to as synthetic metals.[2,3]
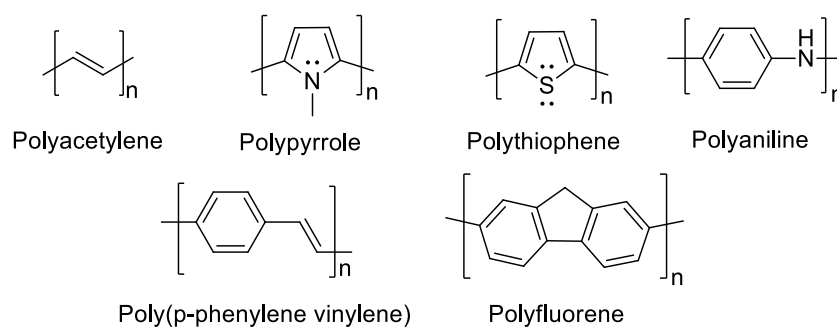
Figure 1: Structure of representative conjugated polymers

Conductivity of a conjugated polymer is related to its bandgap energy, E_g, which is defined as the energy difference between: (*i*) the lowest unoccupied molecular orbital (LUMO) and the highest occupied molecular orbital (HOMO) in a molecule, or (*ii*) the bottom of the conduction band and the top of the valence band in condensed matter. A material in which conduction and valence bands are merged or overlapped has no bandgap and it is referred to as a (metallic) conductor. A material with small bandgap

energy, E_g < ca 3 eV, is referred to as a semiconductor whereas a material with E_g > ca 3 eV is an insulator (Figure 2).
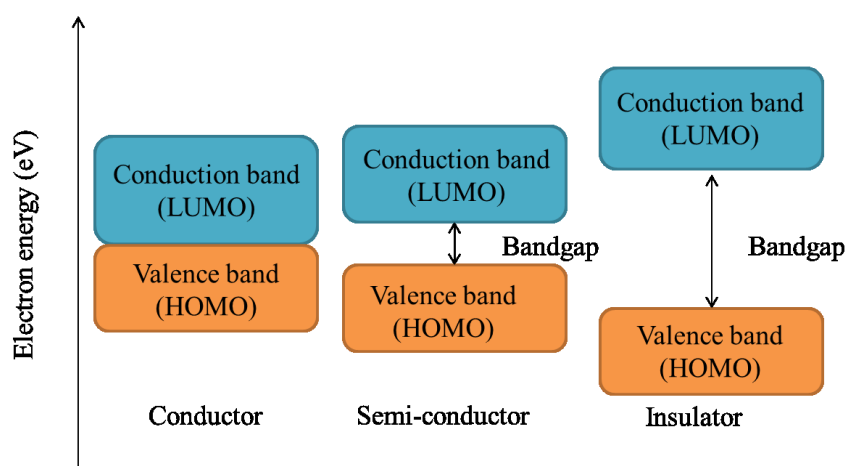
Figure 2: Band model of materials according to their conductivity

Although a fresh doped polyacetylene exhibits excellent functional properties, it has soon been found to exhibit limited stability in air as well as under operational conditions.[4] Subsequent research has led to a development of other, more stable linear π-conjugated polymers comprising arylene or heteroarylene monomeric units, such as polypyrrole,[2,5] polyaniline,[5,6] polythiophene,[7,8] poly(*p*-phenylene vinylene),[9,10] polyfluorene[11,12] (Figure 1) and others. Molecular structure and thus also electronic structure and functional properties of these polymers can be relatively easily tuned by manipulation of the corresponding monomer structure,[7] which is the key issue for most of applications of these materials. Polymers of all these classes have been examined as materials for organic electronics.[13–22] However, the so far developed organic electronic devices have not reached parameters of the devices based on the traditional inorganic materials. Therefore, the search for new well processable and sufficiently stable materials for the construction of organic conductors and semiconductors is of permanent interest since it meets demands of steadily developing organic electronics.

A concerted shift of all double bonds of a linear polyacetylene chain in the same direction to the neighboring positions gives a structurally identical chain (if end-groups are omitted), so that limiting mesomeric forms of this chain are essentially identical. However, if a linear π-conjugated chain is composed of a series of linked aromatic rings, it can acquire two energetically non-equivalent limiting mesomeric forms: *(i)* aromatic (benzenoid), with exclusively single ring-to-ring bonds, and *(ii)* quinoid, with

exclusively double ring-to-ring bonds (Figure 3).[23] These mesomeric forms are energetically non-equivalent. The aromatic form is typical of the ground state because of lower energy and thus higher stability of the π-electron systems, whereas the quinoid form is typical of the energetically enriched first excited state and responsible for the increased extent of delocalization of valence electrons in this state.

RESONANCE FORMS
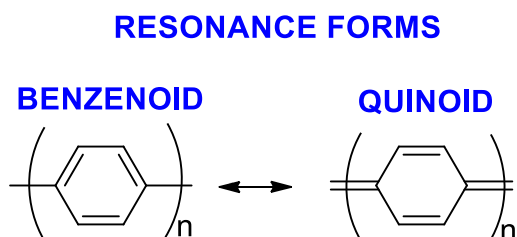
BENZENOID   **QUINOID**

Figure 3: Benzenoid and quinoid resonance forms of a poly(p-phenylene) chain.

The autonomy of aromatic rings in the ground state brings a lowered reactivity and thus increased environmental stability of the polyarylene[24] compared to polyacetylene molecules in the ground state. These rules are essentially valid also for poly(heteroarenes), such as polythiophene and polypyrrole (Figure 4).

LUMO
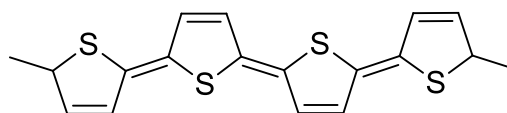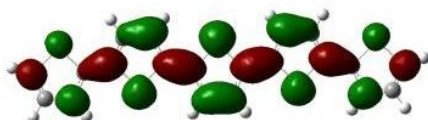
HOMO
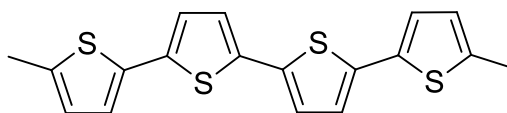
Figure 4: π-Orbital charge density for the HOMO and LUMO state of a polythiophene chain.[25]

Heteroarenes show a lower degree of aromaticity compared to arenes, because they are aromatic only due to the inclusion of non-bonding electrons into aromatic system. Therefore, the valence electrons are substantially more delocalized in the ground-state of polythiophenes and polypyrroles compared to their delocalization in purely

hydrocarbon polyarylenes.[26] Actually, the macromolecules composed of heterocyclopentadienes can be regarded as molecules in which every second single bond is extremely efficiently stabilized in the cisoid configuration by the heteroatom.[27]

Structural versatility of poly(heteroarenes) also allows the tuning of their electronic and electrochemical properties through manipulation of the monomer structure.[7] Diversification of the optical and electronic properties of polyheteroarenes is of high importance as the key issue for applications of these materials. These physical properties of polyheteroarenes strongly depend on the nature of the ring heteroatoms.

One of the main disadvantages of traditional covalent conjugated polymers is the lack of really efficient control of their formation from monomers (their synthesis), due to which the formed chains comprise rather high number of structural defects. These defects, which mostly act as the charge carrier traps, cannot be removed and usually negatively influence properties of material. One approach how to avoid these problems is application of supramolecular polymers instead of traditional covalent conjugated polymers for photovoltaic devices.[28]

1.2. SUPRAMOLECULAR POLYMERS

Polymers that are at least partially formed by self-assembly *via* non-covalent interactions of building blocks (called unimers as proposed by Ciferri[29]) are referred to as supramolecular polymers. A high reversibility of non-covalent bonds ensures that supramolecular polymers are always formed under conditions of thermodynamic equilibrium, and hence the length of their chains is directly related to the concentration of unimer(s) in the system, strength of non-covalent bonds, temperature and solvent. As a result, external parameters such as temperature and mechanical stimuli can significantly affect the polymer chain length and properties.[30–32] Thanks to this fact supramolecular polymers offer increased level of complexity and interesting properties for practical applications including applications in optoelectronic devices.[28,33–37] Although the energy released in the formation of a non-covalent bond is lower than the energy of a covalent bond (*e.g.* 347 kJ/mol for C-C bond)[38] it facilitates assembly of individual molecules to stable supramolecular structures, mainly in the solid state. A thoughtful design of a supramolecular architecture gives an access to molecules (or materials) with highly specific properties that can be obtained by relatively simple assembling of properly designed precursor molecules.

1.2.1 Non-covalent interactions

Non-covalent interactions applied in supramolecular chemistry can be classified into four categories, depending on their origin: electrostatic interactions, dispersion forces, π-effects, and hydrophobic effects.

Electrostatic interactions originate from attractions or repulsions between charged and/or dipolar particles. Therefore they can be divided according to the type of interacting particles. One can thus distinguish the ion-ion interactions, ion-dipole interactions and dipole-dipole interactions. The ionic bonding is in strength comparable to the covalent bonding.[39] Ion-dipole interactions include metal-ligand interactions known as coordination (dative) bond which also belongs to stronger non-covalent interactions (50-200 kJ/mol). *Hydrogen bonding* also belongs among electrostatic interactions. It is a specific type of the dipole-dipole interaction in which a hydrogen atom attached to an electronegative atom (or electron withdrawing group) is attracted to neighboring dipole on an adjacent molecule or functional group. Its typical binding energy is 4–60 kJ/mol, but for highly acidic compounds the total bonding energy can be 120 kJ/mol. Hydrogen bonds are responsible for the overall shape of many proteins, recognition of substrates by numerous enzymes and for the double helix structure of deoxyribonucleic acid, DNA.[40]

Dispersion forces are based on the interactions of temporary induced dipoles, which arise from the polarization of electron cloud by the proximity of adjacent nucleus. These forces are the weakest subset of electrostatic interactions (0.4–4 kJ/mol), but when they are acting among long covalent macromolecules composed of a high number of constitutional units the overall binding energy of each macromolecule in a bulk polymer can be extremely high.

π-Effects are based on the interactions of an electron-rich π-system with another π-system or an electron acceptor.[41] The π-π interactions are inherent to all π-conjugated polymers as well as polymers composed of monomeric units comprising aromatic and/or heteroaromatic rings. Hydrophobic effect results from aggregation of non-polar molecules in aqueous media in order to minimize their contacts with water.[42]

1.3. METALLO-SUPRAMOLECULAR POLYMERS

Metal-ligand interactions provide an excellent way for the synthesis of supramolecular polymers. There are many coordination bonds that are strong enough, show highly directional character, appropriate environmental stability and possibility of fine-tuning

of all these features by a proper choice of metal ions and binding end-groups of unimers. They gave rise to the so called metallo-supramolecular polymers (MSPs) which are a sub-class of the supramolecular polymers where the interaction between monomeric units is processed *via* coordination bonds.

A typical macromolecule of a linear MSP is composed of simple or oligomeric molecules capped with two chelate type end-groups (metal-ion selectors) that enable metal-ion induced reversible self-assembly of the entire molecules (unimer molecules) into chains. When the central parts as well as chelating end-groups of the unimer(s) are fully conjugated, the metal-ion linkers can strongly interact with the π-systems of unimeric units built in the MSP chains and thus strongly influence optical properties of the polymer. The MSP properties are then a merger (superposition) of the properties of both its parts: central blocks of unimers and ligand-ion complexes. As a rule, a significant red-shift of the absorption and emission spectral bands is observed compared with the bands of free unimers in solution.

1.3.1 Stability of metal-ligand complex

The metal-ligand binding constant controls the thermodynamic stability of coordination compounds (thus also the stability of the MSP linkages), which can be understood as the ease of the complex formation from its components or the complex resistance to its disintegration into individual species. Binding constant is also referred to as stability constant, formation constant or association constant; in biological system dissociation constant is widely used. Stability constant β for complex M_pL_q formed from constituents M and L is generally defined as follows:

$$pM + qL \leftrightarrow M_pL_q$$

$$\beta = \frac{[M_pL_q]}{[M]^p[L]^q}$$

Where M stands for metal, L for ligand and p, q for stoichiometric coefficients. Stability constant is a very important quantity since it affects the length of MSP chains. The stability constants are used to be determined by complexation studies, at which changes accompanying addition of metal ions to a ligand solution are followed by various methods such as absorption spectroscopy, ^{1}H NMR spectroscopy or isothermal titration

calorimetry. The stability constant is a function of the solvent and temperature, which both, together with the MSP concentration affect the length of MSP chains in solutions.

Stability constant of a complex is strongly influenced by its central metal ions. The electropositive elements of the groups I.A–III.A can be said that the stability of their complexes increases with the increasing positive charge and decreasing radius of the ions. Transition metals with an open shell electronic structure (not fully occupied d-orbitals) generally show the strong metal-ligand orbital interaction, whereas metal-ligand interaction is weak for metals with fully occupied d-orbitals.[43] In 1953 Harry Irving and Robert Williams observed that the stability of complexes formed by divalent first-row transition metal ions generally increases across the period to a maximum stability for copper ions: $Mn^{2+} < Fe^{2+} < Co^{2+} < Ni^{2+} < Cu^{2+} > Zn^{2+}$.[44]

There are three most important factors for designing materials based on the metal-ligand interactions: (*i*) geometry of the complex, (*ii*) its thermodynamic stability, and (*iii*) kinetic stability (or lability, depending on the point of view). The kinetic stability relates to the rate of decomplexation and is represented by the lifetime of the complex under given conditions,[45] *i.e.*, by the activation Gibbs energy of the metal-ligand bond cleavage. Also, the latter factor should be taken into account when tuning the properties of a complex by appropriate choice of both binding partners: ligand as well as metal.

1.3.2 Terpyridine as chelating ligand

Terpyridine is a tridentate nitrogen ligand, which is known to form complexes with most transition metal ions as do other polypyridine compounds such as 2,2'-bipyridine (*bpy*) and 1,10-phenanthroline. Complexes containing two terpyridine units $M(tpy)_2$ are quite common and apart from the related bipyridine complexes $M(bpy)_3$ are achiral.[46] Terpyridine complexes (Scheme 1) of various metals possess pseudo-octahedral geometry with well-defined structure and reasonable stability. The inherent stability of complexes is caused by strong chelate effect and can be strengthen by the metal-ligand σ-π back donation.[47] Terpyridine forms two basic types of metal complexes: $M(tpy)$ and $M(tpy)_2$ (Scheme 1), which differ in the stability as well as spectroscopic properties.
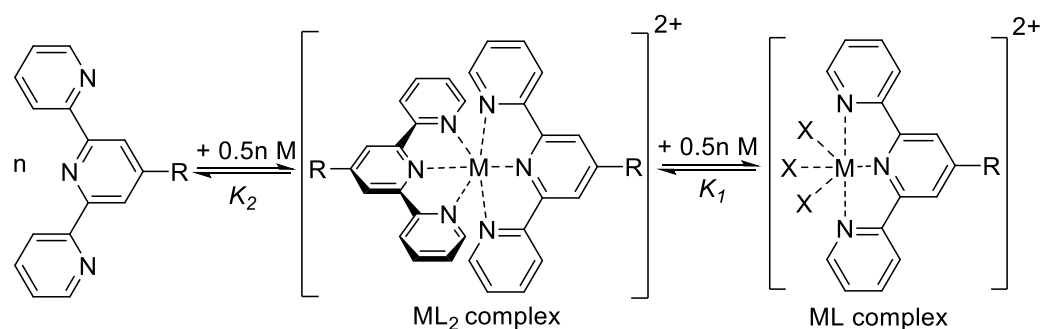
Scheme 1: Complexation of monoterpyridine unit, M= Zn^{2+}, Fe^{2+}, Ru^{2+}, Os^{2+}, …

1.3.3 Optoelectronic properties of metal terpyridine complexes

Metal ions significantly affect optoelectronic properties of terpyridine complexes.[48–52] Metal ions with d^{10} electron configuration (Zn^{2+}) possess complete electron shell, act as Lewis acids and, therefore, they cannot induce a charge transfer in their complexes with terpyridine. Therefore, only ligand centered π–π^* or n–π^* transitions are observed for Zn-*tpy* moieties. In counterpart, utilization of d^6- ions (Fe^{2+}, Ru^{2+} or Os^{2+}) induces formation of the metal-to-ligand charge-transfer (MLCT) states. The electronic transitions associated with MLCT are mostly observed for complexes with ligands having low-lying π^* orbitals and leads to the formation of the absorption band above 500 nm (referred to as the MLCT band) and the intense color of the formed complex: red for Ru^{2+} complexes[53] and violet-blue for Fe^{2+} complexes.[54]

Complexes showing the MLCT band can be non-emissive at room temperature. Absence of luminescence of these complexes is attributed to fast intersystem transition followed by non-radiative transition to the ground state[55] because the high spin triplet metal-centered (^{3}MC) d-d state is located very close to the ground state.[56] The d-d triplet state easy depletes the upper excited states and, since the potential d-d phosphorescence is spin forbidden, decays by unambiguously preferred non-radiative transitions in accord with the energy gap law.[57,58] This path becomes less efficient at lower temperatures, especially for ruthenium-terpyridine complexes as the energy gap between the ^{3}MC state and ground state is higher than in case of iron-terpyridine complexes and, therefore, luminescence can be observed.[59] This behavior is in agreement with experimental observations for complexes of the d^6-d^9 metals, which form low lying ML or LM charge transfer states that quench fluorescence. However weak metal-ligand orbital interactions may exhibit a low quenching response and often enhance fluorescence and increase the red-shift of emission maximum, as observed for

the complexes of d^{10} metals. Changes in emission spectra could be attributed to newly generated emission state of Zn^{2+} induced intraligand π-π* transition.[43]

The other possibility to affect optoelectronic properties of metal-terpyridine complex is functionalization of terpyridine. Various 4'-functionalized terpyridines have been prepared over the past years.[60,61] For example attachment of aromatic group lowering the energy of the ^{3}MLCT state can improve the luminescence lifetime and quantum efficiency.[55]

1.3.4 Stability of terpyridine complexes

Depending on the kinetic stability, the complexes of terpyridine can be divided to kinetically stable and kinetically labile. Hogg et al.[45], who studied terpyridine complexes in aqueous solutions already in 1962, found kinetically stable complexes of Ru^{2+}, Pt^{2+}, Os^{2+} and kinetically labile complexes of Co^{2+}, Zn^{2+}, Fe^{2+}. However, this is valid for aqueous solutions since the stability in a solution is generally a function of the solvent.

The complexes that are kinetically stable in solution as well as at increased temperature behave as covalent molecules and, therefore, they can be readily characterized in solutions with a use of the standard analytical methods. Typical example of the kinetically stable terpyridine complex is $Ru(tpy)_2^{2+}$ which has been widely studied not only because of its stability, but also because of interesting photophysical properties such as phosphorescence,[62,63] metal to ligand charge transfer processes[53] and a potential of the complex to facilitate the charge carrier generation.[64] $Ru(tpy)_2^{2+}$ type complexes are usually prepared by the reduction of $Ru^{III}(tpy)Cl_3$ precursor in the presence of *tpy* species as shown in Scheme 2.
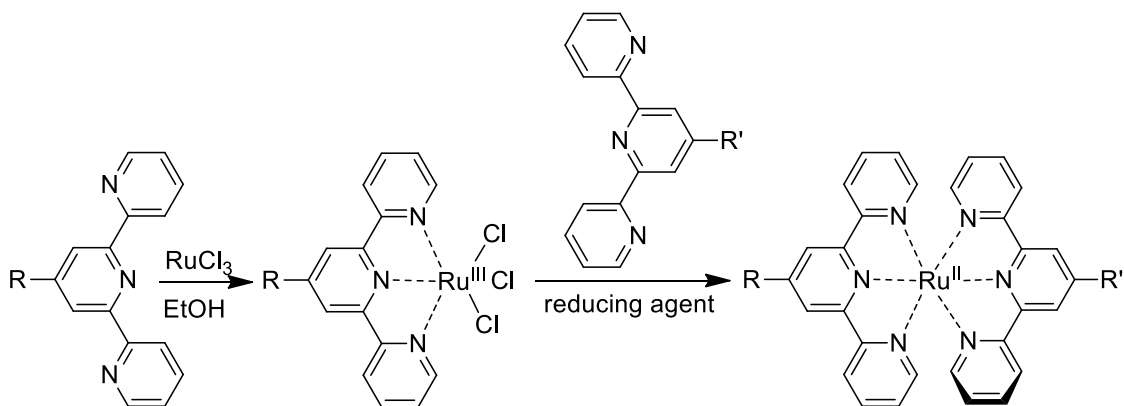

Scheme 2: Formation of Ruthenium-terpyridine complexes

Kinetically labile complexes dissociate at increased temperatures or in solutions or both. Therefore, they can easily undergo post-synthesis modifications by reshuffling or exchanges of their components. This feature could give a self-healing capability to these materials and a possibility of post-synthesis tuning (tailoring) of their properties. These constitutionally dynamic complexes are usually obtained by simple mixing of their constituents.

1.3.5 Dynamers

If coordination linkages between enchained unimer molecules are kinetically labile, the resulting MSPs exhibits constitutional dynamics and, therefore, it is referred to as constitutional dynamic polymer or, shortly, dynamer.[31] The first MSP with kinetically labile linkages was reported by Lahn and Rehahn in 2001.[65] They prepared ditopic bis(phenantroline) derivatives, assembled them with Cu^+ and Ag^+ ions, and studied the influences of the solvent and the unimer concentration in the system on their chemical constitution in solutions. They observed formation of cyclic structures in diluted solutions in solvents coordinating to the ions (acetonitrile, water) and, in contrast, formation of linear chains in a solution in the non-coordinating solvent (tetrachloroethane). The presence of coordinating solvent has been also found crucial for ligand exchanges and recomplexations, as none of these processes has been observed in non-coordinating solvent tetrachloroethane. The exchanges studied are depicted in Scheme 3. The analyses were done by the ^{1}H NMR technique since binding of ligands to Cu^+ or Ag^+ could be resolved from the signal positions.

Ar'= C$_6$H$_5$

Ar= p-C$_6$H$_4$-OMe

A = D$_2$O or CD$_3$CN
B = C$_2$D$_2$Cl$_4$
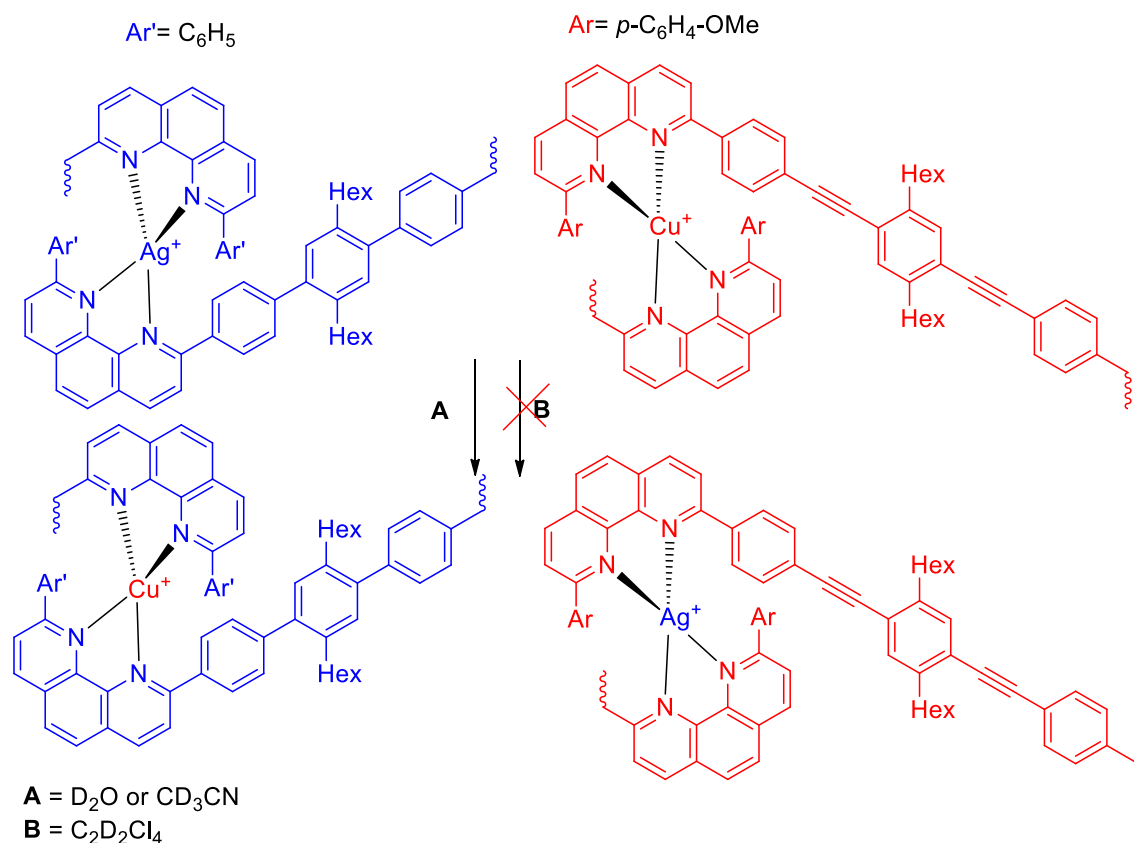
Scheme 3: Study of dynamic properties of Ag and Cu complex reported by Lahn[65]

Constitutional dynamics enables a unique modular approach to the polymer synthesis. This feature was explored for example by Wild et al.,[66] who prepared new white light emitting material of the copolymeric dynamer class by optimizing the mole ratios in which three different homopolymeric Zn-dynamers are mixed (Figure 5). In general, different unimers with identical end-groups but various emission colors can be easily combined in any ratio to obtain new dynamic MSPs of the statistical copolymer class, which shows the desired functional properties. Furthermore, the constitutional dynamics makes difficult determining the molar mass averages of a dynamer owing to its equilibrium dissociation in solutions. Nevertheless, dynamers are supposed to be applied in the solid state where their equilibrium molar mass should be sufficiently high.[28,66–68]
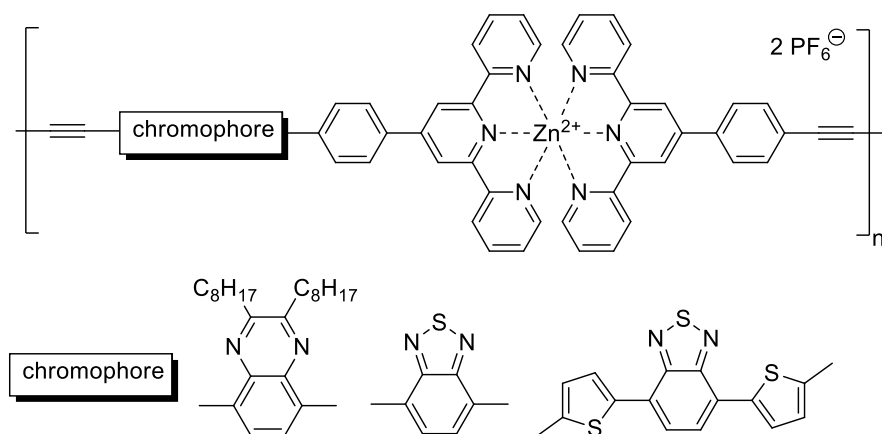
Figure 5: Terpyridine based material to obtain white emission

1.3.6 MSPs based on terpyridine

As indicated above, properties of MSPs should be a superposition of the properties of their organic central blocks and linkages comprising metal ions. If a unimer is composed of fully π-conjugated molecules (conjugated both central block and end-groups), the resulting dynamer can exhibit properties that might be potentially exploited in organic electronics. Terpyridine-4'-yl (*tpy*) end-groups are promising chelating units for fully π-conjugated unimers. An α,ω-bis(*tpy*) unimer can easily undergo spontaneous assembling (supramolecular polymerization) to the corresponding MSP in the presence of a suitable metal ion (ion coupler). Scheme 4 shows the concept of such polymerization. Typical structure motifs of the central blocks of fully π-conjugated α,ω-bis(*tpy*) unimers are oligophenylenes,[48,69–71] oligofluorenes,[72] oligothiophenes[73–77] and their combinations with ethynediyl units[78–82] (see examples in Figure 6). The most widely studied dynamers of this class are based on bis(*tpy*)oligophenylenes[69,83–86] as they are easy to synthesize; the simplest one: bis(*tpy*)phenylene is nowadays even commercially accessible. Recently metallo-supramolecular polymers based on bis(*tpy*)phenylene were reported for electrochromic applications such as smart windows.[70,87,88]
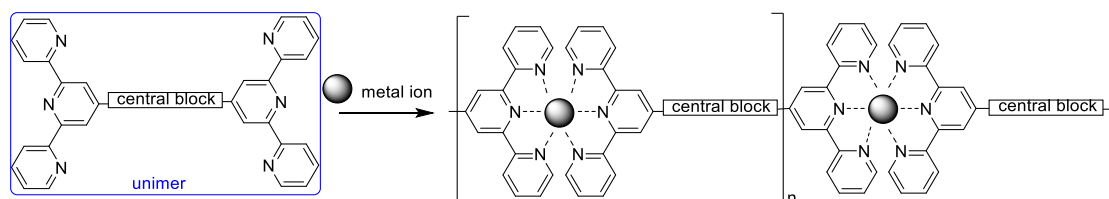
Scheme 4: Supramolecular polymerization of bisterpyridines
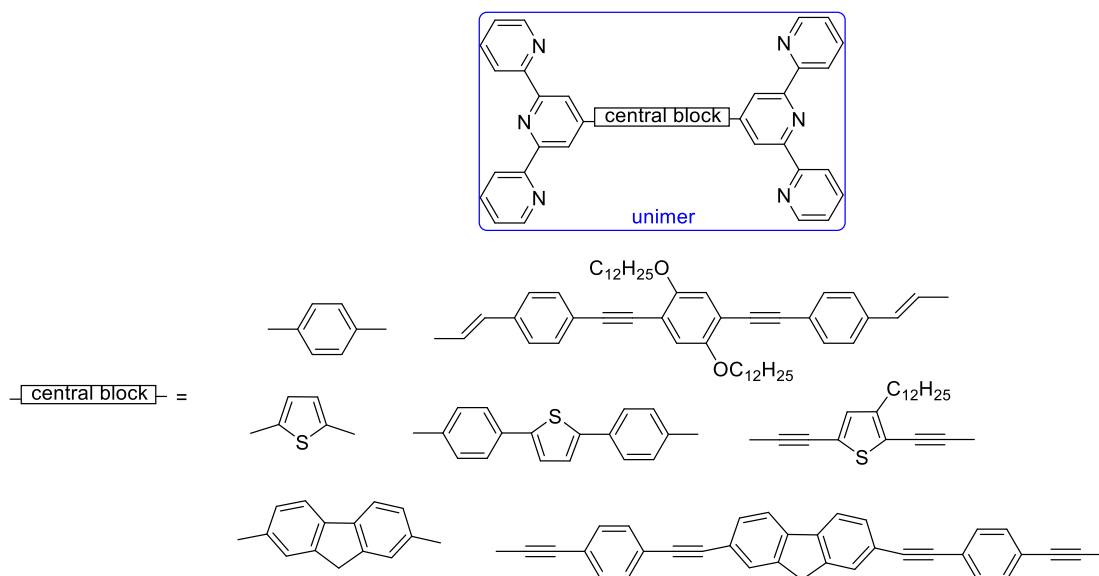
Figure 6: Examples of bis(*tpy*) unimers

Oligothiophenes are a good choice for central blocks of unimers solely derived from heterocycles and capped by *tpy* units. The number of the thiophene rings in unimer and their functionalization can be controlled by synthetic approach and thus used to tune optoelectronic properties of resulting unimers. Svoboda et al. described the synthesis and photophysical properties of the first bis(*tpy*)oligothiophenes[89] (Figure 7) that differed in the central block length and substitution of the thiophene rings. They proved that the optoelectronic properties of resulting MSPs are closely related to the structure of unimers. Increasing number of heterocycles built in the central block of unimer increases the delocalization of electrons along chains and red shifts the positions of both absorption and emission bands. Functionalization of the thiophene rings with alkyl side chains increased solubility of these unimers, however, somewhat distorted coplanarity of the rings and thus decreased the delocalization of π-electrons within unimer molecules. It was manifested by the blue shifts of the absorption and emission spectral bands of unimers compared to their positions for unsubstituted counterparts. The studies continued by synthesis of structurally various bis(*tpy*)oligothiophene (e.g. Figure 7) and their assembly into MSPs with Zn^{2+} and Fe^{2+} ions.[77,90] Recently the same group published synthesis and properties of α,ω-bis(*tpy*)quaterthiophenes with ionic side groups that show enhanced delocalization of electrons and solubility in green solvents such as alcohols or even water.[75]

Figure 7: Examples of bis(*tpy*)oligothiophenes[75,76,89]

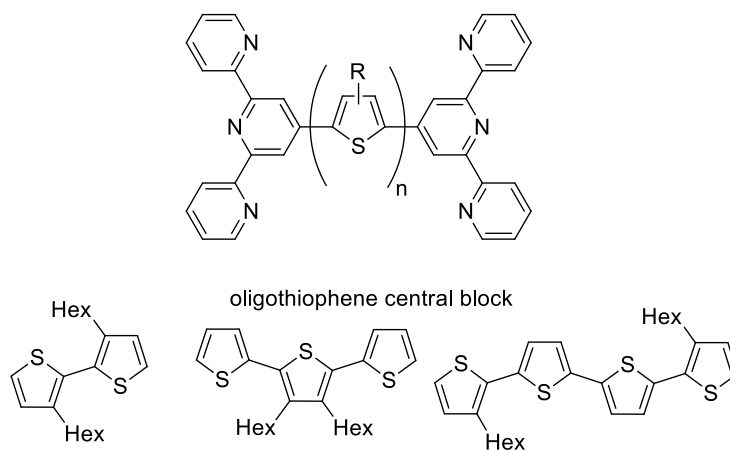## 1.4. PHOSPHOLES

The extent of the delocalization of electrons in a ground-state of poly(heteroarene) chain depends not only on the chain length but also on the aromaticity of the enchained rings. As a rule, the higher aromaticity, the lower extent of the delocalization of valence electrons. Benzene rings are more aromatic than thiophene rings and thiophene rings are significantly more aromatic compared to phosphole or silole rings.[26] Hence, it can be assumed that the replacement of a thiophene unit by a less aromatic phosphole or silole unit in a conjugated oligoheteroarene chain will increase the extent of the electron delocalization (often reported as the effective conjugation length) along the chain.

Phosphole is the phosphorous analogue of pyrrole (Figure 8). A phosphole ring is quite attractive building unit for conjugated systems thanks to its unique properties.[91] A phosphorus atom does not easily form *sp* hybrid orbitals but mainly employs p-orbital electrons to form covalent bonds. Therefore, a coordinated phosphorus atom mostly acquires the pyramidal geometry and its lone electron pair is of highly s character.[92] These geometric and electronic features strongly decrease effective interactions between electrons of the lone pair and the endocyclic diene system, which prevents achieving the truly aromatic state, unlike the case of its nitrogen counterpart, pyrrole (Figure 8).

Due to the foregoing, phosphole ring displays electronic properties that markedly differ from those of the thiophene and pyrrole rings that are widely used in the design of semiconducting polymers. Actually, the phosphole ring possesses: *(i)* only weak aromaticity, which should favor delocalization of the endocyclic diene π-system, *(ii)* low lying LUMO energy level,[93] and *(iii)* reactive heteroatom[94] which offers the possibility of tuning the photo-physical properties (absorption and emission

wavelengths, redox behavior, etc.) of phosphole *via* chemical modification (oxidation, alkylation, coordination).[95–99] These unique properties make phosphole units good candidates for the design of conjugated polymers with enhanced delocalization of electrons along their chains.
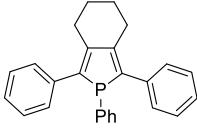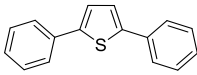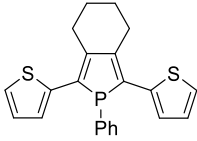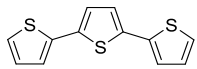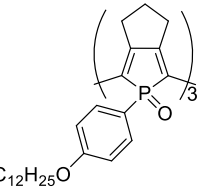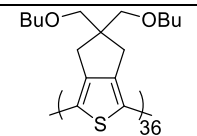
Figure 8: Structural comparison of phosphole and pyrrole; representation of pyramidal geometry of phosphole

1.4.1 Phosphole polymer

The idea of replacing thiophene unit by phosphole unit in a polythiophene chain is quite attractive since structurally similar phosphole ring displays different properties. If the reported spectral characteristics of phosphole oligomers are compared with their thiophene analogues (Table 1), it is clearly obvious that the replacement of the thiophene with phosphole ring lead to the enhanced delocalization of electrons proved by the red-shift of the absorption as well as emission maximum.

Table 1: Comparison of the absorption and emission maxima of selected phosphole and thiophene derivatives.

Compound	Ref.	Absorption maximum (nm)	Emission maximum (nm)
	100	354	466
	101	326	378, 393
	102	412	501
	103	360	435
	104	655	none
	105	524, 546	588, 638

The first example of the incorporation of phosphole ring into π-conjugated polymer backbone was reported by Tilley at al.[106] They envisioned use of zirconocene diyne-coupling as a new general approach to the synthesis of polymers of novel structures comprising phosphole rings (Scheme 5). This approach consists of preparing the polymers with zirconacyclopentadiene units and their conversion into phosphole rings *via* reaction with *P,P*-dichlorophenylphosphine (Scheme 6).
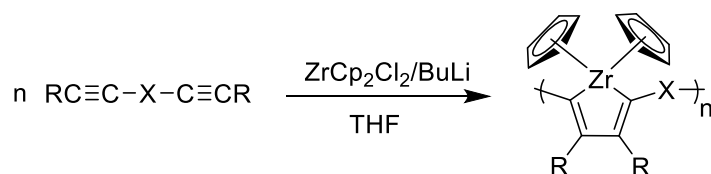
Scheme 5: Synthesis of polymer possessing zirconacyclopentadiene
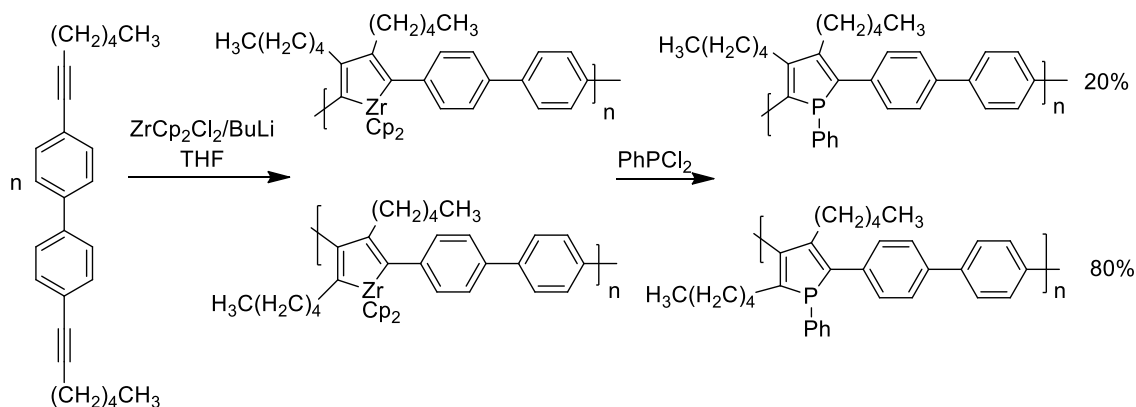
Scheme 6: Structure of phosphole containing polymer prepared by Tilley

Morisaki et al.[107] prepared a regioregular polymer comprising phosphole units by the palladium-complex catalyzed coupling of bis(*p*-bromophenyl)phosphole with diethynylarenes (Scheme 7a). Réau et al.[108] electro-polymerized derivative of 2,5-di(2-thienyl)phosphole to the polymer containing alternating phosphole and 2,2'-bithiophene units (Scheme 7b). In 2010 Matano et al.[104] described the palladium-copper catalyzed Stille cross-coupling of 2,5-bis(tributylstannyl)- and 2,5-diiodo- substituted phosphole affording corresponding poly(phosphole-2,5-diyl) polymer and oligomers (Scheme 7c). These examples illustrate that there are several possibilities (anodic oxidation, coupling reactions) how phosphole derivatives can be polymerized to obtain conjugated polymers containing phosphole units.
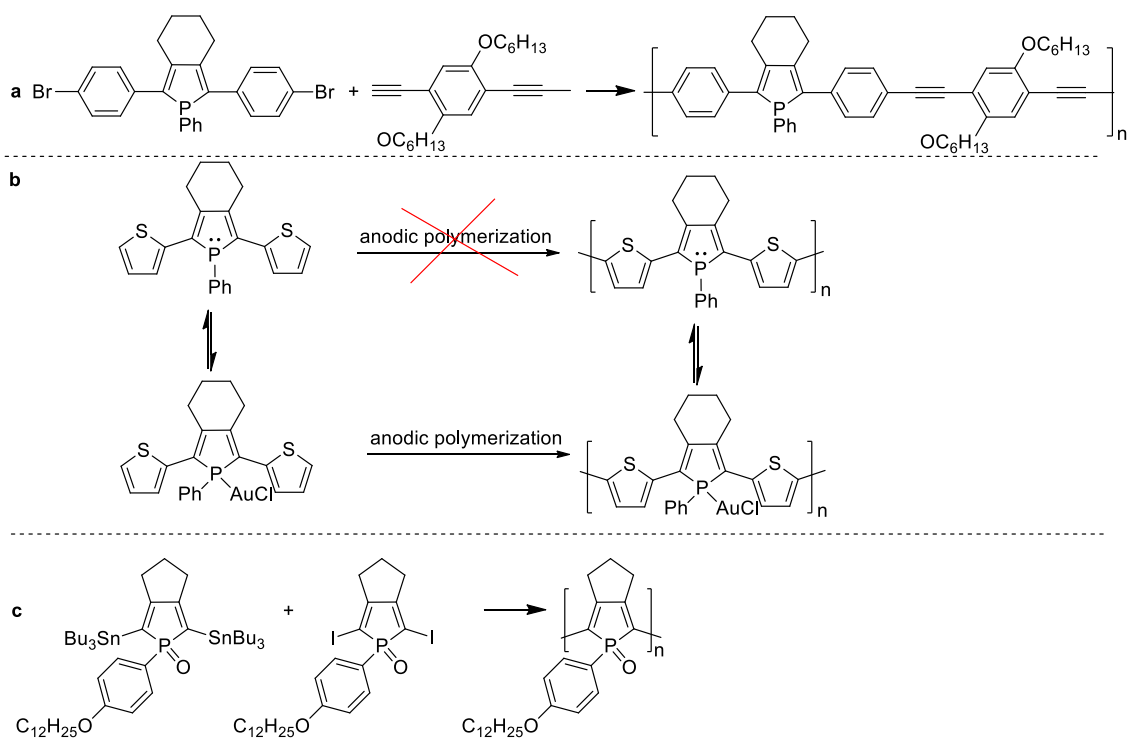
Scheme 7: Examples of already prepared π-conjugated polymers comprising phosphole unit

1.4.2 Supramolecular structures comprising phosphole units

Coordination chemistry of phospholes originates from the ability of phosphorus lone electron pair to form complexes with transition metals (Scheme 8).
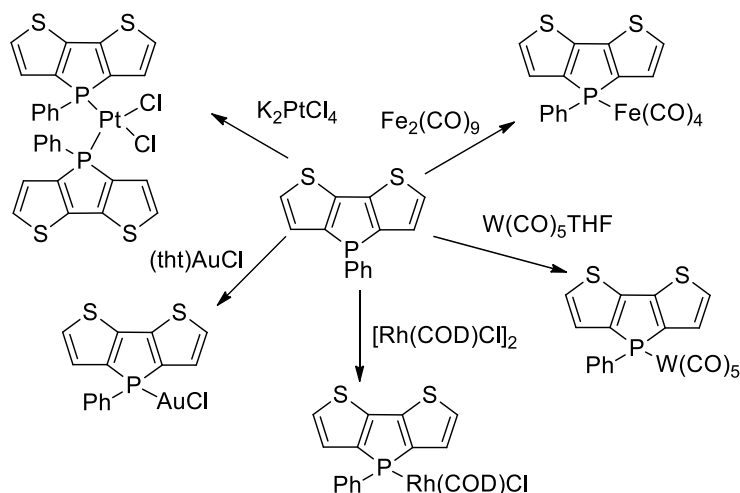
Scheme 8: Transition metal complexes derived from 1-phenyldithieno[3,2-b:2,3-d]phosphole.[109]

2-Pyridylphosphole derivatives[110] (Figure 9) are also useful hetero-ditopic ligands as they offer at least two coordination centers with different stereo-electronic properties. This motif was already applied in the synthesis of molecular pincers[111] and helicands[112] exhibiting original coordination modes.
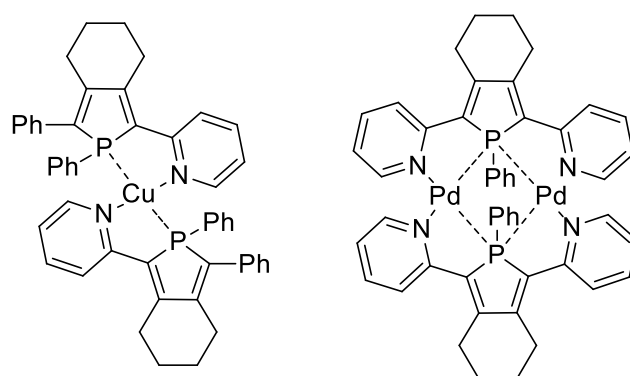
Figure 9: Examples of complexes of 2-pyridylphosphole derivatives.

Phosphole as part of supramolecular assembly without participation on coordination bond is very rare. D. R. Bai et al. prepared bipyridine and terpyridine-extended dithienophosphole chromophores[113,114] (Figure 10). The latter chromophore can be regarded as an α,ω-bis(*tpy*) unimer with the central block comprising phosphole ring.

Complexation of these species with metal ions has not been studied; only the complexation of mono*tpy* derivatives was investigated.
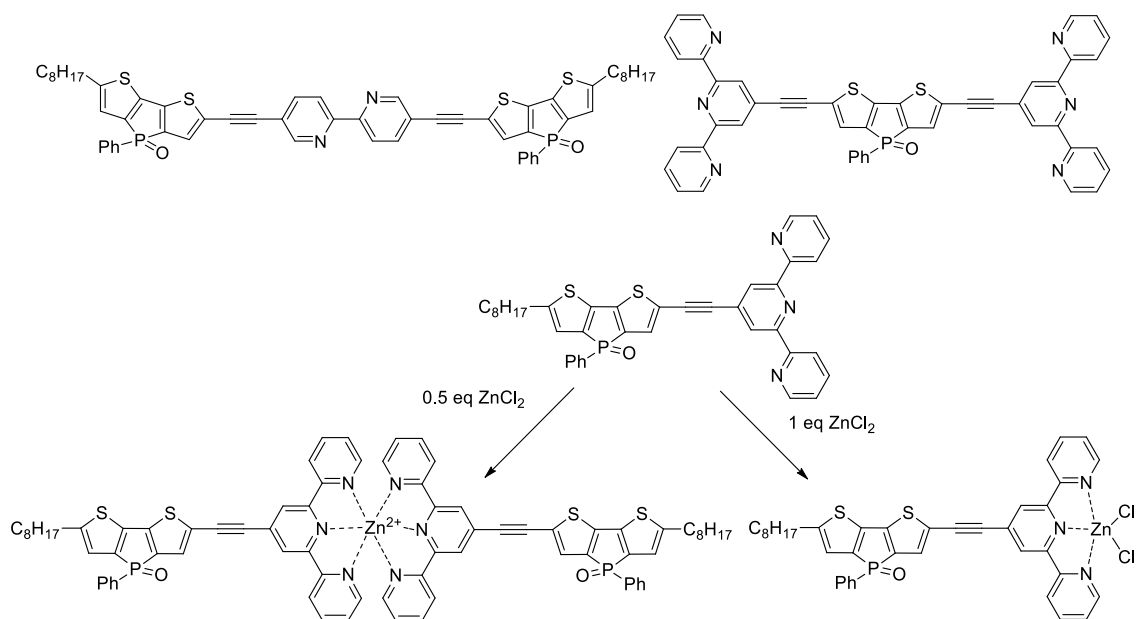
Figure 10: Phosphole chromophores extended by *bpy* and *tpy* units and complexation of mono*tpy* derivative.

2   AIMS OF THESIS

In accordance with the above described requirements for the novel functional materials combining the recent knowledge in supramolecular and phosphole chemistry, the aims of this doctoral project were established as follows:

1. Synthesis of monoterpyridine ligands that were proposed as terminal units of phosphole unimer and a detailed study of their complexation with ions by various techniques; determination of stability constants.

2. Development of synthetic procedures for preparation of conjugated unimers containing phosphole unit in the central block and capped either directly or through a spacer with terpyridine ligands.

3. Study of the course of assembly of metallo-supramolecular polymers from prepared unimers and various metal ions using different spectroscopic techniques.

4. Characterization of prepared unimers and metallo-supramolecular polymers with attention payed to their spectroscopic properties in solutions and thin films. Correlation of the obtained results with structure of unimers and their comparison with properties of bis(*tpy*)oligothiophene unimers of similar structure.

5. Examination of the kinetic stability of chains of prepared metallo-supramolecular polymers in solutions.

3 RESULTS AND DISCUSSION

3.1 Monoterpyridine ligands

3.1.1 Syntheses

The monoterpyridine compound: 4'-(thiophene-2-yl)-2,2':6',2''-terpyridine (Thio-*tpy*) was prepared using the modified Kröhnke synthesis approach[73,115] or, alternatively, Suzuki coupling reaction between 4'-bromo-2,2':6',2''-terpyridine (Br-*tpy*) and boronic derivative of thiophene.[76] 4'-Ethynyl-2,2':6',2''-terpyridine (E-*tpy*) was prepared by a Sonogashira coupling reaction of Br-*tpy* and trimethylsilylacetylene followed by the removal of trimethylsilyl group in presence of potassium carbonate as described earlier.[116] 4'-(Ethynylaryl)terpyridines were prepared using the synthetic pathways shown in Scheme 8.
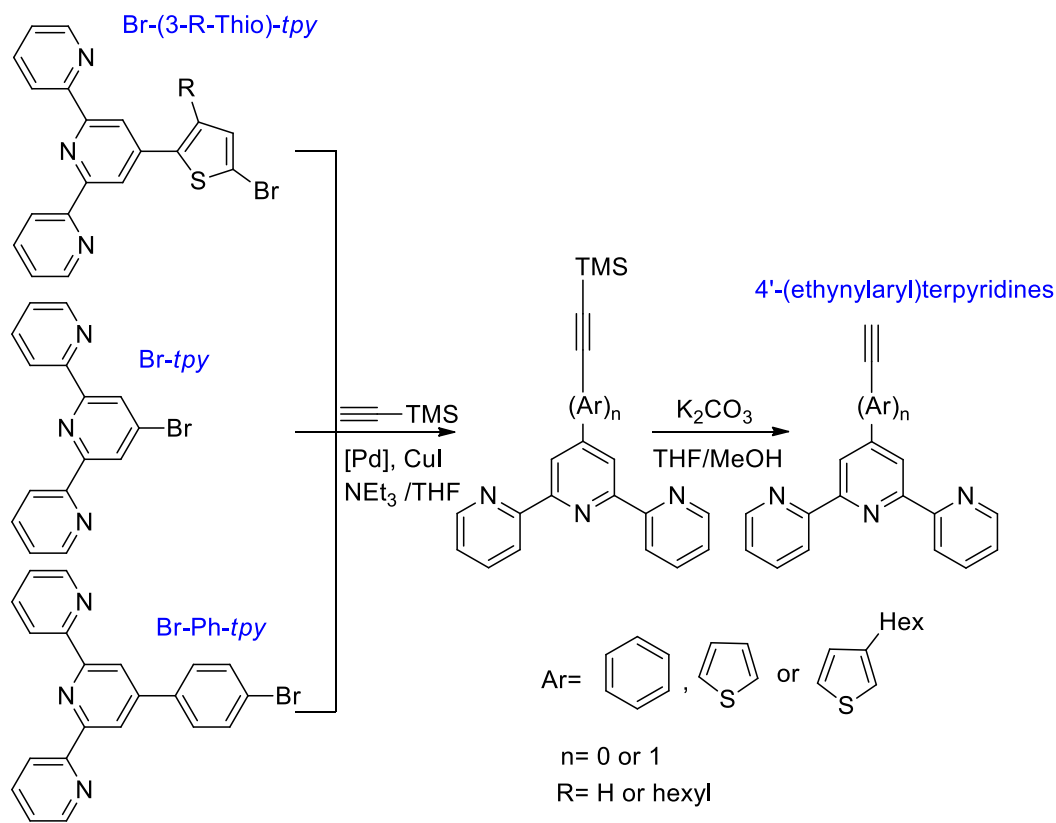
Scheme 8: Functionalization of terpyridine with ethynyl group

Reaction conditions for synthesis of 4'-(ethynylarylterpyridine) were slightly different, depending on the type of aryl unit. For 4'-(4-ethynylphenyl)-2,2':6',2''-terpyridine, the same conditions as for E-*tpy* were applied starting from the appropriate bromo-derivative.[116] The ligands based on 4'-(5-ethynylthiophene-2-yl)-2,2':6',2''-terpyridine

were prepared according to a procedure described by Constable,[117] starting from the appropriate bromo derivative, which was prepared by bromination of substituted thienyl derivative *via* N-bromosuccinimide (NBS)[118] (Scheme 9). General procedures of all mentioned reactions for the ligand synthesis are described in the Experimental part.
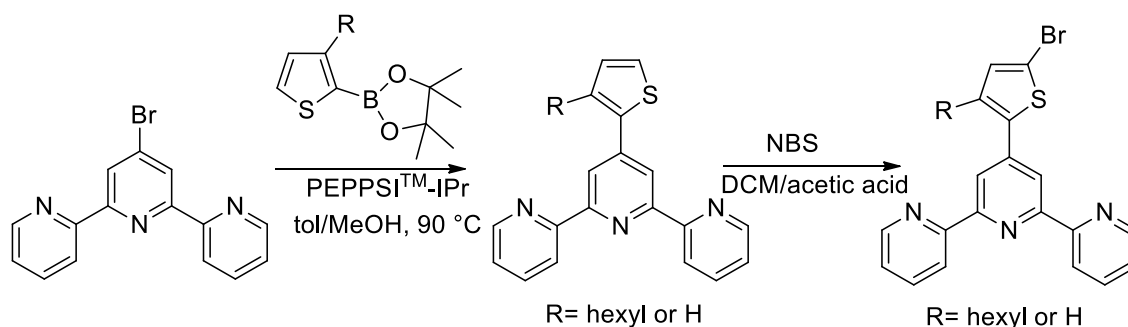
Scheme 9: Synthesis of 4'-(3-R-thiophene-2-yl)-2,2':6',2''-terpyridine

3.1.2 Complexation of terpyridine, Thio-*tpy* and E-*tpy* with metal ions

Complexations of both ligands, Thio-*tpy* and E-*tpy*, with Fe^{2+} and Zn^{2+} ions (for schematic representation see Scheme 10) were studied using UV/vis, fluorescence and ^{1}H NMR spectroscopies. *Tpy* unit possesses different (*syn/anti*) configuration of nitrogen atoms depending if it is coordinated or not. This configuration changes are accompanied by spectral changes as well. Fe^{2+} and Zn^{2+} are known to form complexes with terpyridine with quite high stability constants, yet the atoms are different in the electronic configuration and the complexes possess different kinetic lability.[45,119] The coordination properties of these ligands were compared with coordination properties of unsubstituted terpyridine. A series of solutions with increasing ratios M/L were prepared for each ligand L (terpyridine, Thio-*tpy* and E-*tpy*) by mixing their acetonitrile solutions in specific concentrations a day prior to the measurements and allowed to equilibrate (for details the reader is kindly asked to look into attached publication = ref [120]).

The monitoring of *UV/vis absorption* changes during the complexation process revealed a red-shift of the absorption maximum with the increasing concentration of metal ions in the ligand solution (Table 2). For the systems with Fe^{2+} ion couplers, in addition a new band appeared at above 550 nm, which should be ascribed to the MLCT band in accordance with the earlier reported observations.[121,122]

Table 2: Absorption maxima of various ligands and their Zn^{2+} and Fe^{2+} complexes in acetonitrile, initial ligand concentration 0.05 mmol/L

Ligand→ species↓	Absorption maximum, λ_{max}, nm		
	Terpyridine	Thio-*tpy*	E-*tpy*
L	277	285 (295sh)	316 (328sh)
ZnL_2	334	345	344
ZnL	332	345	341
FeL_2	320	328 (336sh)	327 (334sh)
	551 (MLCT)	576 (MLCT)	570 (MLCT)

The UV/vis spectra also showed the presence of an isosbestic point, which proves a direct transformation of L to ML_2 during addition of metal ions to ligand. Unlike the studies with different terpyridine derivatives[123,124] no isosbestic point was found for the transformation of ML_2 into ML complex species at the M/L ratios above 0.5 (Figure 11).
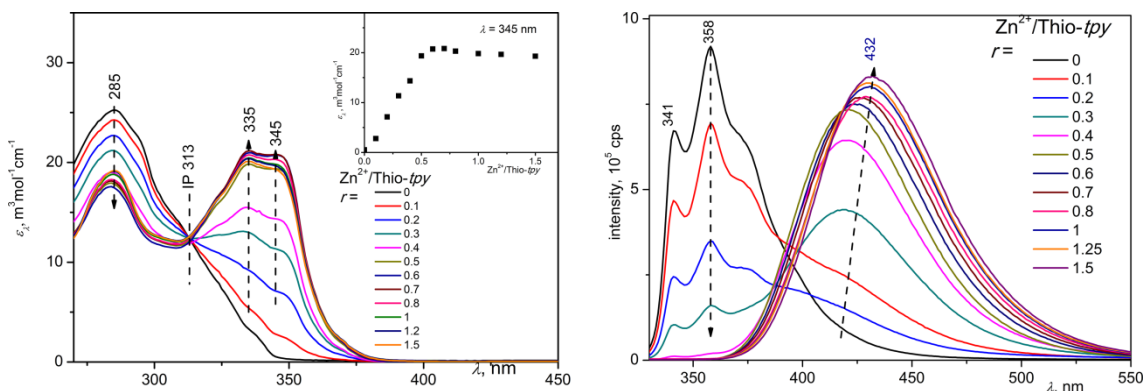
Figure 11: Absorption and fluorescencespectra for the complexation of Thio-*tpy* with Zn^{2+} ions.

Absorption spectra of ML and ML_2 complexes are similar to each other, which is in accord with the results of theoretical calculations (see attached publication[120]). Factorial analysis of all measured spectral series made with HypSpec software[125] gave the values of the stability constants K_1 and K_2 (Table 3) defined by the following equations:

$$M^{2+} + L \rightarrow ML^{2+}; \; K_1 = \frac{[ML^{2+}]}{[M^{2+}]\times[L]}$$

$$M^{2+} + 2L \rightarrow ML_2^{2+}; \; K_2 = \frac{[ML_2^{2+}]}{[M^{2+}]\times[L]^2}$$
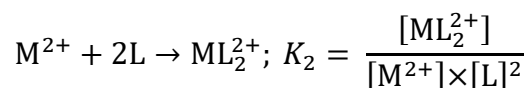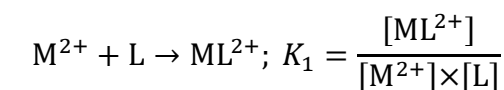
Table 3: Stability constants of studied complexes in acetonitrile or d[3]-acetonitrile at 25°C

Ligand	UV/vis			NMR	
	Zn^{2+}		Fe^{2+}	Zn^{2+}	
	$\log K_1$	$\log K_2$	$\log K_2$	$\log K_1$	$\log K_2$
Thio-*tpy*	7.5±0.4	11.8±0.4	12.8±0.6	7.0±0.8	13.0±1.7
E-*tpy*	7.0±0.2	13.0 ± 0.2	13.3±0.6	6.8±0.7	12.4±1.3

Fluorescence spectra were measured with the same adjustment of machine for all experiments by using the excitation wavelength equal to the position of the isosbestic point (UV/vis spectra intersection) in order to exclude an influence of differences in molar absorption coefficient (within a given series) on the fluorescence intensity. Fluorescence studies of the complexation revealed a massive enhancement of the fluorescence band and its small red-shift upon introduction of Zn^{2+} ions in the case of the systems with terpyridine and E-*tpy* ligands. In contrast, the system with Thio-*tpy* ligand showed a strong red-shift of the fluorescence maximum (Figure 11). The fluorescence intensity was firstly decreasing for the [Zn^{2+}]/[Thio-*tpy*] ratios up to 0.25 and then continuously increasing keeping its position (420 nm) for the ratios [Zn^{2+}]/[Thio-*tpy*] up to 0.5. Then, the intensity is further increasing and, in addition, showing a continuous red shift of the fluorescence maximum for the ratios [Zn^{2+}]/[Thio-*tpy*] above 0.5 (see Figure 13), introducing Zn^{2+} to *tpy* derivatives causing red-shift and decrease of fluorescence intensity was repeatedly described.[75,77,90,121,126,127] In contrast, the introduction of Fe^{2+} ions to a solution of any tested ligand led to a gradual fluorescence quenching as already reported[128] because of fast intersystem transition followed by non-radiative transition to the ground state.

Complexation of both synthesized ligands with Zn^{2+} and Fe^{2+} ions was also monitored by *^{1}H NMR spectroscopy* in d[3]-acetonitrile. ^{1}H NMR spectra of L, ML2 and ML are well differentiated as the nitrogen atoms adapts *anti* conformation in a free *tpy* group but *syn* conformation in a *tpy* group coordinated to a metal ion. The changes in ^{1}H NMR spectra accompanying the increase in the molar ratio of Zn^{2+} ions to *tpy* ligand in the system Zn^{2+}/E-*tpy* are shown in Figure 12; assignment of the NMR signals is done using proton positions shown in Scheme 10. ^{1}H NMR spectra of E-*tpy*, Zn-(E-*tpy*)2 and Zn-(E-*tpy*) are well differentiated as (*i*) the nitrogen atoms of pyridine rings prefer the *anti*-conformation in the free (not coordinated) species, but they acquire the *syn*

conformation when they are bound to metal ion (*ii*) A-rings (Scheme 10) of two E-*tpy* ligands in ML_2 complex shield each other due to their close proximity, which results in a high up-field shift of the signal of A6 protons; shielding by the adjacent L unit is absent in the monoterpyridine Zn-(E-*tpy)* ligand.
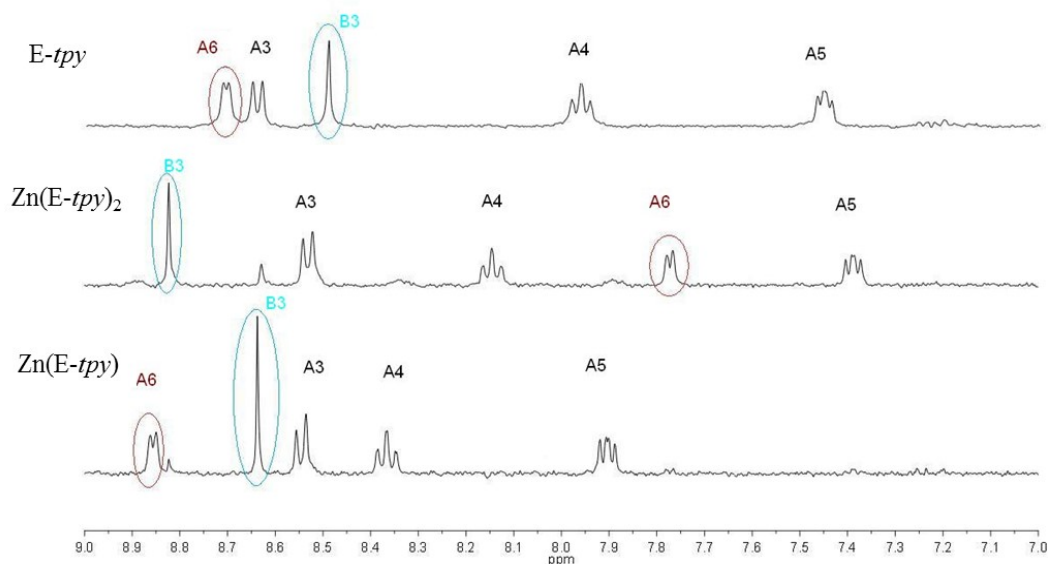
Figure 12: Position of specific ^1H NMR signals of E-*tpy* dependent of present species (free ligand, ML_2 complex and ML complex)
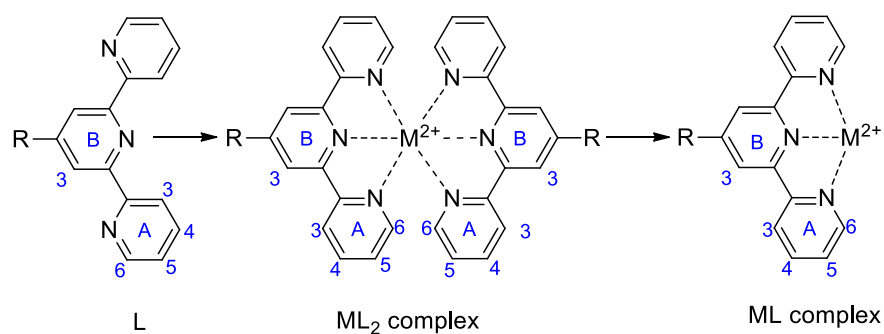
Scheme 10: Scheme of complexation of monoterpyridine ligands

NMR spectra obtained for the systems Fe^{2+}/*tpy* ligands showed exclusively formation of ML_2 species even at the Fe^{2+}/*tpy* ratios exceeding the value of 1; formation of the mono-*tpy* ML species was not observed for this system.

As the signal resolution of the measured NMR spectra was high, the distributions of L, ML and ML_2 species in the systems as a function of the M/*tpy* ligand ratio could be estimated. Factorial analysis of the spectra made with the HypSpec

software[125] gave the values of the stability constants K_1 and K_2 that are close to the values obtained by the factorial analyses of the UV/vis spectra (see Table 3).

The determined stability constants are similar nevertheless the type of experiment (UV/vis or NMR) and also the substituents. Furthermore stability constants of ZnL_2 and FeL_2 complexes were comparable with those observe in aqueous solutions[119], however formation of FeL complex reported in aqueous solution[47,119] was not observed in acetonitrile.

Different *tpy* derivatives were shown to be easily synthesized and to provide stable complexes with various metal ions. Metal ions as well as ligand structure played the role in final properties. Yet due to their structure and coordination behavior these ligands are ready to be used in more evaluated systems such as polymer with pending E-*tpy*-substituent or bis(*tpy*) unimers and related metallo-supramolecular polymers.

3.1.2 Terpyridine functionalized by phosphole unit

Presented monoterpyridine ligands can be used as pendant substituents of polymer chain. For example, the E-*tpy* was exploited for preparation of a phosphole unit carrying *tpy*-ethynyl group attached to phosphorus atom: P-E*tpy* (Scheme 10, this work was done in collaboration with Mathieu Denis and Wylliam Delaunay from the University of Rennes 1). Thus the effect of the complexation of the terpyridine and phosphorus on the physicochemical properties of the π-conjugated system could be studied. The synthesis of P-E*tpy* was carried out by means of the reaction of lithium acetylide with corresponding 1,1'-biphosphole (see Scheme 11). The acetylide derivative was formed *in situ* by the reaction of E-*tpy* with butyllithium. 1,1'-Biphosphole was synthetized from octa-1,7-diyne-1,8-diyl-2,2'-bis(thiophene) *via* Sato method (*vide infra*) using titanium isopropoxide and phosphorus tribromide as already reported by Fave *et al.*[93]
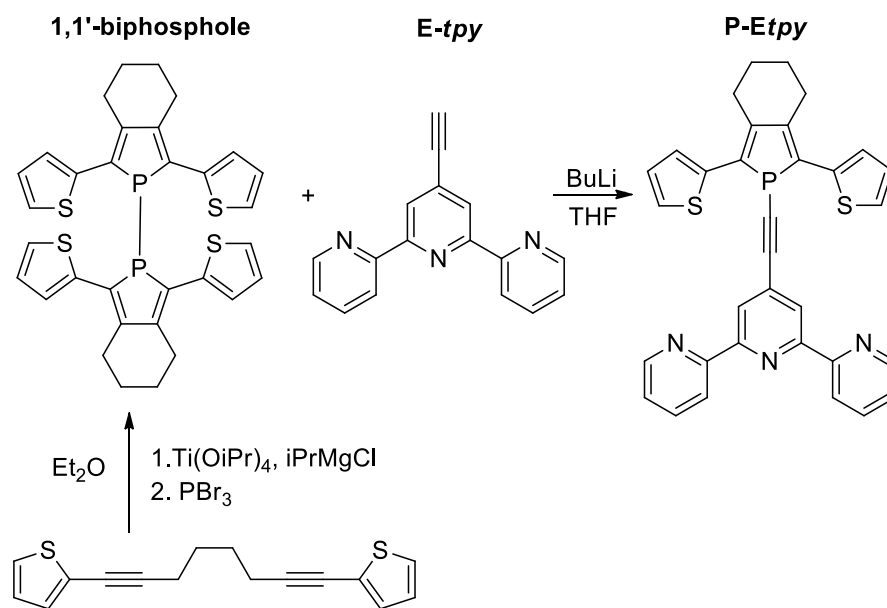
Scheme 11: Synthesis of P-E*tpy*

Since the ^{31}P atom is active in NMR spectroscopy, the synthesis of organophosphorus compounds can be monitored by ^{31}P NMR. The ^{31}P NMR spectrum of the obtained crude product showed 5 signals: the signal of the desired product at –26.20 ppm, two doublets at 19.85 ppm (J = 16.46 Hz) and –5.63 ppm (J = 16.46 Hz), the signal of 1,1'-biphosphole as starting material at –0.94 ppm and signal of an impurity at –11.05 ppm (Figure 13). The two doublets indicate the presence of a compound comprising two phosphorus atoms bonded to sp^2 carbons. Therefore, we decided to oxidize the P atom with sulphur for better separation and isolated this side product from the reaction mixture.
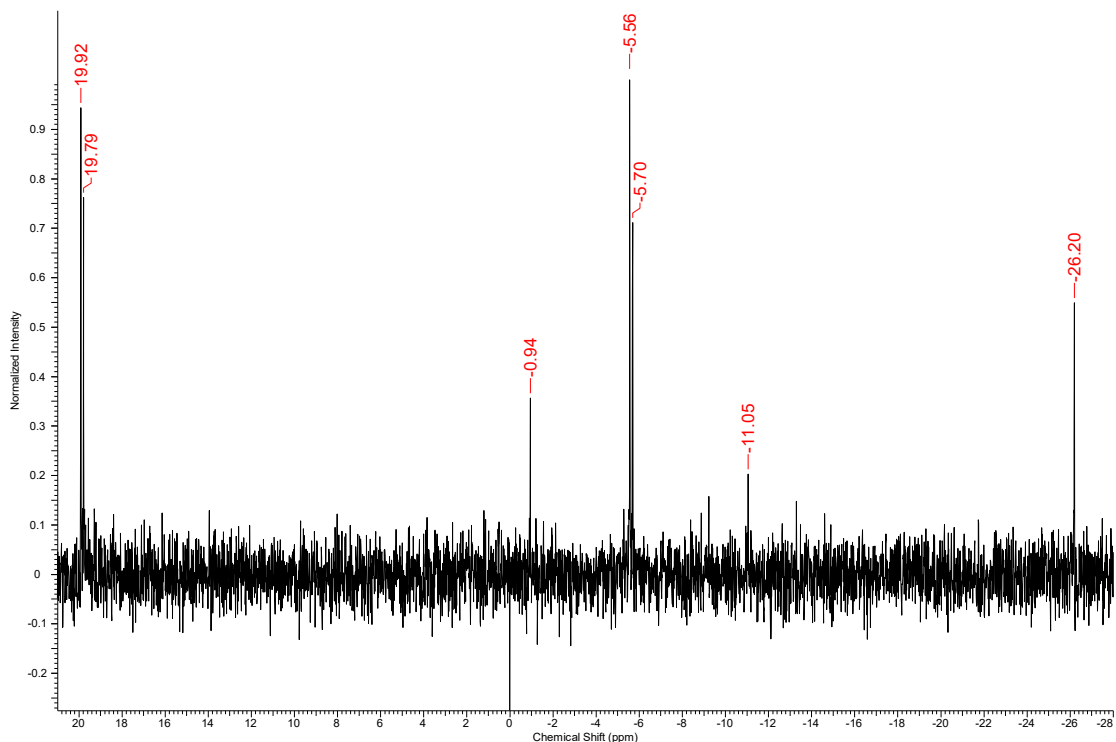
Figure 13: ^{31}P NMR spectra of terminated reaction mixture of synthesis P-E*tpy*

The separation was successful and the ^{1}H NMR spectrum of this side product allowed us to propose its structure that is shown in Figure 14.
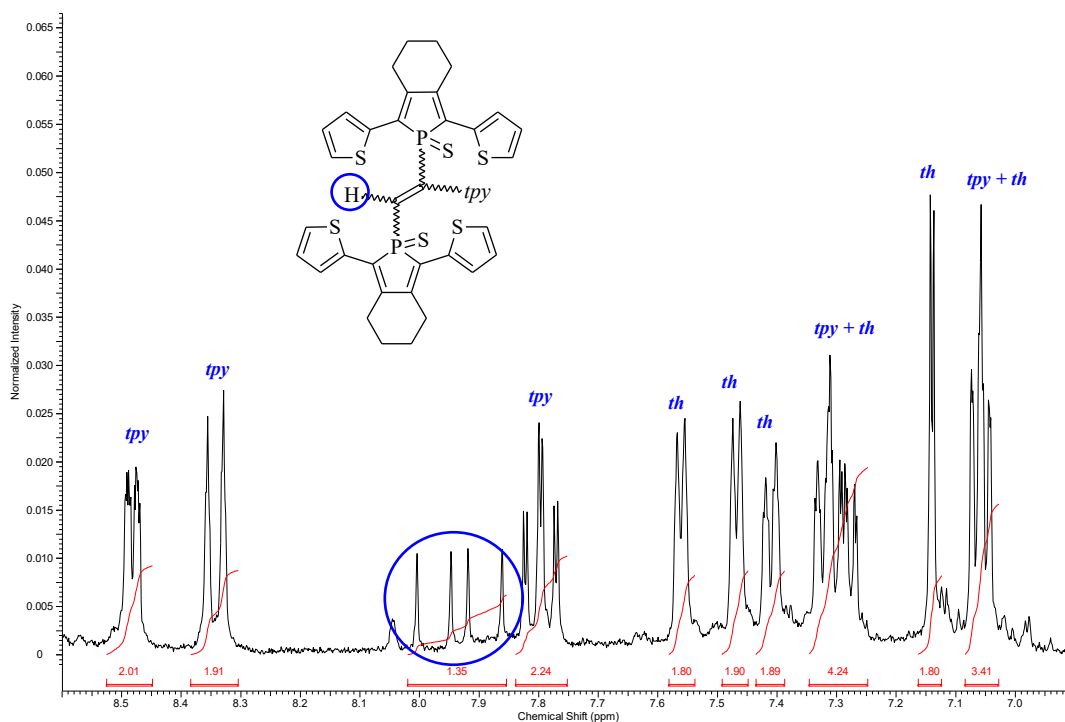
Figure 14: ^{1}H NMR signals in aromatic region and proposed structure of isolated side product

It should be mentioned here that this side product is exclusively formed upon addition of E-*tpy* into the reaction mixture. No side product of this type is observed when phenylacetylide is added to the reaction mixture. The first step involving P–P bond cleavage by acetylide anion has been proposed to proceed as a nucleophilic substitution that gives pholide anion as the intermediate (leaving nucleophile) that has clearly been detected in the reaction mixture[129] without E-*tpy* (see Scheme 12). As terpyridine is a highly electron-withdrawing group, the triple bond in P-E*tpy* is electron-deficient, which allows nucleophilic addition of pholide anion on the triple bond giving the above described bis(phosphole) type side product comprising double bond.
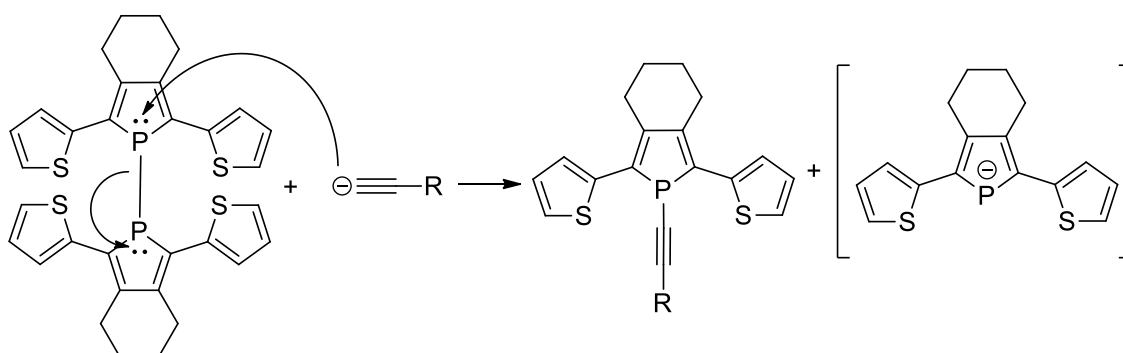
Scheme 12: Proposed mechanism of the formation of "P-E" species.

Despite the above described complications we were able to synthesize P-E*tpy* and perform its physical characterization. In addition, the prepared P-E*tpy* was successfully modified using several methods (Scheme 13). As obtained results were already discussed in dissertation thesis,[129] only brief overview is presented here. Zn^{2+} ions were chosen to coordinate to *tpy* fragment because as implemented in the Introduction they possess d^{10} configuration and Zn^{2+} ions are well known to form complexes with *tpy* group and effect the photophysical properties.[52,62,121,128,130–133] Reactivity of phosphorus lone pair can be used to tune the properties.[108–110,134–136]
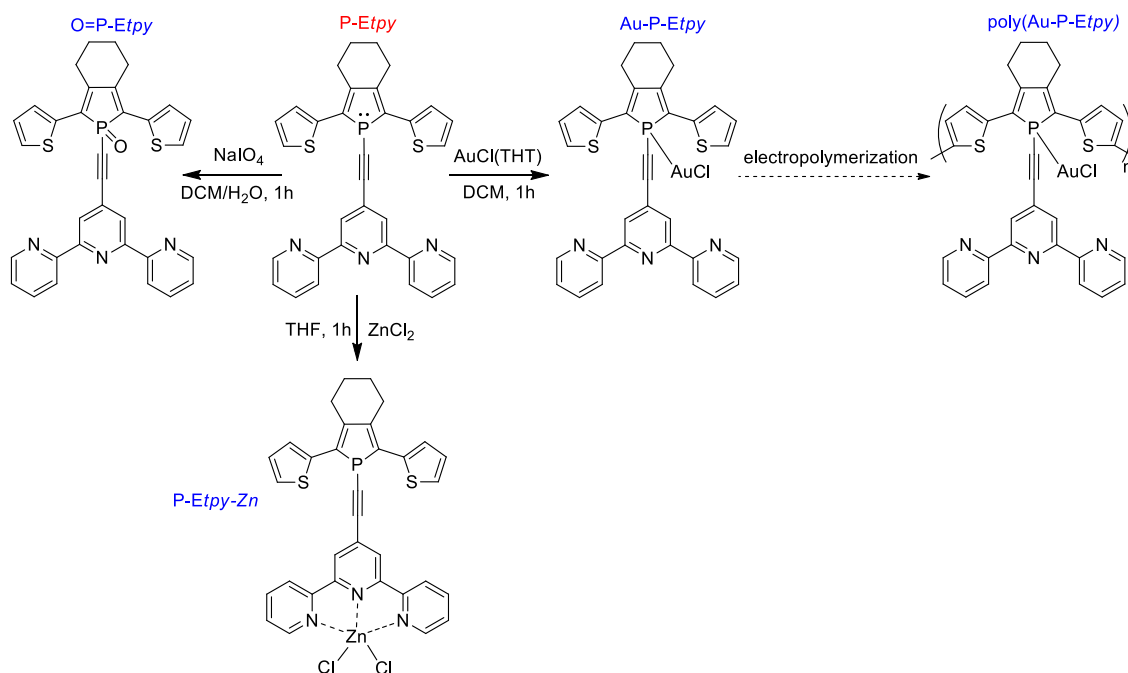
Scheme 13: Modifications of P-E*tpy* and employed abbreviations for their appellation

Absorption and emission spectra of P-E*tpy* and its derivatives were recorded in DCM solutions of the concentration 0.1 mmol/L. The spectroscopic properties are summarized in Table 4 and clearly illustrates that the substitution at P atom (contrary to coordination of Zn^{2+}) has significant influence of absorption of π-system as the absorption maximum is red-shifted. Influence of Zn^{2+} ions coordination to *tpy* group on the absorption was clearly observable with a bathochromic shift accompanied by a hyperchromic effect of the absorption bands of the terpyridine leading to the occurrence of a bimodal band at 334 and 347 nm.

Table 4: spectroscopic properties of P-E*tpy* and its modifications

Compound	Absorption maximum, nm	Emission maximum, nm	Fluorescence quantum yield, %
P-E*tpy*	410	511	1
O=P-E*tpy*	448	-	-
Au-P-E*tpy*	437	560	3
P-E*tpy*-Zn	407	-	-

The previous paragraphs definitely showed ability of Thio-*tpy* and E-*tpy* to be reasonable choice for designing terpyridine complexes, thus they are relevant candidates
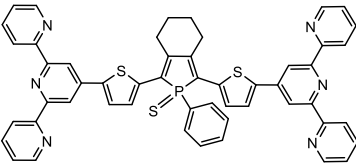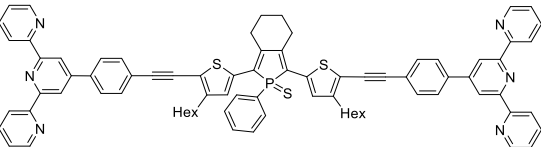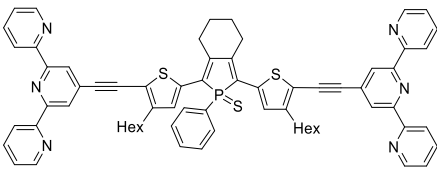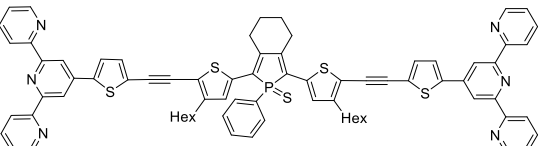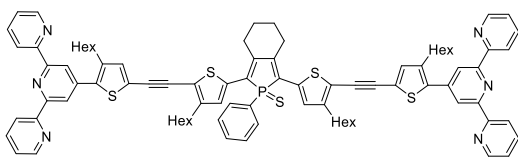
to be used in design more composed systems like bis(*tpy*) unimers and related metallo-supramolecular dynamers.

3.2 Unimers

3.2.1 Syntheses

The structure and abbreviations of prepared phosphole unimers are shown in Table 5 and the synthetic pathway to the unimers in Scheme 14. All prepared unimers contain the core unit denoted as **TPT** (abbreviation based on the sequence of heterocycles **T**hiophene-**P**hosphole-**T**hiophene). The same abbreviation is used for the simplest unimers in molecules of which the *tpy* end-groups are linked directly to free α-positions of the thiophene rings of the central block. All other unimers in addition comprise linkers connecting the *tpy* end-groups to the free α–positions of thiophene rings of the **TPT** core unit. These unimers are simply denoted by abbreviations of the first letters of the groups comprised in the linkers. The simplest extended unimer of this class that contains **e**thynediyl linkers (–C≡C–) is denoted as **E**; the unimer containing **E**thynediyl-1,4-**Ph**enylene, **E**thynediyl-**T**hiophene-2,5-diyl or **E**thynediyl-(3-**hexyl**)**T**hiophene-2,5-diyl linkers are named **ET, EPh** and **ET6,** respectively. If needed, these unimers with extended linkers are generally mentioned as the E-type unimers.

Table 5: Structures and abbreviation of unimers used throughout the thesis

TPT	EPh

E	ET

	ET6

Synthetic pathways to phosphole unimers consist of three steps: *(i)* synthesis of the central sequence of heterocycles containing P-substituted phosphole ring surrounded with two thiophene rings, *(ii)* functionalization of the free α–positions of thiophene rings of the central block, and *(iii)* connecting of the *tpy* end-groups or linkers capped with *tpy* end-groups to the functionalized central block (see Scheme 14).
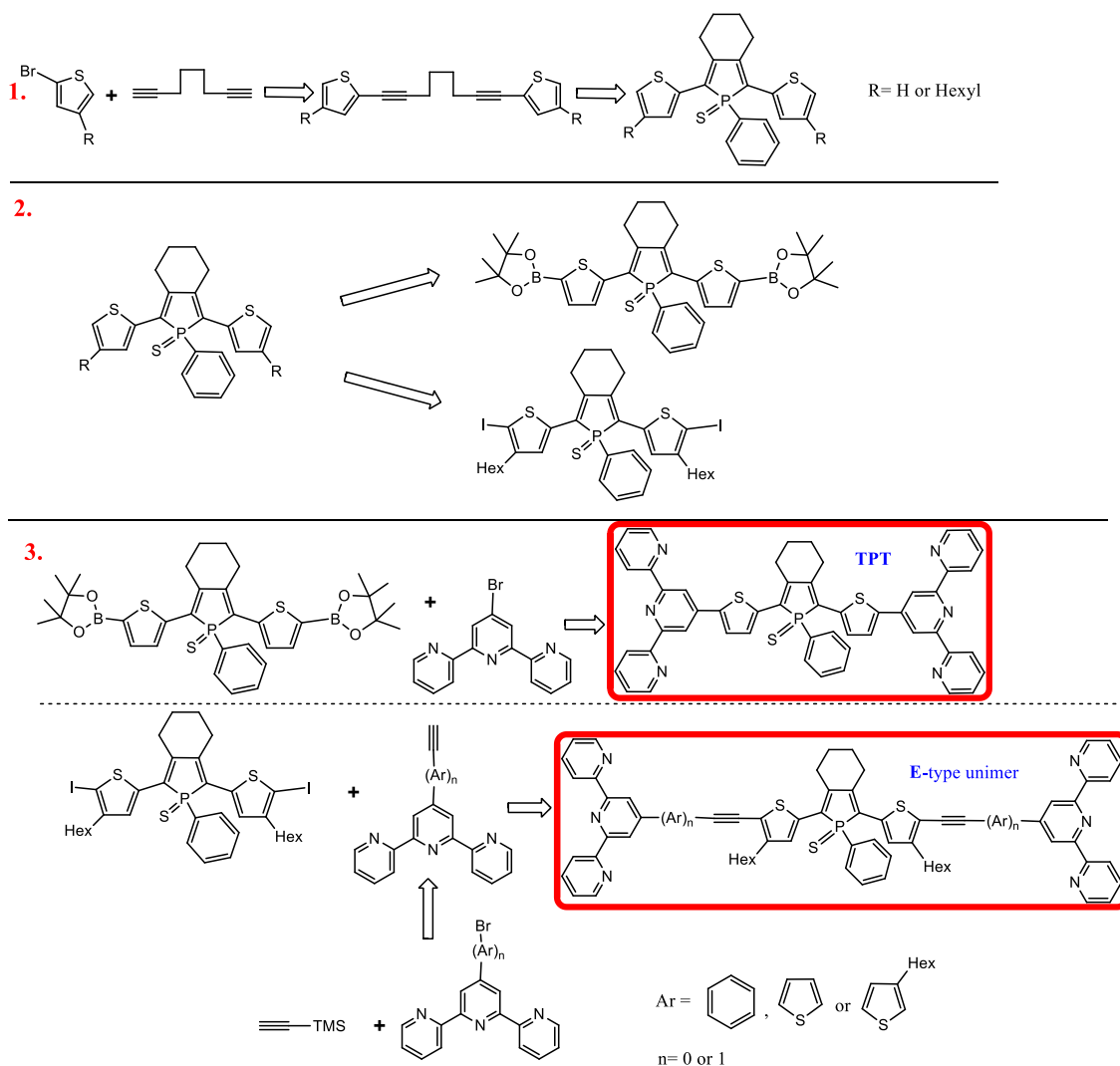
Scheme 14: Synthetic strategies towards unimers

The synthesis of the phosphole containing central block started by Sonogashira coupling of 1,7-octadiyne with 2-bromo- or 2-iodothiophene to obtain (1,7-octadiyne-1,8-diyl)dithiophene with a reasonably high yield up to 70%, from which the desired phosphole can be obtained by two different synthetic pathways (Scheme 15). The Fagan-Nugent[137,138] method uses *in situ* generated low valent zirconium species that undergo cycloaddition with the diyne giving zirconacyclopentadiene species that are readily converted to phosphole species by subsequent treatment with dibromophenylphosphine (PhPBr$_2$). The Sato-Urabe protocol[139] uses *in situ* generated titanium species that similarly give functionalized titanacyclopentadiene[140] species which, in a consecutive low temperature reaction with dichlorophenylphosphine (PhPCl$_2$), afford corresponding phosphole species. After phosphole formation the

45

phosphorous atom was oxidized by addition of sulfur using the procedure described in ref [100].
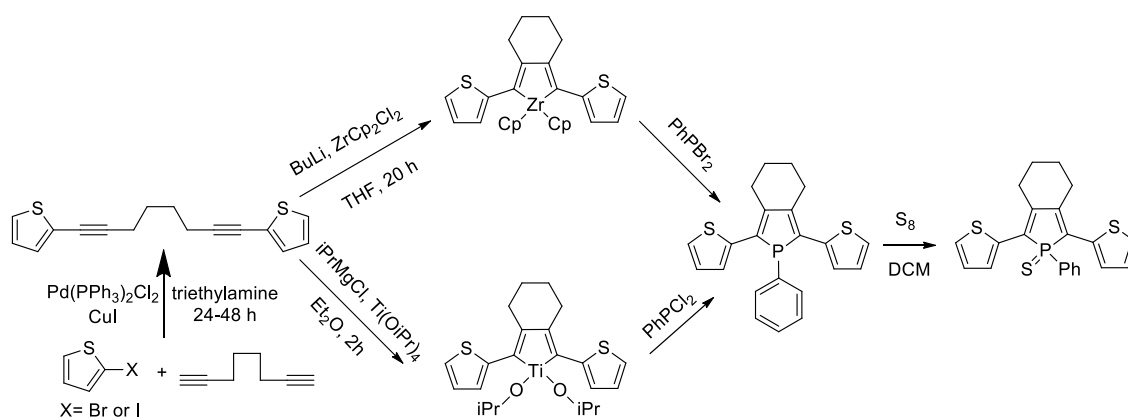
Scheme 15: Fagan-Nugent (up) and Sato (down) method of bis(thienyl)phosphole synthesis

Although the Fagan-Nugent protocol[137] is well known to give high yields of bicyclic 2,5-diarylphospholes bearing both electron-rich and electron-deficient aryl groups,[94,100] in the synthesis of bis(2-thienyl)phosphole the Sato method was found to give higher yield (60% yield) of the desired product compared to the Fagan-Nugent method (40% yield).

Functionalization of the 2,5-bis(2-thienyl)phosphole central block was accomplished by the direct borylation of terminal thiophene rings in their α-positions using iridium catalyst and protocol described in ref [141]. Functionalization of the 2,5-bis[(4-hexyl)2-thienyl]phosphole core unit was performed by the iodination of the thiophene rings at their α-positions using N-iodosuccinimide (see Scheme 16).[104]
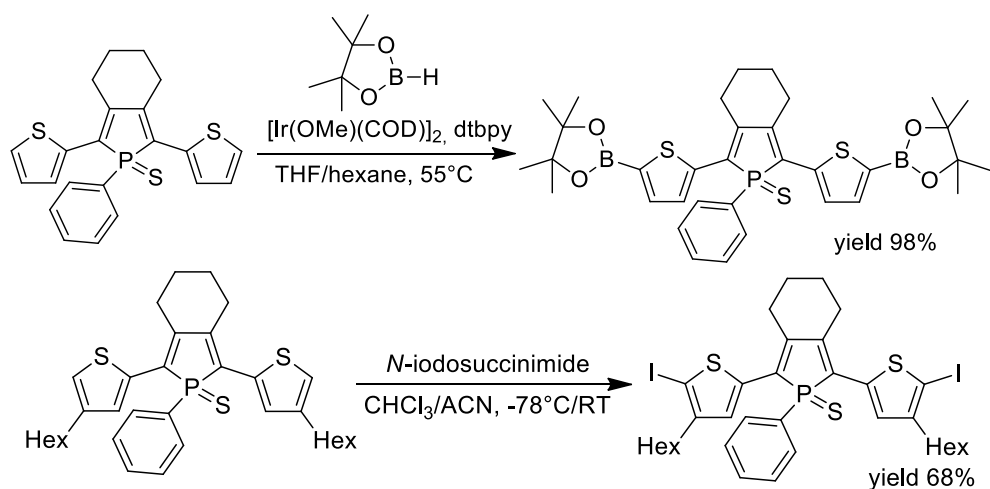
Scheme 16: Functionalization of bis(R-thienyl)phosphole

The direct borylation was realized using the C–H activation approach. Up to my best knowledge, it is the first application of this approach in the field of phosphole chemistry. This reaction step was achieved reproducibly after optimization of various factors (temperature, solvent, reactant equivalent). It should be mentioned here, that the borylated compound is not too stable and thus it should be used instantly without further purification. The direct borylation approach was also applied for 1-phenyl-2,5-bis(4-hexylthiophene-2-yl)thioxophosphole, but it was not successful, most probably owing to the steric hindrances and electronic effects of the pendant hexyl groups. Therefore, this phosphole core unit was functionalized by means of its halogenation which had to be executed at low temperature and in the dark to obtain the desired diiodo product in a reasonably high yield. Unlike the boronic derivative, the diiodo derivative of the **TPT** central block is sufficiently stable and thus can be purified by column chromatography.

As indicated above, two different cross-coupling reactions were used: (*i*) Suzuki coupling of the diboronic derivative and Br-*tpy*, and (*ii*) Sonogashira coupling of the dihalogeno derivative and E-(aryl)*tpy*. Suzuki coupling was firstly accomplished using the conditions (toluene/methanol 1/1 mixed solvent, 90 °C, PEPPSI^{TM}-IPr catalyst) that were successfully applied in the synthesis of α,ω-bis(*tpy*)oligothiophenes.[76] However, unlike that case, it gave only very low yield (around 4 %) of the desired product. Upon optimization of the solvent system: toluene/water 1/1 mixed solvent allowing higher reaction temperature and other reaction conditions: Aliquat$^®$ 336 as the interphase transfer catalyst, temperature of 130 °C, the product was obtained in the isolated yield of 15 %.

E-type unimers were synthetized by same protocol as E-*tpy* ligand, described by Grosshenny[116] (in which diisopropylamine is used as the solvent as well as the base and Pd(PPh$_3$)$_4$ as the catalyst). However, the desire unimers were obtained in quite low isolated yield (around 5 %). Therefore, this coupling reaction had to be optimized. Synthesis of unimer **E** having the simplest structure was taken as model reaction for optimization. Reaction was monitored by TLC and also by the ^{31}P NMR spectra. Firstly, we changed the solvent to toluene instead of THF and the temperature from 60 °C to 100 °C. However, the efficiency of the reaction was not significantly increased. Secondly, we tried to use a milder base: 1,8-diazabicyclo[5.4.0]undec-7-ene (DBU) and the product was not formed under these conditions.

When tuning the reaction conditions, a decomposition of Pd(PPh$_3$)$_4$ catalyst has been observed, which conducted us to use other catalysts. First, we tested

bis(dibenzylideneacetone)palladium(0) (Pd(dba)$_2$, but only one terpyridine was introduced on the central block after 24 h. The prolongation of the reaction time did not bring about any improvement. Secondly, we tested two-component catalytic system consisting of Pd(PPh$_3$)$_2$Cl$_2$ and CuI, but homocoupling of E-*tpy* units was found preferable over cross-coupling reaction. The use of the very stable PEPPSI[TM]-IPr palladium catalyst doesn't gave the desired product in an increased yield. Thus the change of the structure of the catalyst for this reaction did not improve the yield of the reaction.

During the above catalytic tests, we also observed formation of a side product: bis(*tpy*)phospholene[142], which could be potentially caused by base-catalyzed isomerization. Bis(*tpy*)phospholene species with a double bond shift into cyclohexene (originally cyclohexane) ring are characterized by bluish luminescence in difference of reddish fluorescence of bis(*tpy*)phosphole species and a significant shift of ^{31}P NMR signal (bis(thienyl)thioxophospholene: + 65 ppm/ bis(thienyl)thiooxophosphole: + 53 ppm[142]). Since phospholene analogue (in difference of phosphole) is soluble in Et$_2$O, it could be washed away and isolated. Therefore, also reactions without additional base were tested since the present terpyridine groups could by itself act as a base but neither of these attempts were successful.

Regarding the results of the above-described experiments and in order to avoid the formation of phospholene side product, we have used another synthetic approach based on Stille coupling of tin derivative of phosphole and Br-*tpy* derivative (Scheme 17).
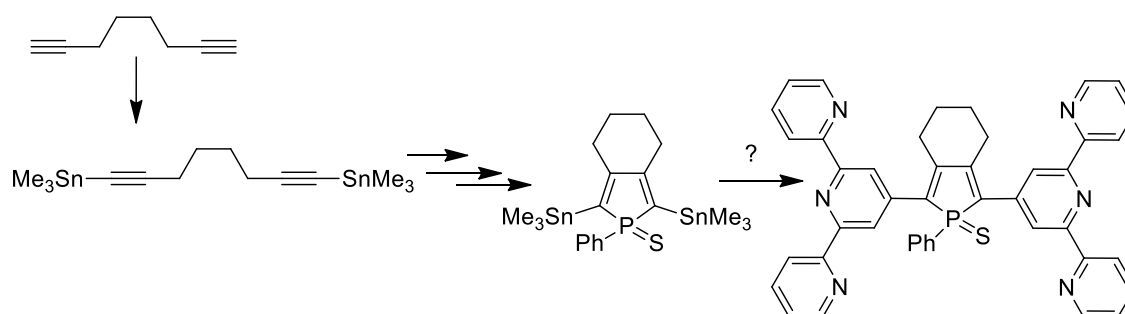
Scheme 17: Stille coupling based synthetic approach to phosphole unimer

The tested conditions are described in details in the Experimental part. Parallel project has been performed in the group in Rennes, including successfully promoted Stille coupling of structurally similar compound. The conditions used in this project:

Pd(PPh₃)₄ and CuI as catalysts and toluene as solvent, were chosen to be tested first. In addition to the TLC method, the reaction was monitored by ^{31}P NMR spectroscopy of crude reaction mixture since a chemical shift around +68 ppm is characteristic of the tin derivative and the shift around +52 ppm typical of the resulting unimer with P=S group. Unfortunately, any applied experimental conditions (described in Experimental part, Table 11) ended up with desired product. Since no Stille coupling were found suitable for the synthesis of phosphole based unimers, the previously mentioned approaches based on Suzuki and Sonogashira couplings were used for preparing the desired unimers though the isolated yields of the desired products were rather low (see Experimental part).

3.2.2 Characterization

All unimers were characterized by UV/vis, luminescence, NMR spectroscopies and cyclic voltammetry. UV/vis and fluorescence characteristics of unimers are summarized in Table 5.

Table 5: Spectral properties of synthesized unimers in solutions ($c = 0.02$ mmol/L; chloroform/acetonitrile mixed solvent) and thin films (glass support)

	Absorption		Fluorescence				Stokes shift	
	λ_{max}, nm		λ_{max}, nm		Φ, %		$\overline{\nu}_s$, cm^{-1}	
	Solution	Film	Solution	Film	Solution	Film	Solution	Film
TPT	482	521	603	685	19	0.7	4210	4600
E	497	511	623	705	8.7	0.2	4070	5390
EPh	500	526	635	669	14.4	0.3	4250	4060
ET	506	545	641	730	21.7	0.3	4160	4650
ET6	505	538	642	700	8.2	0.5	4230	4300

Solution absorption spectra of all unimers show two major bands: the band located at around 280 nm that is mainly contributed with n-π* and π-π* transitions in *tpy* end-groups,[90,120] and the band located at above 400 nm that is associated with the transitions from HOMO to LUMO that both are spread over the unimer central block and adjacent central rings of *tpy* end-groups[77,81,89,90,113,120] (Figure 15). It worth mentioning that second band is unusually broad and structureless, which might indicate a charge transfer (CT) within the unimer molecule. The unimers molecules namely contain electron-

withdrawing thio-oxophosphole and terpyridine group linked to an electron-donating (thiophene) group, which may promote CT along the unimer axis.
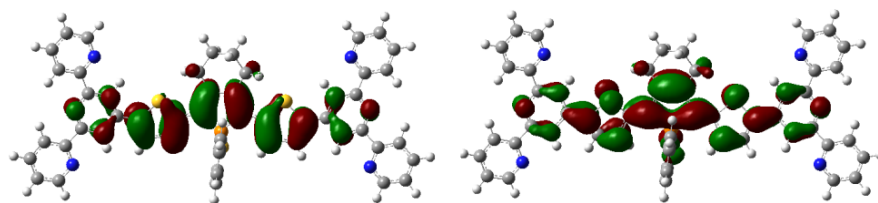
Figure 15: Electron density contours for HOMO (left) and LUMO (right) of **TPT** obtained by the DFT calculations, namely the Becke's three parameter functional with the non-local Lee-Yang-Parr correlation functional (B3LYP) with the standard 6-31G(d) basis set as implemented in Gaussian 09.[143]

Positions of the absorption maxima reflect effectiveness of the delocalization of electrons along unimer molecules (Figure 16). Obviously, **TPT** comprising only three heterocycles in the central block shows the lowest electron delocalization. The insertion of two triple bonds into the structure gives unimer **E**, that, as compared to the **TPT**, shows the absorption maximum red-shifted about 13 nm (from 482 to 495 nm), which proves a slight increase in the delocalization of electrons. The ethynediyl linkers are known to reduce the steric effects imposed by interactions of near-neighboring rings.[144] Accordingly, removal of the steric hindrances between *tpy* groups and thiophene rings by inserted ethynediyl linker should be regarded as the main reason for the observed small red shift of the absorption band associated with HOMO to LUMO transitions and its slight enhancement.

Unimers with prolonged linkers (**EPh**, **ET** and **ET6**) show an additional slight red shift and enhancement of the absorption band. In these molecules *(i)* the backbone is extended about four double bonds in conjugation, *(ii)* the steric interactions between the linker and central sequence of heterocycles are the same as in molecules **E**, and *(iii)* the interactions between the linker and *tpy* end-groups comparable to those existing in molecules of **TPT**. There is no doubt that the extension of the conjugated backbone is mainly responsible for the observed small red shifts and enhancement of the absorption bands. The smallest red shift is observed for unimer **EPh** with linkers containing highly aromatic benzene ring, which well corresponds with well-known fact that the rings with a high aromaticity exhibit reduced capability of sharing the intracyclic π-electrons with neighboring conjugated units. In accord with the latter rule, the unimers **ET** and **ET6**

with linkers comprising less aromatic thiophene rings exhibit a higher red shift of the HOMO/LUMO band than unimer **EPh**. The λ_{max} values of **ET** and **ET6** are practically equal, the difference between them being mainly seen in the lowered intensity of the bands of **ET6**. This observation can be qualitatively explained as a result of interplay of two opposing effects of hexyl pendants in **ET6**: *(i)* donation of electrons into thiophene ring, and *(ii)* slight chain distortion caused by the hexyl groups.
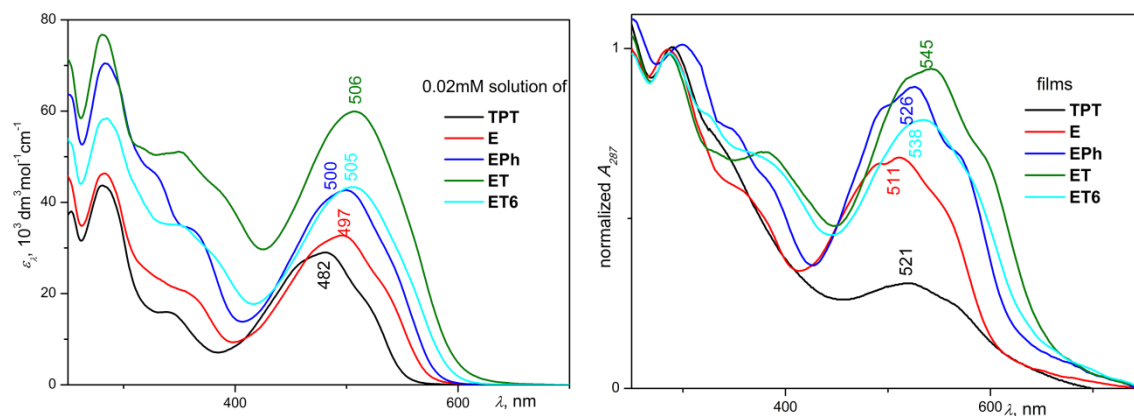
Figure 16: Absorption spectra of all prepared unimers in solution and thin films

Absorption spectra of thin films of unimers show the absorption bands red shifted about 10 to 40 nm compared to their positions in the solution spectra (Figure 16). At least two factors: planarization and intermolecular packing interactions are responsible for the spectral changes when going from solution to the solid state. It is known, that molecules comprising *P*-substituted phosphole chromophores mostly behave as isolated molecule even in the solid state owing to the geometry and surrounding of phosphorus atom, which preclude close cofacial organization (packing) of P chromophores in the solid state.[96] Hence the observed shift of optical spectral bands should be mainly ascribed to small differences in the molecular geometry between molecules in solution and bulk films, respectively. The highest shift in absorption maxima when going from a solution into thin film is shown by unimers **ET** and **TPT** (shift about 39 nm), somewhat lower by unimers **ET6** (33 nm, owing to the effect of hexyl pendants) and **EPh** (26 nm, owing to higher distorsion between benzene and central *tpy*-pyridine rings) and the lowest by the unimer **E** (only 14 nm) for which mainly restriction of the free rotation around single bonds should take place in the solid state (Table 5, Figure 16).

Fluorescence spectra show broad emission bands with maxima at 600 to 645 nm in solutions and 665 to 735 nm in thin films (Figure 17). For the solution spectra, the

position of the fluorescence maximum steadily increases along the same sample sequence as in the case of the absorption spectra: **TPT < E < EPh < ET ~ ET6** and moreover, their positions are uniquely high for non-assembled bis(*tpy)* unimers. The solution fluorescence spectra of unimers also show almost the same values of the Stokes shift, in average $4\,160 \pm 90$ cm^{-1} (Table 5). This suggests similar changes in the geometry of excited states during their conformational relaxation regardless the unimer structure, which might indicate that the most important is the conformational change of the molecules in central block. The fluorescence quantum yields vary from 8 to 22 % without any correlation with the unimer structure.
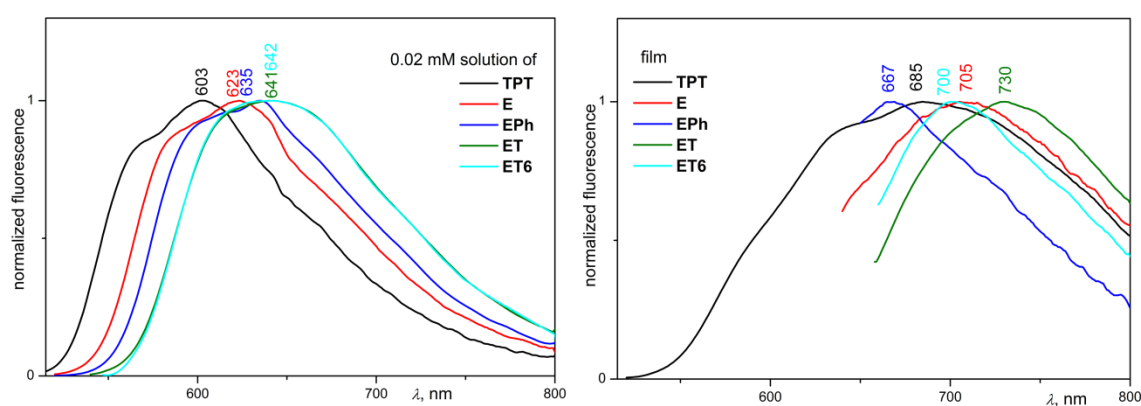
Figure 17: Fluorescence spectra of all prepared unimers in solution and thin films.

The fluorescence spectra of unimer in thin films are red-shifted to those obtained in solution by about ca 85 nm for **TPT**, **E** and **ET**, somewhat less, about ca 60 nm, for **ET6** (the influence of hexyl pendents) and only about 35 nm for **EPh**, which should be ascribed to the aromaticity of the 1,4-phenylene linkers. The Stokes shift values observed for solid unimers varied in the rather large range from ca 4 050 to 5 400 cm^{-1}, the largest being found for unimer **E** while the lowest one for unimer **EPh**, as can be expected. The largest Stokes shift found for **E** molecules proves fast conformational relaxation to lower-energy structures with more coplanar rings also implying lowered rigidity[144] of molecule **E**. Quantum yields of solid unimer thin films are below 1 %, which means that the excitation energy is preferably dissipated by non-radiative transitions.

3.3 Metallo-supramolecular polymers

Metallo-supramolecular polymers were prepared by mixing the solutions of a metal salt and a unimer in the metal ions to unimer mole ratio M/U = 1. Thin films of related MSPs were prepared by casting the MSP solution on a quartz glass support and subsequent evaporation of the solvent. Spectral properties of MSPs in solution were taken from assembly experiments for equimolar systems. Abbreviations of MSPs have general format P(U/M), where P denotes a polymer composed of a given unimer **U** (**U** is **TPT**, or **E**, or **EPh**, or **ET**, or **ET6**) and M stands for a given metal ion (2+).

3.3.1 Absorption spectra

Zn²⁺ metallo-supramolecular polymers

Positions of the UV/vis absorption bands of Zn-MSPs are summarized in Table 6. Compared to the absorption spectra of free unimers, the absorption spectra of Zn-MSPs (Figure 18) show sharpening and slight red-shift of the band attributed to transitions within terpyridine group, broadening of the band attributed to HOMO/LUMO transitions within unimer backbone, and formation of a new bimodal band located at around 330 nm. This band can be attributed to transitions attributed to coordinated terpyridine units in *syn* conformation of nitrogen atoms, since the band at similar position has been reported for the protonized terpyridine[121] and monoterpyridine ligands.[120] Bimodal character of the band has probably a vibrational origin.

Table 6: Spectroscopic characteristics of Zn-MSPs; λ_{max} – apex of spectral maximum, Φ fluorescence quantum yield

	Absorption		Fluorescence				Stokes shift	
	λ_{max}, nm		λ_{max}, nm		Φ, %		$\overline{v_s}$, cm^{-1}	
	Solution	Film	Solution	Film	Solution	Film	Solution	Film
P(**TPT**/Zn)	507	509	634	641	-	0.5	3950	4050
P(**E**/Zn)	518	533	642	702	-	6.75	3730	4520
P(**EPh**/Zn)	506	515	649	673	-	3.8	4350	4560
P(**ET**/Zn)	515	527	680	723	-	2.6	4710	5140
P(**ET6**/Zn)	508	528	674	692	-	4.58	4850	4490

Positions of absorption maxima of Zn-MSPs solutions are located between 506 and 518 nm and they are red-shifted by maximally 26 nm in comparison of free unimers.

Larger shifts of absorption maximum are observed for P(**TPT**/Zn) and P(**E**/Zn), polymers derived from unimers comprising shorter central blocks. For P(**EPh**/Zn), P(**ET**/Zn) and P(**ET6**/Zn), the difference between the absorption maxima of the polymer and free unimer is almost negligible. This observation indicates that the extent of the electronic delocalization within Zn-MSP chains approaches its limiting value. It should be emphasized that unimer **E** comprises 14 conjugated multiple bonds (taking into account adjacent terpyridine rings), which was previously found as the limiting value for the extent of delocalization.[144,145]

The positions of absorption maxima of the solution and solid state UV/vis spectra are close to each other for all studied MSPs (Figure 18). This indicates almost absence of organized stacking of polymer molecules in casted films. Positions of absorption maxima of Zn-MSPs in thin films are located between 509 and 533 nm. Absorption maximum of the P(**E**/Zn) film is slightly red-shifted while the absorption maxima of films of other prepared Zn-MSPs are slightly blue-shifted compared to the maxima of films of corresponding unimers which indicates disordered packing of the MSP chains in films.
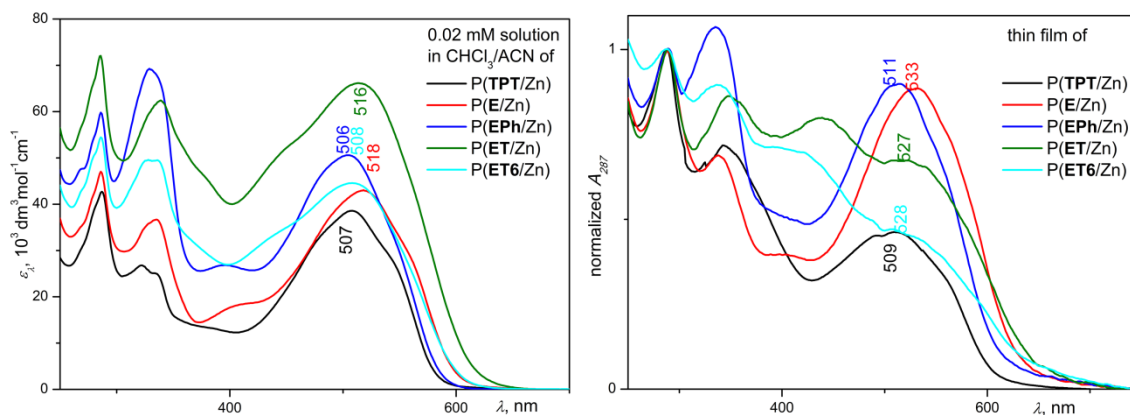
Figure 18: Absorption spectra of Zn-MSPs in solution and thin films

Fe²⁺ metallo-supramolecular polymers

Absorption characteristics of prepared Fe-MSPs are summarized in Table 7. Absorption spectra of Fe-MSPs exhibit four to five bands (Figure 19). The band at around 285 nm belongs mainly to n-π* and π-π* transitions within *tpy* groups. The band located at around 325 nm is related to the conformationally changed *tpy* groups in *syn*-conformation of nitrogen atoms bound to metal ions. For Fe-MSPs, this band is more significant compared to Zn-MSPs. The band at around 360 nm is clearly observed only

for P(**ET**/Fe), P(**ET6**/Fe) and P(**TPT**/Fe), which indicates that it is contributed with transitions involving the thiophene rings connected to *tpy* groups. It should be stressed out, that this band is not observed for analogues Zn-MSPs, which indicates that it might be related to the metal to ligand charge transfer (MLCT) transitions as well. The band at around 500 nm involves HOMO/LUMO transitions in polymer backbone same as in the case of Zn-MSPs. The most intense band occurring above 580 nm belongs to the MLCT band that is typical of all $[Fe(tpy)_2]^{2+}$ complexes in majority of solvents. This band is responsible for a purple-blue color of these complexes. The spectra of Zn-MSPs cannot exhibit similar band, as Zn^{2+} comprises closed d^{10} electron shell.

Table 7: Spectral characteristics of Fe-MSPs, λ_{max}- absorption maxima

	Absorption			
	λ_{max}, nm			
	solution	(MLCT)	film	(MLCT)
P(**TPT**/Fe)	491	625	499	626
P(**E**/Fe)	508	609	511	616
P(**EPh**/Fe)	509	580	518	590
P(**ET**/Fe)	518	601	538	615
P(**ET6**/Fe)	518	585	540	592

The position of the MLCT band varies from 580 nm to 625 nm depending on the constitution of the central blocks of unimeric units. This means that this band should contributed not only with MLCT transitions within bound *tpy* end groups but also with transitions involving the central block part as already mentioned above (band at ca 360 nm). This observation has been proved through the resonance Raman spectra of Fe-MSPs taken with different excitation wavelengths, see attached publication **B** (ref.[146])

The apex of MLCT band is located at the longest wavelength for P(**TPT**/Fe) thus polymer comprising the shortest distance between metal centers. Subsequent aggregation of Fe^{2+} centers is proposed to causes a shift of the MLCT band to longer wavelengths due to dipolar coupling between metal centers.[86,147] An increased distance

between Fe^{2+} ions should weaken dipolar coupling between metal centers. Weak electronic interactions between *tpy* subunits within molecule, were already reported by Barbieri for Ru-MSPs derived from α,ω-bis(*tpy*)oligomers of diethynyl-thiophenes, particularly for large molecules.[148] However, the extent of delocalization of electrons is also important for the MLCT position as can be deduced from differences between P(**ET**/Fe), P(**ET6**/Fe) and P(**EPh**/Fe) (see Table 7) and also triple bond can act as separator of electronic communication.[127]
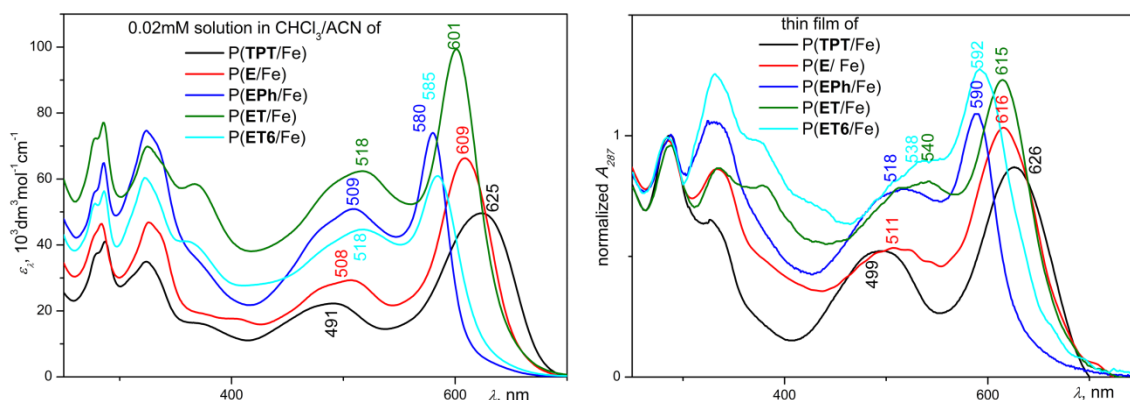
Figure 19: Absorption spectra of prepared Fe-MSPs

Spectra of Fe-MSPs taken from solid films are closely similar to the spectra taken from solutions. This indicates a low extent of planarization of Fe-MSPs molecules in films. Only spectra of P(**ET**/Fe) and P(**ET6**/Fe) show an increased red shift of the HOMO/LUMO band (Table 7, Figure 19) indicating somewhat increased planarization of molecules of these MSPs.

Co^{2+}, Cu^{2+} and Ni^{2+} metallo-supramolecular polymers derived from TPT

The assembly of **TPT** was performed also with other metals than Zn^{2+} and Fe^{2+}, thus other MSPs have been prepared and characterized. Co^{2+}, Cu^{2+} and Ni^{2+} as representatives of d^7-d^9 metals were chosen to be used. Spectral characteristics of these MSPs are shown in Table 8.

Table 8: spectral characteristics for P(**TPT**/Co), P(**TPT**/Cu) and P(**TPT**/Ni)

	Absorption maximum λ_{max}, nm		Shift from free **TPT**, nm	
	Solution	Film	Solution	Film
P(**TPT**/Co)	529	554	48	33
P(**TPT**/Cu)	514	531	33	10
P(**TPT**/Ni)	509	526	28	5

The UV/vis solution absorption spectra of P(**TPT**/Co), P(**TPT**/Cu) and P(**TPT**/Ni) (Figure 20) did not show dramatic differences from the recorded spectrum of P(**TPT**/Zn). The band attributed to complexed terpyridine is bimodal for P(**TPT**/Cu) and P(**TPT**/Ni) and unimodal for P(**TPT**/Co) (same as for P(**TPT**/Fe)). The P(**TPT**/Co) showed slightly broader band ascribed to transitions within central block of unimer. This broadening can be due to contribution of transitions originated from the d-d interaction of cobalt centers as it was suggested before[86] and can be also regarded as the reason for the observed larger red shift of this absorption band with respect to the band of free **TPT**. The solid-state UV/vis spectra of Co-, Cu- and Ni-MSPs showed similar features as their solution spectra. Compared to the solid-state spectrum of Zn-MSP, they show significantly higher red shift of the HOMO/LUMO band, which suggests more planar conformations.
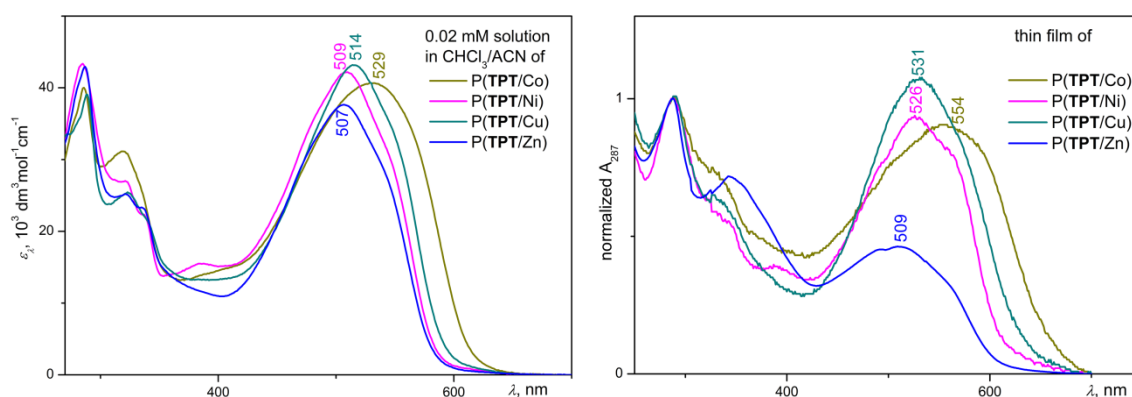
Figure 20: Absorption spectra of P(**TPT**/Co), P(**TPT**/Cu) and P(**TPT**/Ni) with P(**TPT**/Zn) as reference in solution and thin films

3.3.2 Fluorescence spectra

Besides Zn-MSPs, all other prepared MSPs were detected to be non-emissive. The reason for it should be seen in the fact that they contain ion-couplers metals with the

open-shell electron configuration, which typically lead to very strong metal-to-ligand orbital interaction resulting in quenching of electronically excited states.[43]

The fluorescence spectra of prepared Zn-MSPs are shown in Figure 21 and their spectral characteristics are summarized in Table 6. All spectra show single broad emission band covering red and infrared region, with maximum located at 634 nm for P(**TPT**/Zn**)**, 642 nm for P(**E**/Zn), 649 nm for P(**EPh**/Zn), 674 nm for P(**ET6**/Zn) and 680 nm for P(**ET**/Zn) (Figure 21). The wavelength of the fluorescence maximum is increasing with prolongation of effective conjugation length. Solution emission maxima of Zn-MSPs are red-shifted compared to those recorded for unimers by 35 ± 4 nm for **TPT**, **ET** and **ET6** and 17 ± 3 nm for **E** and **EPh**. Hence the highest difference of fluorescence maxima of the free unimers and related Zn-MSPs are observable for systems with *tpy* groups attached to thiophene ring. This is in agreement with observations obtained in the complexation of monoterpyridine ligands.[120] The red-shift caused by coordination to Zn^{2+} ions is in agreement with literature as Zn^{2+} ions lower and stabilize the LUMO, which induces the intramolecular charge transfer in non-charge transfer compounds that causes the red-shift and significant decrease of the fluorescence.[113,126,149]

The solid state fluorescence spectral bands of Zn-MSPs are red-shifted compared to the bands of the solution spectra. Emission bands of solid Zn-MSPs are blue shifted compared to the bands of solid unimers, except for the case of **EPh** and P(**EPh**/Zn). This indicates more planar geometry of unimers compared to that of unimeric units in Zn-MSPs in thin films. This might be caused by fixed octahedral geometry of *tpy* units in Zn(*tpy*)$_2$ linkages within MSPs chains that should hinder planarization of the chains. The fluorescence quantum yields of Zn-MSPs in thin films are higher than the quantum yields of related unimers in films.
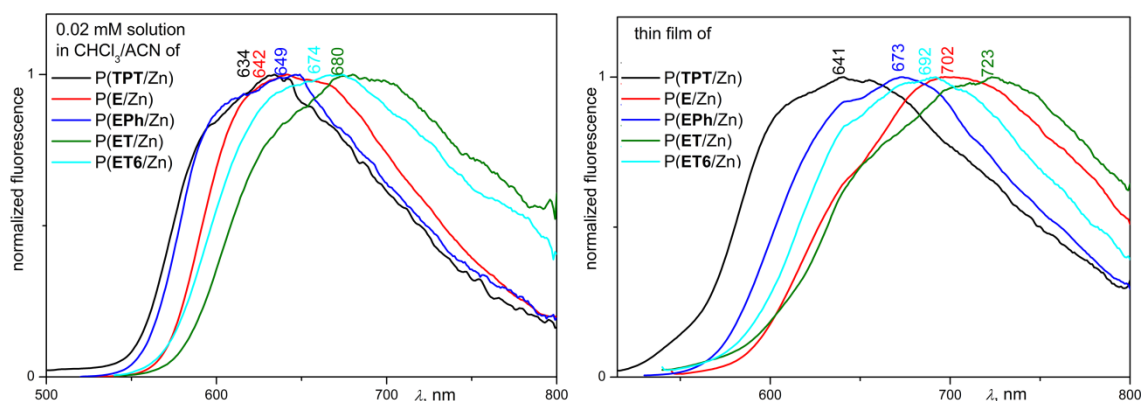
Figure 21: Fluorescence spectra of Zn-MSPs in solution and thin films

3.4 Comparison with bis(*tpy*)oligothiophenes and related MSPs

As mentioned above (Section 1.4.1) the replacement of thiophene unit in oligothiophenes or polythiophenes by phosphole ring leads decreased band-gap energy. Unimers comprising oligothiophenes capped by *tpy* group[75,76] were already reported, thus we can easily compare spectroscopic properties of unimer comprising just thiophenes and unimer comprising phosphole. MSPs from these unimers were also prepared; the effect of incorporation of phosphole could be examined even in MSP chain. Structurally similar bis(*tpy*)terthiophene (**T**) and bis(*tpy*)quaterthiophene (**Q**) (Figure 22) and related MSPs synthetized by Pavla Štenclová[145] were chosen to be compared with unimer **TPT** and related MSPs. Spectroscopic characterization of compared unimers and related MSPs are summarized in Table 9.
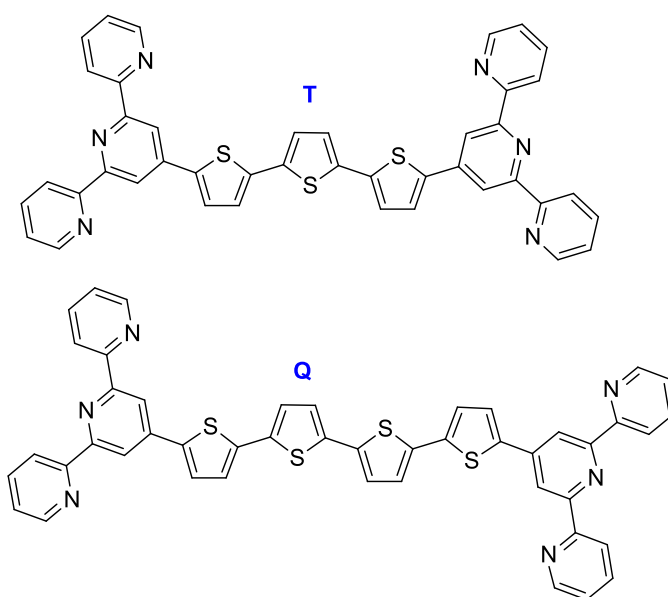
Figure 22: Structure of unimers **T** and **Q**

Table 9: Absorption maxima and fluorescence characteristics of unimer **TPT** in comparison with structurally similar thiophene comprising unimers

	Absorption		Fluorescence		Stokes shift	
	λ_{max}, nm		λ_{max}, nm		$\overline{v}_s$, cm^{-1}	
	Solution [a]	Film [b]	Solution [a]	Film [b]	Solution	Film
TPT	482	521	603	685	4210	4600
T[76]	420	425	484, 516	730	3150	9780
Q[75]	441	435	514, 546	645	4350	7450
P(**TPT**/Zn)	507	509	634	641	3950	4100
P(**T**/Zn)[76]	479	470	635	686	5130	6750
P(**Q**/Zn)[75]	486	500	656	~690	5350	5050
P(**TPT**/Fe)	491 625[c]	499 626[c]	-	-	-	-
P(**Q**/Fe)[75]	471 603[c]	475 621[c]	-	-	-	-

a) solution characteristics were measured in mixed solvent chloroform/acetonitrile (1/1 by volume), for **TPT** and **Q** and related MSPs, and in THF for **T** and related MSPs; b) glass support; c) values of apex of MLCT band

The UV/vis band of unimer **TPT** is substantially red shifted compared to the corresponding band of unimer **T** (by 62 nm) and also unimer **Q** (by 41 nm), even if central block of the latter unimer involves longer conjugated central sequence of heterocycles. Moreover the absorption maximum of central block of unimer **TPT** (432 nm[96]) is located at higher wavelength region itself in comparison with unimer **T**, thus clearly declaring substantial decrease in the band gap energy caused by replacing the middle high aromatic thiophene ring in the unimer central block with a low aromatic phosphole ring. Comparoing the thin film spectra of the unimers, **TPT** shows the main UV/vis band (λ_{max} = 521 nm) considerably red shifted compared to the bands of **T** (λ_{max} = 425 nm) and **Q** (λ_{max} = 435 nm). This confirms decrease in the band-gap energy even in the thin films. This is quite interesting considering that intermolecular packing in phosphole species is precluded.

The observed red-shift in UV/vis might but need not directly relate to increased delocalization of electrons. The results of DFT calculation (see Figure 15, p. 48) namely show that the HOMO of **TPT** is delocalized rather equally over all three central rings, while the LUMO is localized primarily on the phosphole ring with more minor

contributions from thiophene rings. This indicates that the observed spectral red shift is very likely contributed by charge-transfer interactions within **TPT** molecules.

Solution fluorescence spectra of **TPT** showed a broad band red-shifted with respect to the well distinguished bimodal band of fluorescence spectra of **T** (by 87 nm) and **Q** (by 57 nm). Remarkably the maximum of the thin film fluorescence of unimer **T** is located exceptionally high (λ_{max} = 730 nm, Stokes shift approaches 10^4 cm^{-1}), thus in longer wavelength than for unimer **TPT**. Such large Stokes shift proves extensive conformational relaxation of excited **T** molecules, which could be due to their regular packing in aggregates allowing so high relaxation, as it was already reported for oligothiophenes.[150] Large Stokes shifts accompanied with low fluorescence quantum yields are typical of H-aggregates.[151] To examine this hypothesis more in detail the fluorescence spectra of **T** and **TPT** were recorded on samples of unimers dispersed at various concentrations in KBr pellets as matrix (Figure 23).
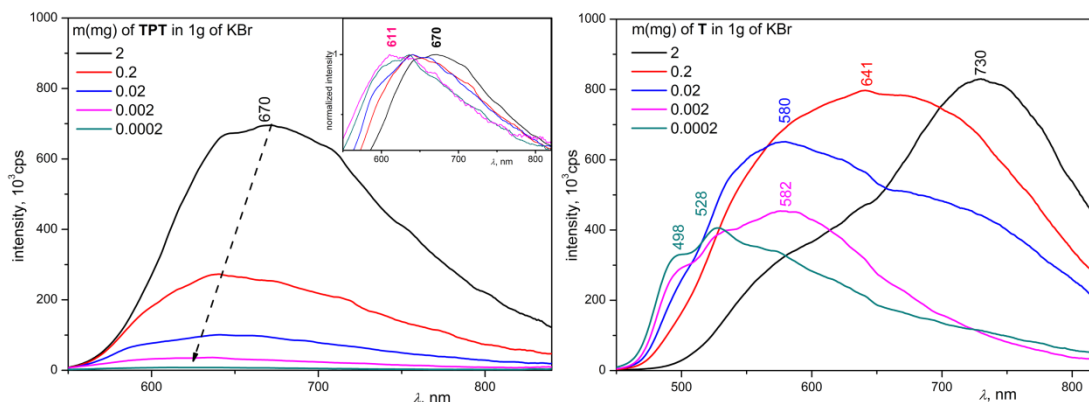
Figure 23: The solid-state fluorescence spectra of various concentrations of unimers **T** and **TPT** in KBr pellets; inset contains normalized spectra

The unimer **T** showed a gradual blue-shift of the fluorescence band (up to –232 nm) and a relatively low decrease in the intensity with decreasing concentration of **T** in the KBr matrix. On the contrary, fluorescence spectra of unimer **TPT** showed a small blue-shift (up to 60 nm) and rather high intensity decrease upon dilution. These observations are consistent with the hypothesis of regular packing of **T** molecules and poor packing of **TPT** molecules in solid films. For the unimer **TPT** the pyramidal geometry of the phosphorus atom precludes a regular cofacial molular packing in the solid state.[96]

Comparison of related Zn-MSPs and Fe-MSPs showed similar features as in the case of free unimers. Absorption maxima of P(**TPT**/Zn) and P(**TPT**/Fe) are red-shifted compared to the maxima of P(**T**/Zn), P(**Q**/Zn) and P(**Q**/Fe). The exceptionally high

position of MLCT band of P(**TPT**/Fe) need to be highlighted, as the apex of MLCT band of P(**Q**/Fe) is located at about 20 nm lower position for solution and at about 5 nm lower position for thin film. This clearly indicates enhanced electron delocalization within coordinated **TPT** units compared to **Q** units though the latter one comprises more heterocycle units in the backbone.

Regarding fluorescence spectra of P(**TPT**/Zn), P(**T**/Zn), and P(**Q**/Zn), they are all located in comparable region in solution as well as in thin films. Thus suggesting that Zn/*tpy* complex is the key part of polymer chain, mainly responsible for radiative transitions from excited state towards ground state.

3.5 Assembling of unimers to metallo-supramolecular polymers

Assembly of MSPs from prepared unimers (**U**) and metal ions (M^{2+}) was monitored by the UV/vis and fluorescence spectroscopies and size exclusion chromatography (SEC). A set of solutions of the constant unimer concentration (0.02mM for spectroscopic measurements and 0.5mM for SEC) and the ion-to-unimer mole ratio $r = M^{2+}/U$ increasing from 0 to 3, was prepared for each M^{2+}/U couple and the solutions were allowed to equilibrate for one day before monitoring their spectra. Perchlorate salts were used as source of metal ions. All experiments were performed in chloroform/acetonitrile (1/1) mixed solvent.

3.5.1 Absorption spectra

Assembling with Zn^{2+} ions can be formally divided into three stages depending on the Zn^{2+}/unimer ratio (Figure 24). First stage is characterized mainly by appearance of isosbestic point, which indicates direct conversion into another defined species which, according to the ratio of M/**U** up to 0.5–0.6, are attributed to be dimers. Other changes accompanying absorption spectra during the first stage of assembly of Zn^{2+} and unimers are in general as follows:

(*i*) The band at around 282 nm attributed to transitions within *tpy* group is narrowed, slightly decreased in intensity and red-shifted

(*ii*) New band at around 330 nm is occurred and the intensity of this band is enhanced with increasing ratio Zn^{2+}/U. Appearance of this band is contributed to changed conformation of nitrogen atoms in *tpy* end groups.

(*iii*) Red-shift and enhancement of the absorption band involving transitions centered on the central block (originally with maxima at 481–506 nm). This feature is divergent from oligothiophene unimers where the original bands of free unimer gradually

decreased while new band occurred at longer wavelengths during assembly into MSPs.[75,76] The absorption bands of all prepared phosphole unimers and related dimers are obviously not differentiated because of very close positions of their maxima. Incorporation of phosphole lead to major increase of conjugation length in free unimers, and thus the changes in conjugation length after complexation into longer chains are not dramatically enhanced.

Second stage of assembling occurs for the ratio Zn^{2+}/U between 0.5 and 1 (or 1.25 respectively). This stage is characterized by the continued red shift and intensity increase of main absorption band, but without occurrence of a clear isosbestic point. These features are typical of the prolongation of MSP chains.[75,77,90,32,152] Other differences are as follows:

(*i*) The band at around 300 nm is becoming bimodal for systems of unimers **TPT** and **ET6**. The splitting is probably due to the vibrational origin as it was also observed for Thio-*tpy* ligand.[120]

(*ii*) Formation of new band is exceptionally observed for systems with **ET** and **ET6** accompanied by decrease of intensity of main transition band. In fact as the main transition band is very complex according to origin of involved transitions, the formation of this band could be attributed to redistribution of energy involved by different transitions.

(*iii*) Third stage of assembly is characterized by only minor changes in the absorption spectra in both band maxima and band intensity. The over stoichiometric amount of metal ions present in this stage could result in end-capping of polymer chain and fractionating the polymer chain to shorter species. In the case of **ET** and **ET6**, the band at around 440 nm is attenuated, thus another redistribution of energy occurs, implementing that the latter band is significant for longer polymer chain. The ability to form species where one Zn^{2+} ion is linked to one *tpy* group was observed before for monoterpyridine ligands[114,120] as well as bis(terpyridines).[153]

Figure 24: The UV/vis spectral changes accompanying three stages of assembling various unimers with Zn²⁺, third stage in the insets

Assembling with Fe^{2+} can be also followed within three stages (Figure 25). During the *first stage* the similarities with assembly of Zn^{2+} can be observed, the band attributed to transitions within *tpy* group is also sharpened, red-shifted and decreased in intensity. Formation of new band attributed to *syn* conformation of nitrogen atoms in terpyridine is observed around 330 nm; in case of **ET** and **ET6** this band is split. It is interesting that in the case of monoterpyridine ligand, the intensity of splitting of latter band is reverse thus more intense for complexation with Zn^{2+} than Fe^{2+}.[120] Appearance of new band above 570 nm attributed to MLCT was observed, the position of MCLT maximum remains stable during first stage of assembly for all unimers. Intensity of HOMO/LUMO transition band is weakened for systems of unimers **E** and **TPT**, thus the unimers comprising clearly separated HOMO/LUMO and MLCT band in their absorption spectra. In the case of assembling of unimers **EPh**, **ET** and **ET6** the latter band is located very close to MLCT band, thus instead of weakening it is enhanced. The HOMO/LUMO transition band is red-shifted nevertheless the intensity changes.

During *the second stage of assembly* the band located at around 325 nm is noticeably enhanced in comparison with Zn^{2+} assembly. The band contributed to transitions within *tpy* group remains almost same, while the main transition band generally followed the trend established during first phase of assembly. The position of MLCT band remained stable except of unimer **TPT**. In this case the position of MLCT band is further red-shifted with cumulating Fe^{2+} ions in polymer chain and it reached the maximum intensity in Fe^{2+}/**U** equaled 1. The red-shift is caused by dipolar coupling of metal centers as discussed above. Hence the distance between Fe^{2+} centers in this unimer is close to limit of effective dipolar coupling. Intensity decay of main transition band as well as MLCT band during *the third stage of assembly* can be attributed to shortening of polymer chain and end-capping of unimers as reported before.[75,77]
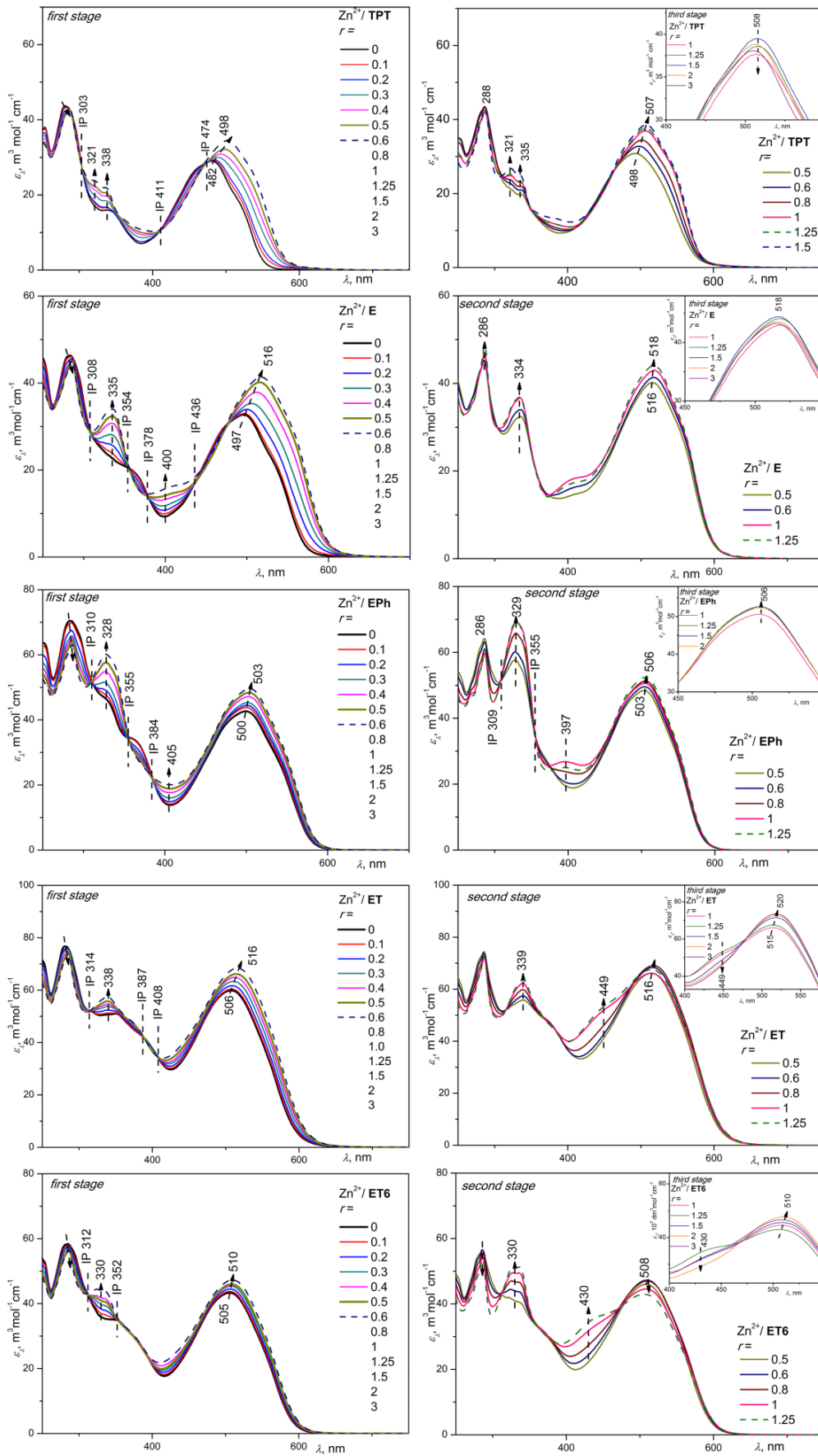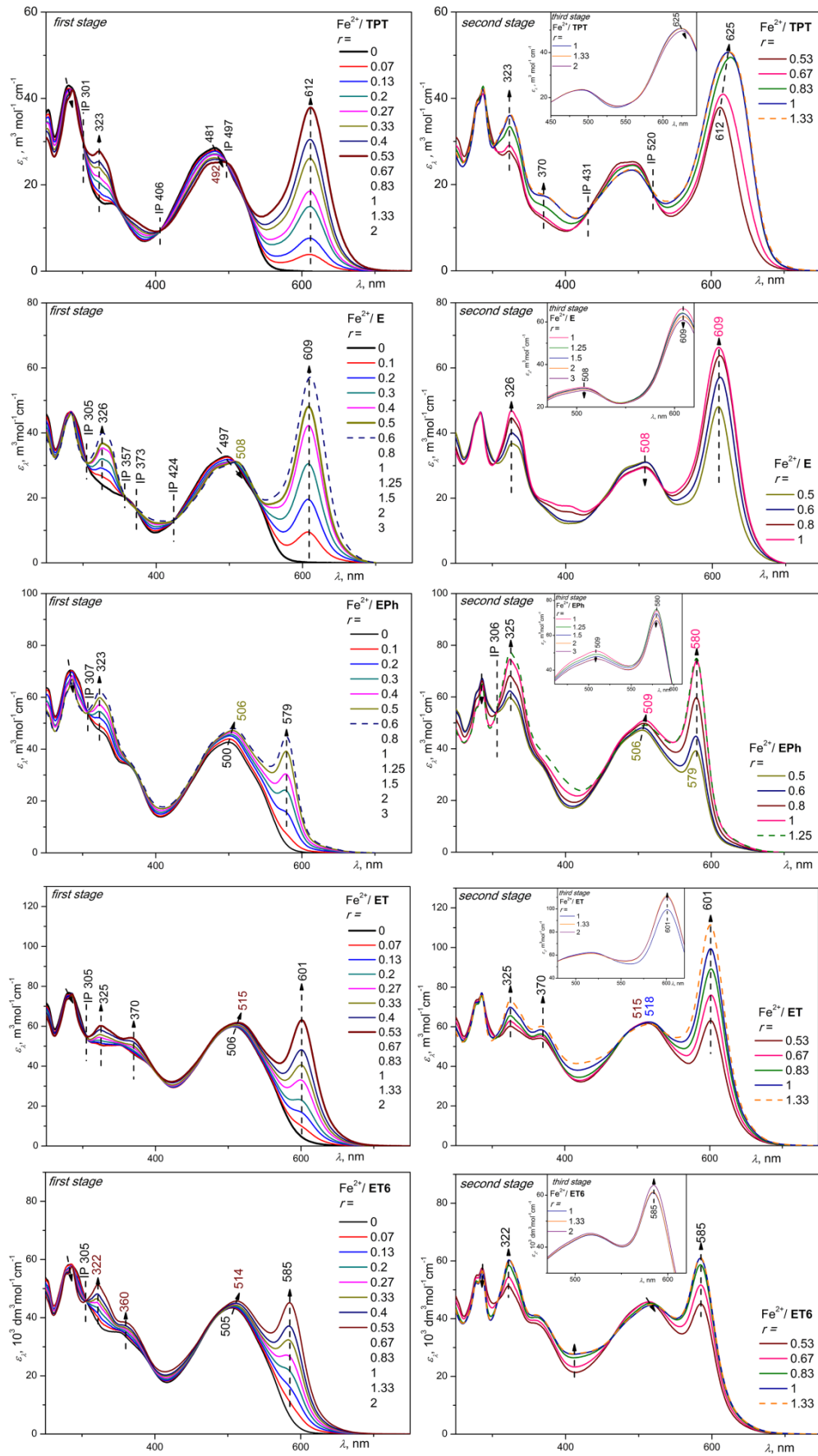
Figure 25: The UV/vis spectral changes accompanying three stages of assembling various unimers with Fe^{2+}, third stage in the insets

66

Major difference in *assembling* of **TPT** *with Co²⁺, Cu²⁺* and *Ni²⁺* occurs in the case of Cu^{2+}, where this is the only metal with clearly differentiate second and third stage of assembly in absorption spectra (Figure 26). In surplus of Cu^{2+} ions the band at 287 nm is extremely enhanced and also slightly red-shifted up to 290 nm. Difference in absorption spectra of Cu(*tpy*)²⁺ and Cu(*tpy*)₂²⁺ complexes was already reported.[154] Another interesting feature was observed for the third stage of assembly, where hypsochromic shift and enhanced of intensity of HOMO/LUMO transition band was observed for excess of Co^{2+} ions. During assembly with Co^{2+} major shift of HOMO/LUMO transition band was observed, suggesting involvement of d-d transitions of cobalt centers.[86]
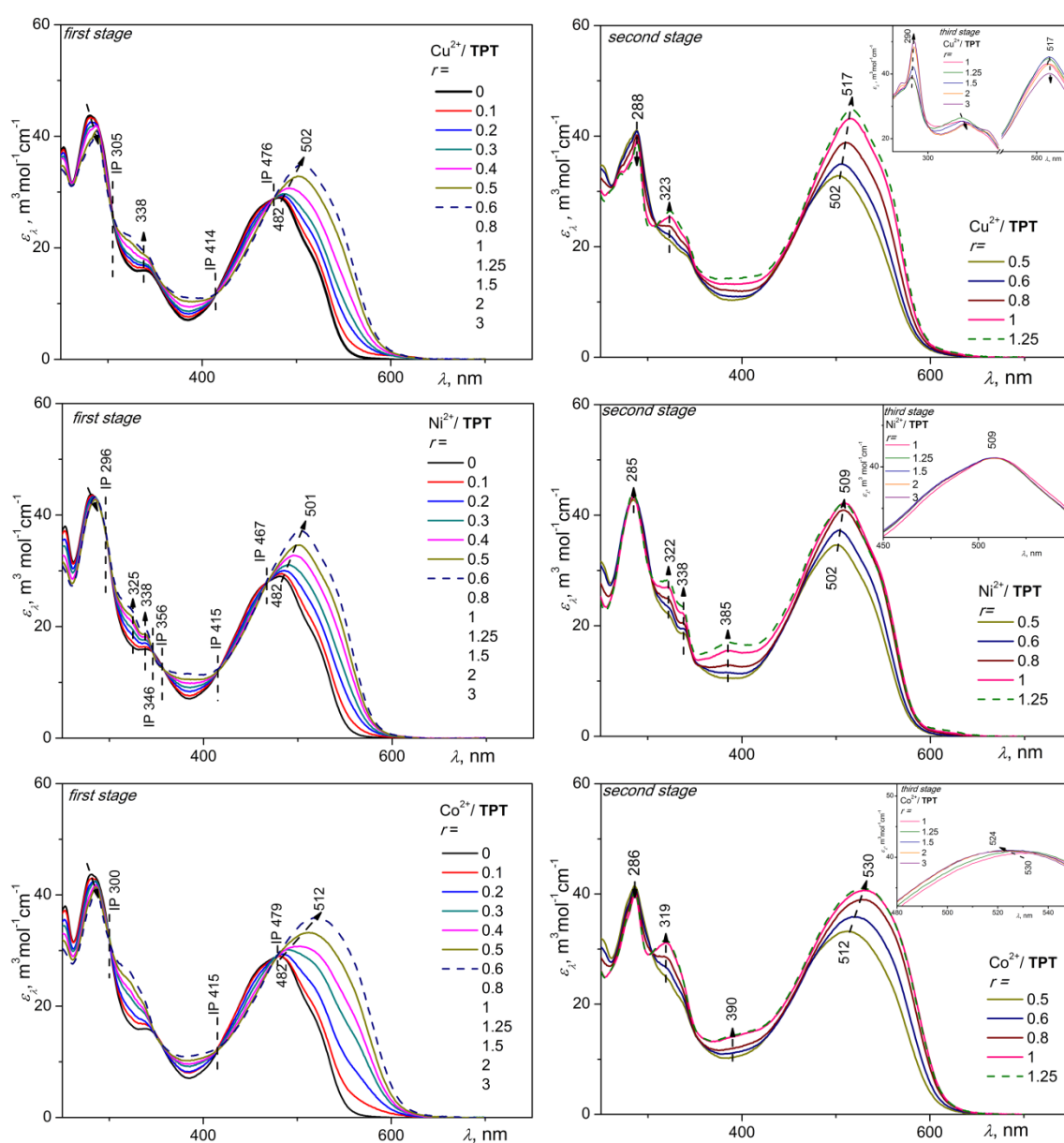
Figure 26: The UV/vis spectral changes accompanying three stages of assembling of **TPT** with Co²⁺, Cu²⁺ and Ni²⁺, third stage in the insets

3.5.2 Fluorescence spectra

Spectral changes accompanying the assembling process were also followed by fluorescence spectra. The same set of samples as for absorption measurement were also examined by fluorescence spectroscopy, position of apparent isosbestic point at around 400 nm observed in absorption spectra was used as excitation wavelength. From all metal ions only Zn^{2+} exhibit fluorescence. Introduction of Fe^{2+}, Co^{2+}, Cu^{2+} and Ni^{2+} ions led to gradual quenching of fluorescence without shift of band maxima upon increasing amount of ratio and fluorescence is totally quenched at the ratio 1 (Figure 27). Interestingly the emission band showed vibrational splitting during quenching for unimer **E**.
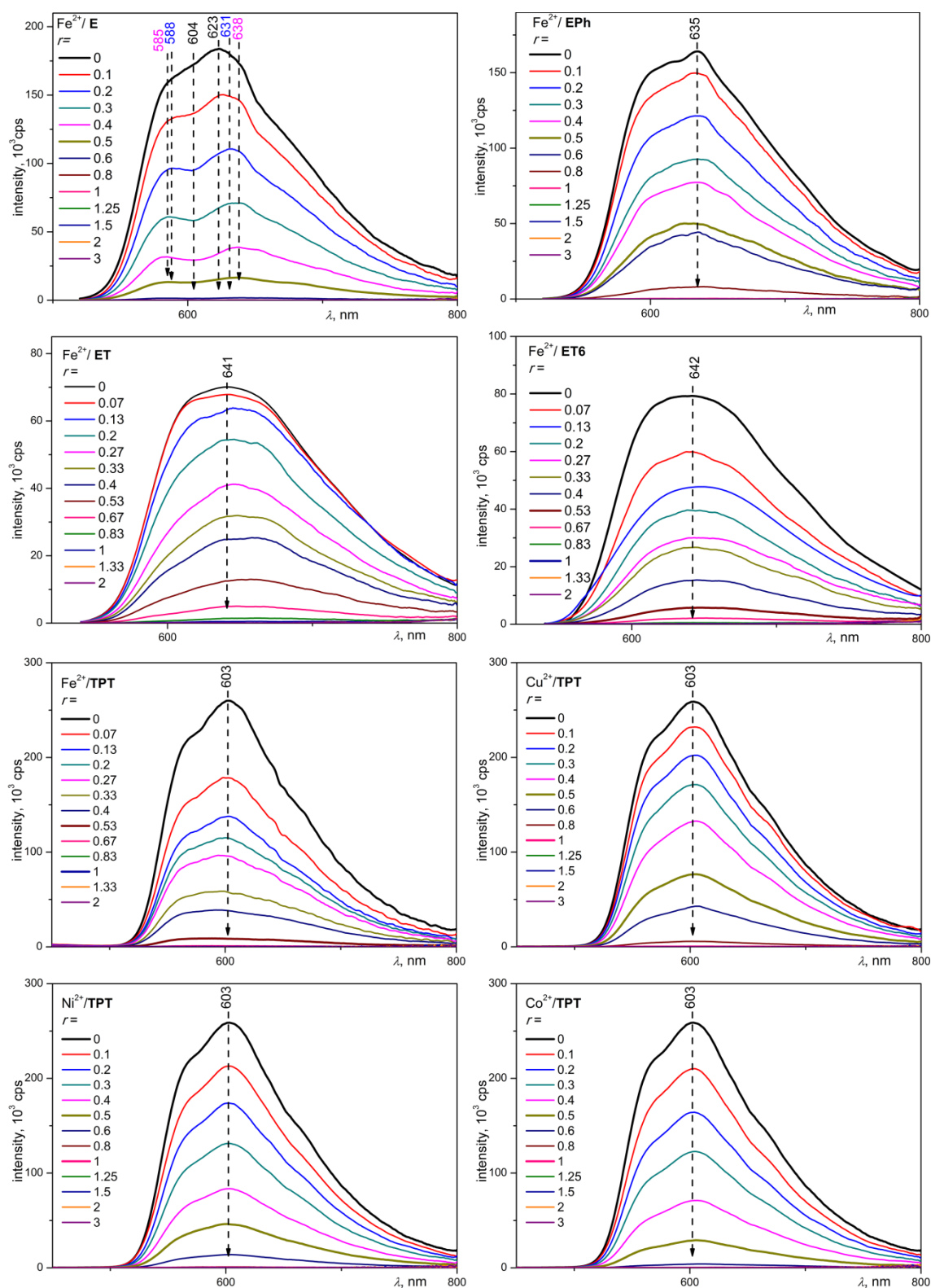
Figure 27: Gradual quenching of fluorescence observed during assembling of various systems

Therefore only assemblies with Zn^{2+} ions, which exhibit fluorescence at all examined ratios, will be discussed. Assembly of Zn^{2+} ions and unimers can be also formally divided into three stages; contrary to absorption spectra the three stages could be clearly

determined (Figure 28). During *the first stage* of assembly the intensity of original band of free unimer is gradually lowered while the bathochromic shift of fluorescence maxima can be observed. The decrease of fluorescence intensity is detected generally up to $Zn^{2+}/U = 0.6$ (0.8 in case of **ET** and **ET6**). Thus one can conclude that dimer formed in this stage exhibits less intense fluorescence than free unimers. During *the second stage* of assembly the fluorescence intensity is enhanced. On average, the fluorescence of species presented in solution with composition $Zn^{2+}/U = 1$ is two times higher than for the ratio $Zn^{2+}/U = 0.5$. This clearly illustrates that species with longer chains, *i.e.* Zn^{2+} ions located close to each other, exhibit enhanced fluorescence intensity. The fluorescence maxima were in most cases further red-shifted. Final changes of intensity and position of fluorescence maxima occurred in *the third stage* of assembly. Reaching the maximum intensity (often for ratio 1.25) of shifted band is followed by decrease and shift of maxima to slightly shorter wavelengths, thus illustrating of shortened polymer chain and end-capping. It need to be mentioned that the band attributed to polymer chain is located at exceptionally high wavelengths in comparison with polymers derived from unimers comprising quaterthiophenes[75] and terthiophenes.[76]
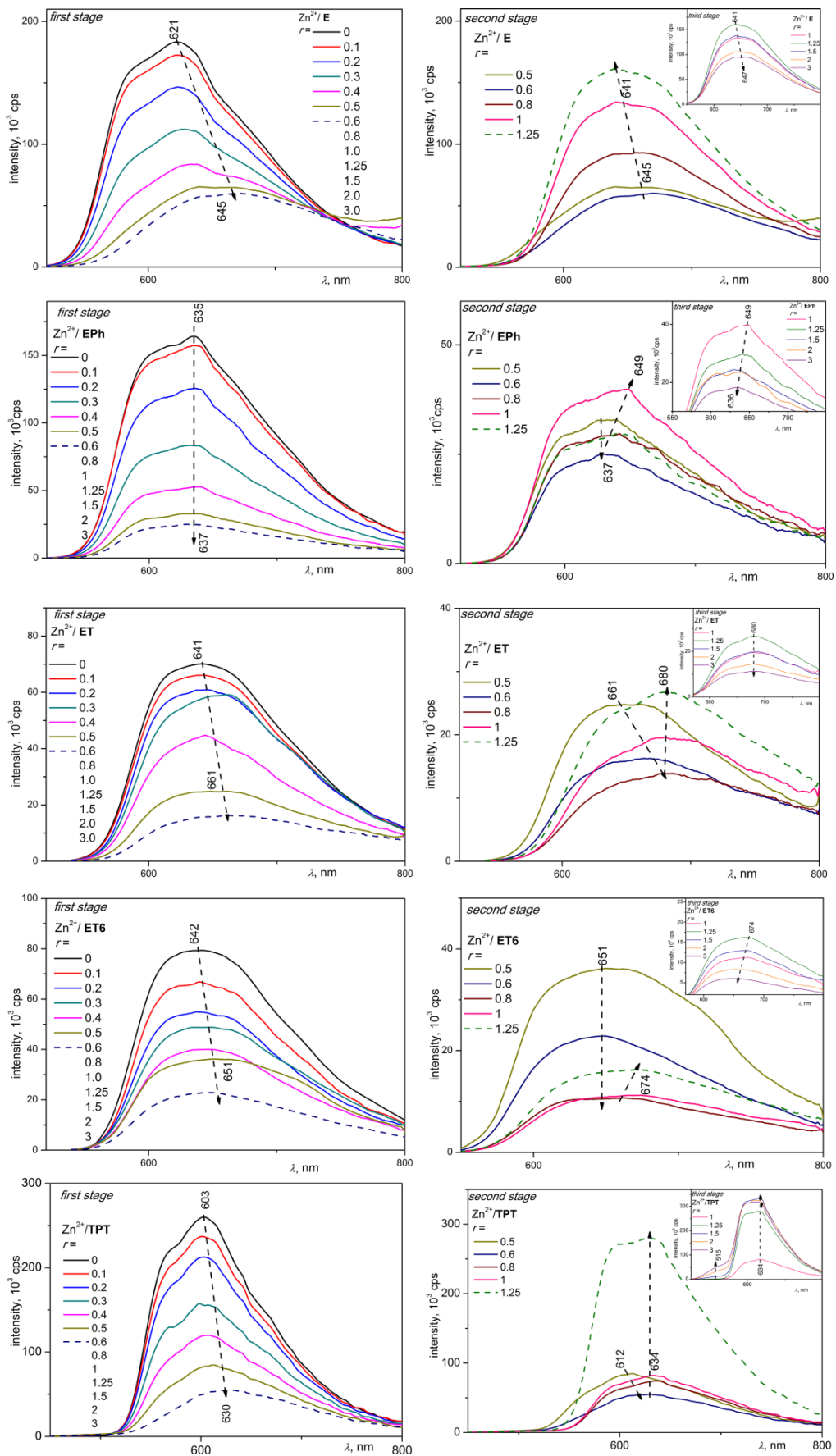
Figure 28: The fluorescence spectral changes accompanying three stages of assembling various unimers with Zn^{2+}, third stages in the insets

71

3.5.3 Size exclusion chromatography

The size exclusion chromatography (SEC) method can provide qualitative information on the constitutional dynamics of MSPs in the solvent used as a mobile phase.[77,67] The SEC is method suitable for systems with very stable coordination bonds (Ru^{2+} and Os^{2+}) and slow kinetics and several successful examples of SEC analysis were reported in literature.[48,155–157] Determination of MW distribution and DP is yet quite challenging for MSPs, as the values are highly dependent on the concentration[32], the charged compound can interact with columns in SEC system[155] and high binding strength of metal complexes is required.[67] If an MSP with fast establishing assembly equilibrium (fast constitutional dynamics) is analyzed by SEC, only a peak for the free unimer is observed due to the fast disassembly of MSP upon multiple dilution of the injected solution inside columns (injected 20 µL, elution volume of ca 40 mL). However, if an MSP with slow constitutional dynamics is injected, its chains do not completely or substantially dissociate during the SEC analysis and an SEC record resembling the record of an oligomer or polymer is obtained, from which the average degree of polymerization can be calculated. If the SEC device is fitted with a diode-array UV/vis detector, it also provides the spectra of SEC fractions from which the type of chains present in the fractions (dimers, longer or end-capped chains) can be identified or at least ascertained.

For the SEC analysis, one day old solution of **TPT** (0.5 mM) and M^{2+} ions (r from 0 to 1.3) was injected and a chloroform/acetonitrile (1/1 by volume) solvent mixture containing $Bu_4N^+PF_6^-$ (0.5 % by weight; to suppress aggregation) was used as the mobile phase. Samples with Co^{2+} ions were also considered suitable as half time of Co^{2+}/tpy complexes is quite high[45] and they also exhibit reasonable stability[119], but they were not analyzed since they provided opalescent solutions indicating the presence of aggregates. The Zn^{2+}/**TPT** and Cu^{2+}/**TPT** systems provided SEC records showing just a peak of free **TPT**, which proves fast constitutional dynamics for **P(TPT/Zn)** and **P(TPT/Cu)**. This agrees with earlier observations made for other MSPs and complexes derived from tpy and Zn^{2+} or Cu^{2+} ions.[45] The systems Fe^{2+}/**TPT** and Ni^{2+}/**TPT** provided SEC records similar to covalent polymers proving slow constitutional dynamics of these MSPs. Fe^{2+}/**TPT** assembly will be discussed as representative system.

Good resolved SEC records were given by the systems with $r \leq 1$ (Figure 29). The systems with $r \geq 1$ gave poorly resolved records showing a decrease in the elution peak area with increasing value of r, which should be ascribed to the retention of chains end-capped with M^{2+} ions in the SEC columns. The UV/vis spectra of SEC fractions within Fe^{2+}/**TPT** system show a continuous development from the spectral pattern comparable with absorption studies of assembling. Thus the dependence between elution time and length of polymer chain is clearly demonstrated (Figure 29).
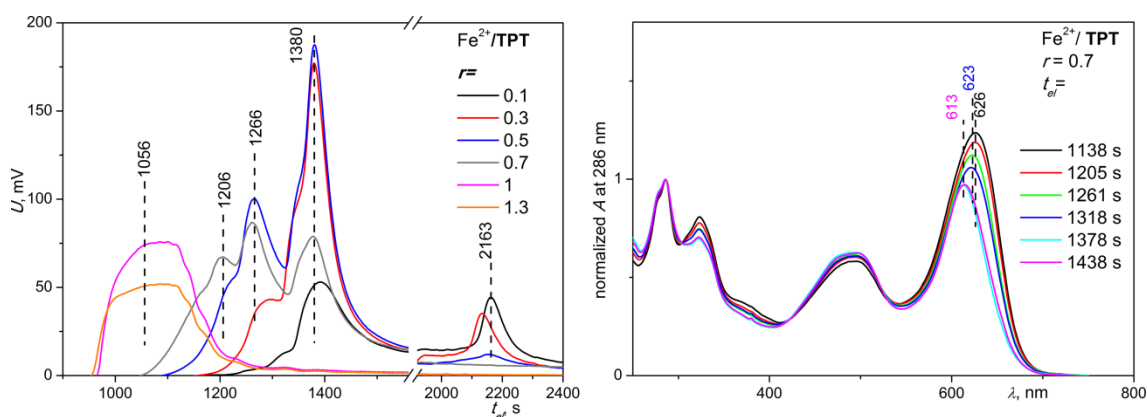
Figure 29: SEC chromatograms for different compositions Fe^{2+}/**TPT** (left), UV/vis DAD spectra of SEC fractions of Fe^{2+}/**TPT** system with composition $r = 0.7$ at various elution times

The number-average, $\langle X \rangle_n$, and weight-average, $\langle X \rangle_w$, degrees of polymerization of the **P(TPT/Fe)** chains formed in the solution with $r = 1$ have been estimated using the PMMA calibration: $\langle X \rangle_n = 4$ and $\langle X \rangle_w = 5.7$. These values should be underestimated owing to the retention of polymer higher fractions in the SEC columns. However, a recent time-resolved transient optical absorption study on solutions of **P(Zn/T)** and its derivative **P(Zn/T16)** (with hexyl groups on carbons next to the *tpy* groups), in which equilibrium fractions of the free unimers **T** and **T16** have been determined,[158] gave values of $\langle X \rangle_n = 11$ and $\langle X \rangle_w = 21$ for **P(Zn/T)** and $\langle X \rangle_n = 5$ and $\langle X \rangle_w = 9$ for **P(Zn/T16)** calculated using the Carothers equations. The latter values are close to those found for **P(TPT/Fe)**.

4   EXPERIMENTAL PART

4.1 MATERIALS

- Ligands

4'-(4-Bromophenyl)-2,2':6',2"-terpyridine and 4'-bromo-2,2':6',2"-terpyridine were purchased from TCI Europe N.V. and used as received. 2-Thienylboronic acid, 3-hexylthiophene-2-boronic acid pinacol ester, trimethylsilylacetylene (TMSAc), *N*-bromosuccinimide (NBS) were all purchased from Sigma Aldrich and used as received.

- Phosphole compounds and their functionalization

2-Bromothiophene, 4-hexyl-2-bromothiophene, 1,7-octadiyne, titanium(IV) isopropoxide, bis(cyclopentadienyl)zirconium(IV) dichloride (ZrCp$_2$Cl$_2$), sulphur, 4,4,5,5-tetramethyl-1,3,2-dioxaborolane (HBpin), *N*-iodosuccinimide (NIS) (all Sigma Aldrich) were used as obtained. Isopropylmagnesiumchloride (2.0M solution in diethylether) and n-butyllithium (2.5M solution in hexane) (Sigma Aldrich) were analyzed for exact concentration with menthol/bipyridine titration before use. *P,P*-dichlorophenylphosphine and phosphorous tribromide (PBr$_3$) (both Sigma Aldrich) were distilled trap to trap before use and P,P-dibromophenylphosphine was prepared by halogen exchange from P,P-dichlorophenylphosphine and phosphorous tribromide (PBr$_3$).[159]

- Catalysts

Bis(triphenylphosphine)palladium(II) dichloride (Pd(PPh$_3$)$_2$Cl$_2$), [1,3-bis(2,6-diisopropylphenyl)imidazol-2-ylidene](3-chloropyridyl)palladium(II) dichloride (Peppsi^{TM}-IPr), tetrakis(triphenylphosphine)palladium(0) (Pd(PPh$_3$)$_4$), bis(1,5-cyclooctadiene)di-*μ*-methoxydiiridium(I) ([Ir(OMe)(COD)]$_2$), copper iodide (CuI), 4,4'-di-*tert*-butyl-2,2'-dipyridyl (dtbpy) were all purchased from Sigma Aldrich and used as received.

- Other chemicals and metal salts

Zinc(II) perchlorate hexahydrate, nickel(II) perchlorate hexahydrate, copper(II) perchlorate hexahydrate, cobalt(II) perchlorate hexahydrate, iron(II) perchlorate hydrate were all purchased from Sigma Aldrich and used as received. Potassium carbonate, Celite and magnesium sulphate (VWR or Lach-Ner) were used as received.

- Solvents

Diisopropylamine and trimethylamine were purchased from Sigma Aldrich and used as received. Tetrahydrofuran (THF) was purchased from Sigma Aldrich and was distilled from suspension with lithium aluminium hydride or from sodium/benzophenone system before use in reactions. For column chromatography tetrahydrofuran was either distilled from suspension with lithium aluminum hydride or freshly dried by MBraun drying solvents system (SPS-800). Toluene (Lach-Ner or Sigma Aldrich) was distilled from sodium/benzophenone system prior to use in reactions otherwise it was used as received. Pentane, diethyl ether (Et$_2$O) and dichloromethane (DCM) were purchased from Sigma Aldrich, VWR or Lach-Ner and dried by MBraun drying solvents system (SPS-800) if needed (for reactions or sensitive compounds), otherwise it was used as obtained. Hexane was only used in laboratories in Prague and it was purchased from Lach-Ner chemical company and for reactions stored over active molecular sieves and bubbled with argon. Otherwise it was used as obtained. Acetonitrile was purchased from Sigma Aldrich and stored over active molecular sieves and bubbled with argon prior to use in reaction, otherwise it was used as obtained.

- General information

All experiments were performed under an atmosphere of dry argon using standard Schlenk techniques. Column chromatographies were performed in air unless stated in text. Reactions including phosphole were followed by ^{31}P NMR spectra. The following paragraphs describe only general procedures applied in this project. For detailed reaction conditions as well as for product characterizations the reader is kindly asked to view attached publications.

4.2 METHODS

- Nuclear magnetic resonance (NMR)

^{1}H, ^{31}P NMR and ^{13}C NMR spectra were recorded on a Varian ^{UNITY}INOVA 400, Varian SYSTEM 300 instruments or Bruker GPX (400 MHz) spectrometer in CD$_2$Cl$_2$ or CDCl$_3$. ^{1}H and ^{13}C NMR spectra were referenced to the solvent signal: 7.25 ppm (CDCl$_3$) or 5.32 ppm (CD$_2$Cl$_2$) for ^{1}H and 77.0 ppm (CDCl$_3$) or 53.84 ppm (CD$_2$Cl$_2$) for ^{13}C spectra. ^{13}C NMR spectra of unimers were recorded on Bruker AVANCE III (600 MHz) spectrometer by Dr. Hybelbauerová (Charles University in Prague). More sophisticated NMR experiments (monoterpyridine titrations and EXSY) were

performed by Dr. Zedník (Charles University in Prague). Coupling constants, J (in Hz), were obtained by the first-order analysis.

- Infrared and Raman spectroscopy

Infrared spectra were recorded on a Thermo Nicolet 7600 FTIR spectrometer equipped with a Spectra Tech InspectIR Plus microscopic accessory using KBr-diluted samples and diffuse reflectance technique (DRIFT) (128 or more scans at resolution 4 cm^{-1}). Raman spectra were recorded on a DXR Raman microscope (Thermo Scientific) using excitations across the whole visible region (λ_{ex} = 445, 532, 633 and 780 nm) and usual laser power at the sample 0.1 to 0.4 mW. Raman and IR spectra of unimers and MSPs were recorded by Dr. Šloufová (Charles University in Prague)

- Gas chromatography

Synthesis of ligands was followed by consumption of starting materials via gas chromatograph Shimadzu GC-2010 with SLB^{TM}-5ms (Supelco) column (30 m × 0.25 mm id × 0.25 μm). Samples were diluted with suitable solvents and 1μl of diluted sample was injected.

- Absorption spectroscopy

Absorption spectra of solutions as well as of thin films were recorded on a Shimadzu UV-2401PC instrument. Blank solvent was used as reference for solution spectra. Films were coated on quartz cuvette from solution and gained after subsequent evaporation of solvent. Absorption spectra of thin films were referenced to air.

- Photoluminescence spectroscopy

Photoluminescence spectra were recorded on a Fluorolog 3-22 Jobin Yvon Spex instrument, using four-window quartz cuvette (1 cm) for solutions and glass support as substrate for films. Absolute quantum yields, ϕ_F, of photoluminescence were determined by integration sphere Quanta-φ F. Pellets for fluorescence measurement were made by grounding specific amount of sample and potassium bromide using ball mill Vibrator DDR-GM 9458 Narva and then pressed by hydraulic press H62 TRYSTOM. Determination of quantum yields as well as photoluminescence spectra in solid state was performed by Dr. Svoboda (Charles University in Prague).

- Size exclusion chromatography (SEC)

SEC records were obtained using a Spectra Physics Analytical HPLC pump P1000 with two SEC columns: Polymer Labs (Bristol, USA) Mixed-D and Mixed-E. The system was equipped with a Thermo UV6000 DAD detector. 0.05M tetrabutylammonium

hexafluorophosphate in chloroform/acetonitrile (1/1, v/v, Sigma Aldrich, HPLC grade) was used as an eluent (0.7 mL min^{-1}).

- High resolution mass spectroscopy (HR-MS)

HR-MS were measured by Dr. Cvačka's group at the Institute of Organic Chemistry and Biochemistry AS CR, v. v. i. in Prague.

- Calculations

Theoretical calculations were done using the density functional theory (DFT), namely the Becke's three parameter functional with the non-local Lee-Yang-Parr correlation functional (B3LYP) with the standard 6-31G(d) basis set as implemented in Gaussian 09 package.[143] We employed the Becke's three parameter functional with the non-local Lee-Yang-Parr correlation functional (B3LYP) with the standard 6-31G(d) basis set. Electron density and vibrational spectrum of the unimer **TPT** was calculated for the optimized geometry. The wavenumbers values computed contained systematic errors and were thus scaled by the factor 0.946 for Raman and 0.972 for IR spectra. All theoretical calculations were done by Dr. Svoboda (Charles University in Prague).

4.3 SYNTHESES

The following paragraphs should provide a scope to tested synthetic pathways, which were used in order to fulfil the aims of the Thesis. That's why only general procedures of syntheses are described. For detailed reaction conditions as well as for individual characteristics of synthesized product the reader is kindly asked to look into attached publications. Synthesis and complexation studies of 4'-functionalized terpyridine ligands are described in Attachment A (Ref.[120]). Attachment B (Ref.[146]) contains preparation of unimer **TPT** and related MSPs.

4.3.1 Syntheses of ligands

4'-(4-ethynylphenyl)-2,2':6',2''-terpyridine and 4'-ethynyl-2,2':6',2''-terpyridine were synthesized according to procedure described by Grosshenny[116]. 4'-(thiophen-2-yl)-2,2':6',2''-terpyridine and 4'-(3-hexylthiophen-2-yl)-2,2':6',2''-terpyridine were synthesized using the Suzuki coupling as described by Bláhová[76], then brominated in a standard way using NBS[118] and 4'-(5-ethynylthiophen-2-yl)-2,2':6',2'' was prepared as in ref [117]. Recorded characterizations of products (NMR, IR) were in good agreement with the spectra available in referenced literature. Thus detailed synthesis and

characterization of 4'-(5-ethynyl-3-hexylthiophen-2-yl)-2,2':6',2''-terpyridine and is described below.

- General procedure to functionalize terpyridine by 3-R-thiophene

Bromo-terpyridine (1 eq), boronic derivative of 3-R-thiophene (1.1 eq), potassium carbonate (3 eq) and PEPPSI^{TM}-IPr (cat.) were dissolved in toluene/methanol (1/1, v/v) mixture and stirred under 90 °C for at least 2 hours. Conversion of reactants was followed by GC. After consumption of starting material, reaction mixture was washed with water (extraction of water soluble inpurities), organic phase was collected, dried with MgSO$_4$, filtrated over small column of Celite and evaporated. Purification (if needed) was performed using column chromatography (basic alumina, hexane/THF). Product was pale yellow powder.

- General procedure to brominate 4'-(3-R-thiophene-2-yl)-2,2':6',2''-terpyridine

3-R-Thio-*tpy* (1 eq) was dissolved in DCM/acetic acid (1/1, v/v) mixture and *N*-bromosuccinimide (1.1 eq) was added. The reaction flask was covered by aluminium foil and the mixture was reacted overnight. Then the mixture was diluted by DCM and appropriate amount of potassium carbonate was added to neutralize the reaction environment, followed by extraction of water soluble materials. Organic phase was dried over magnesium sulphate, filtered off and evaporated resulting into whitish product.

- General procedure to synthetize EPh-*tpy* and E-*tpy*

Bromo-(phenyl)*tpy* (1 eq), Pd(PPh$_3$)$_4$ was dissolved in THF/diisopropylamine mixture, then trimethylsilylacetylene (2 eq) was added and reaction mixture was heated at 80 °C, conversion of starting materials was followed by GC. After consumption of starting material, all volatiles were evaporated and resulting solid was dissolved in small amount of THF and filtrated over basic alumina (THF) to remove the catalyst. Formation of product was confirmed by ^{1}H NMR and GC. Product was then dissolved in THF/methanol mixture and introduced to potassium carbonate which leads to removal of the TMS group. Column chromatography on basic alumina (hexane/THF 3/2) was performed to obtain pure product.

- General procedure to synthetize ET-*tpy* and ET6-*tpy*

Bromo-(thiophene-2-yl)*tpy* or bromo-(3-hexyl-thiophene-2-yl)*tpy* (1 eq), copper iodide and Pd(PPh$_3$)$_2$Cl$_2$ was dissolved in THF/diisopropylamine mixture, then trimethylsilylacetylene (2eq) was added and reaction mixture was heated at 40 °C,

conversion of starting materials was followed by GC. After consumption of starting material, all volatiles were evaporated and resulting solid was dissolved in small amount of THF and filtrated over basic alumina (THF) to remove the catalyst. Formation of product was confirmed by ^{1}H NMR and GC. Product was then dissolved in THF/methanol mixture and introduced to potassium carbonate which leads to removal of the TMS group. Column chromatography on basic alumina (hexane/THF 3/2) was performed to obtain pure product.

- Synthesis of 4'-(5-ethynyl-3-hexylthiophen-2-yl)-2,2':6',2''-terpyridine

Reactants: Bromo-(3-hexyl-thiophene-2-yl)*tpy* (0.200 g, 0.42 mmol), copper iodide and Pd(PPh$_3$)$_2$Cl$_2$, trimethylsilylacetylene (0.12 mL, 0.84 mmol), then for removal TMS group potassium carbonate (69 mg, 0.5 mmol); solvents : THF/diisopropylamine mixture (20 mL), then THF/methanol mixture (20 mL) for removal TMS group; temperature: 40°C.The desired product was obtained as yellowish solid (0.098 g, yield = 55%) after purification by column chromatography on basic alumina (hexane/THF 3/2).
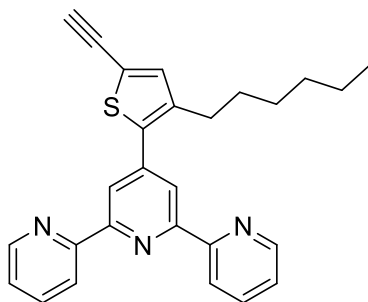
^{1}H NMR (300 MHz, CD$_2$Cl$_2$, δ/ppm): 8.70 (ddd, *J*=4.71, 1.77, 0.86 Hz, 2 H, A6), 8.66 (dt, *J*=8.01, 1.01 Hz, 2 H, A3), 8.57 (s, 2 H, B3), 7.90 (td, *J*=7.00, 1.70 Hz, 2 H, A4), 7.37 (ddd, *J*=7.45, 4.77, 1.29 Hz, 2 H, A5), 7.25 (s, 1 H, thiophene), 3.49 (s, 1 H, ethynyl), 2.78 (t, *J*=8.10 Hz, 2 H, Hex1), 1.62 - 1.75 (m, 2 H, Hex2), 1.48 - 1.50 (m, 2 H, Hex3), 1.24 - 1.32 (m, 4 H, Hex4 + Hex5), 0.82 - 0.87 (m, 3 H, Hex6)

^{13}C NMR (101 MHz, CD$_2$Cl$_2$, δ/ppm): 156.50, 156.31, 149.81, 143.79, 141.70, 138.09, 137.37, 136.74, 124.54, 121.84, 121.57, 120.97, 82.66, 77.27, 32.16, 31.35, 29.59, 29.48, 23.16, 14.37

HRMS found m/z 424.1842 [M + H$^+$], C$_{27}$H$_{26}$N$_3$S requires 424.1847

FT-IR (cm^{-1}): 3217.16 (m), 3172.81 (s), 3072.53 (m), 3061.92 (m), 3048.91 (m), 3012.75 (m), 2953.93 (s), 2930.79 (s), 2868.59 (m), 2854.13 (s), 1601.59 (s), 1584.72 (s), 1567.84 (s), 1557.24 (s), 1538.92 (s), 1465.64 (s), 1435.26 (m), 1393.80 (s), 1377.89 (m), 1267.00 (m), 1124.30 (m), 1096.33 (w), 1088.62 (m), 1072.71 (m), 1022.57 (m), 989.30 (m), 964.23 (w), 894.33 (m), 852.86 (m), 792.60 (s), 776.69 (s),

751.14 (s), 741.98 (s), 676.41 (s), 658.57 (m), 616.63 (s), 586.74 (m), 549.61 (w), 403.53 (w)

- Preparation of 1,1'-biphosphole

Octa-1,7-diyne-1,8-diyl-2,2'-bis(thiophene) (1eq) and Ti(O-iPr)$_4$ (1.1 eq) were dissolved in Et$_2$O. At -78 °C, Et$_2$O solution of isopropylmagnesiumchloride (2.1 eq) was slowly added and the resulting mixture was stirred for 2 hours at –50 °C. Then phosphorus tribromide (2.1 eq) was dropwise added, resulting suspension allowed to warm up to 0 °C within one hour and stirred for next 20 hours after which all volatile materials were evaporated. The obtained residue was diluted with DCM, filtrated over basic alumina under inert atmosphere and the filtrate was evaporated and washed with freshly distilled pentane. Purity of the desired product was checked by the ^{1}H, ^{31}P NMR spectra which were in good agreement as the spectra in literature.[93]

- Synthesis of 4'-{[2,5-di(thiophene-2-yl)phosphole-1-yl]ethynyl}-2,2':6',2"-terpyridine (P-E*tpy*)

To a THF solution (30 mL) of 4'-ethynyl-2,2':6',2"-terpyridine (0.257 g, 1.5 mmol, 3 eq) was added dropwise, at -78°C, a hexane solution of 2.2M n-BuLi (0.62 mL, 1.37 mmol, 2.74 eq). The reaction mixture was stirred in the cold bath for 30 min and another 15 min after its removal. Then a THF solution (45mL) of 1,1'-biphosphole (0.301 g, 0.5 mmol, 1 eq) was slowly added *via canula* and the reaction mixture allowed to stir at room temperature for 1h. The solution was filtered on basic alumina with THF and all the volatile materials were removed under vacuo. The product was purified on neutral alumina column (eluent heptane/DCM 6/4). After washing with freshly distilled pentane, the desired compound was obtained as an orange powder (yield: 34 %, 90 mg, 0.20 mmol).
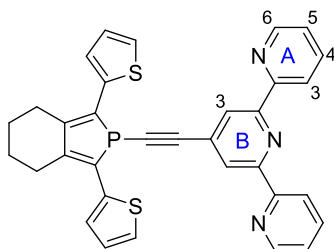
^{1}H NMR (300 MHz, CD$_2$Cl$_2$, δ/ppm): 8.65 ppm (d, *J* = 4.8 Hz, 2H, A6), 8.55 (d, *J* = 7.9 Hz, 2H, A3), 8.36 (s, 2H, B3), 7.84 (m, 2H, A4), 7.43 (d, *J* = 3.8 Hz, 2H, C*H*3thienyl), 7.40 (d, *J* = 5.1 Hz, 2H, C*H*5thienyl), 7.33 (m, 2H, A5), 7.16 (dd, *J* = 5.1 Hz, 3.8 Hz, 2H, C*H*3thienyl), 2.87 (m, 4H; CH2-C*H2*-C=C), 1.82 (m, 4H; C*H2*- CH2-C=C).

^{13}C NMR (101 MHz, CD$_2$Cl$_2$, δ/ppm): 156.2 ppm (s; C$_{tpy}$), 155.9(s; C$_{tpy}$), 149.8 (s; CH$_{tpy}$), 146.6 (d, J = 11.0 Hz; C$_\beta$), 139.2 (d, J = 22.9 Hz; C$_\alpha$), 137.4 (s; CH$_{tpy}$), 132.9 (s;Ctpy), 130.1 (d, J = 4.7 Hz, C$_{thienyl}$), 128.1 (s; CH$_{tpy}$), 126.9(d, J = 9.6 Hz; CH$_{thienyl}$), 126.1 (d, J = 2.0 Hz; CH$_{thienyl}$), 124.6 (s; CH$_{tpy}$), 121.5 (s, CH$_{tpy}$), 105.7 (s; PC≡C), 88.1 (d, J = 22.3 Hz; P-C≡C), 30.2 (d, J = 2.0 Hz; CH$_2$-CH$_2$-C=C), 23.3 (s; CH$_2$CH$_2$-C=C).

^{31}P NMR (121 MHz, CD$_2$Cl$_2$, δ/ppm): –26.3 ppm (s).

HRMS found m/z 557.1157 [M + H$^+$]; C$_{33}$H$_{24}$N$_3$PS$_2$ required 557.1149

4.3.2 Synthesis of phosphole unimer

Synthetic pathways to phosphole unimers consist of three steps: *(i)* synthesis of the central phosphole block, *(ii)* functionalization of the central blocks, and *(iii)* final coupling towards unimer.

4.3.2.1 Synthesis of central phosphole blocks

Phosphole central blocks were synthesized from functionalized 1,7-octadiyne following Sato[139] or Fagan- Nugent method.[137] 1,7-Octadiyne was functionalized *via* Sonogashira coupling with appropriate halogenated thiophene derivative. Reaction conditions for octa-1,7-diyne-1,8-diyl-2,2'-dithiophene[140] and for octa-1,7-diyne-1,8-diyl-2,2'-bis(4-hexyl-thiophene)[160] were used as described in quoted references.

- General procedure to synthesize 1-phenyl-2,5-bis(4-R-thiophene-2-yl)thioxophosphole (Fagan-Nugent method)

Octa-1,7-diyne-1,8-diyl-2,2'-bis(thiophene) (1 eq) and ZrCp$_2$Cl$_2$ (1.1 eq) were dissolved in THF. At –78°C, hexane solution of butyllithium (2.1 eq) was slowly added and the resulting mixture stirred for 1 hour at –78 °C and then 18 hours at room temperature. Then *P,P*-dibromophenylphosphine (1.1 eq) was added dropwise at –50 °C under argon atmosphere, and reaction mixture was stirred at –50 °C for 20 min. Then reaction mixture was allowed to warm up to room temperature and formation of product was followed by ^{31}P NMR. After consumption of starting materials the reaction was terminated by filtration over basic alumina (THF). Filtrate was evaporated and the purity was checked by ^{31}P NMR. Excess of sulfur was added to the filtrate after dissolution in DCM. Oxidation of P atoms was monitored by ^{31}P NMR (signal changes from 12 to 52 ppm). The crude product was purified by chromatography on silica (heptane/DCM) and isolated as a yellow-orange solid.

- General procedure to synthesize 1-phenyl-2,5-bis(4-R-thiophene-2-yl)thioxophosphole (Sato method)

Octa-1,7-diyne-1,8-diyl-2,2'-bis(4-R-thiophene) (1eq) and Ti(O-iPr)$_4$ (1.1 eq) were dissolved in Et$_2$O. At –78 °C, Et$_2$O solution of isopropylmagnesiumchloride (2.1 eq) was slowly added and the resulting mixture stirred for 2 hours at –50 °C. Then *P,P*-dichlorophenylphosphine (1.1 eq) was dropwise added, resulting suspension allowed to warm to 0 °C within one hour and stirred for next 20 hours after which all volatile materials were removed by vacuum distillation. The obtained residue was diluted with DCM, filtrated over basic alumina under inert atmosphere and excess of sulfur was added to the filtrate. Oxidation of P atoms was monitored by ^{31}P NMR (signal changes from 12 to 52 ppm). The crude product was purified by chromatography on silica (heptane/DCM) and isolated as a yellow-orange solid.

- Characterization of the 1-phenyl-2,5-bis(4-hexyl-thiophene-2-yl)thioxophosphole

Synthesis and characterization of 1-phenyl-2,5-bis(4-thiophene-2-yl)thioxophosphole was published earlier and recorded spectra of the product were in a good agreement with those already published.[100] Synthesis and characterization of 1-phenyl-2,5-bis(4-hexyl-thiophene-2-yl)thioxophosphole was performed by both methods, but details of the Sato method (which deliver higher yield) are described further: reactants: octa-1,7-diyne-1,8-diyl-2,2'-bis(4-hexylthiophene) (0.55g, 1.25 mmol), Ti(OiPr)$_4$ (0.4ml, 1.375 mmol), iPrMgCl (1.4 ml; 2.62 mmol),PhPCl$_2$ (0.18 ml, 1.3 mmol), sulfur; solvent diethylether (50 mL), DCM (50 mL). Resulting product was then purified by column chromatography, using silica gel and heptane/DCM (4/1 by volume) as mobile phase and isolated as yellow-orange solid in 73%yield (0.53 g, 0.92 mmol).
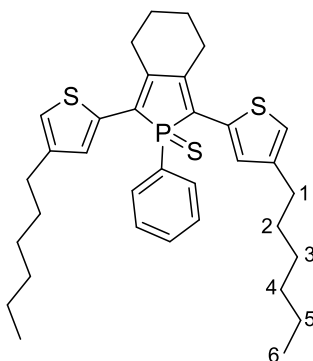
^{1}H NMR (400 MHz, CD$_2$Cl$_2$, δ/ppm): 7.88 (ddd, J = 14.0, 8.3, 1.5 Hz, 2H, *o*-H Ph), 7.48 (ddd, J = 7.0, 5.3, 1.8 Hz, 1H, *p*-H Ph), 7.42 (ddd, J = 8.5, 6.5, 3.0 Hz, 2H, *m*-H Ph), 7.21 (s, 2H, th3), 6.95 (s, 2H, th5), 2.9 (m, 4H, C-*CH$_2$*-CH$_2$), 2.51 (t, J = 7.6 Hz, 4H, hex1),

1.87 (m, 4H,C-CH$_2$ *CH$_2$*), 1.50 (t, *J* = 7.4 Hz, 4H, hex2), 1.26 (m 12H, hex3-5), 0.87 (m, 6H, hex6)

^{13}C NMR (101 MHz, CD$_2$Cl$_2$, δ/ppm): 145.92 (d, *J*(P,C) = 21.3 Hz), 144.13, 134.96 (d, *J*(P,C) = 17.1 Hz), 132.50 (d, *J*(P,C) = 3.0 Hz), 131.18 (d, *J*(P,C) = 11.6 Hz), 129.51 (d, *J*(P,C) = 5.6 Hz), 129.85 (d, *J*(P,C) = 73.00 Hz), 129.33 (d, *J*(P,C) =12.72 Hz), 128.85 (d, *J*(P,C) =85.00 Hz), 122.41, 32.20, 30.83, 30.68, 29.70 (d, *J*(P,C) =13.51 Hz), 29.41, 23.16, 22.99, 14.43

^{31}P NMR (162 MHz, CD$_2$Cl$_2$, δ/ppm): 51.77

FT-IR (cm^{-1}): 3073.49(w), 3062.89(w), 2963.09(m), 2870.04(w), 1455.03(w), 1435.74(w), 1422.73(w), 1416.46(m), 1308.46(w), 1292.07(w), 1261.22(s), 1228.43(m), 1185.04(m), 1093.92(s), 1019.68(s), 935.79(w), 920.84(w), 908.31(m), 863.47(m), 799.35(s), 749.69(m), 740.05(m), 695.69(m), 666.77(m), 640.73(w), 626.27(m), 606.50(w), 579.50(w), 565.52(m), 539.97(m), 517.31(m), 508.63(m), 478.26(m), 460.42(w), 437.76(w), 402.09(m)

HRMS found m/z [M + H$^+$] 579.2337, C$_{34}$H$_{44}$PS$_3$ requires 579.2342

4.3.2.2 Functionalization of central phosphole blocks

Prior to use in the reaction mentioned later, the phosphole central block had to be functionalized. Procedure of borylation was performed under the conditions reported by Chotana[141] whereas procedure of halogenation was performed as described by Saito.[104]

- Borylation of 1-phenyl-2,5-bis(4-R-thiophene-2-yl)thioxophosphole

[Ir(OMe)(COD)]$_2$ (4 mg, 3 mol%) and dtbpy (2 mg, 3 mol%) were added to a solution of 1-phenyl-2,5-bis(thiophen-2-yl)thioxophosphole **1** (82.5 mg; 0.2 mmol) in dry THF/hexane (7/5 mL) mixed solvent under argon atmosphere, then HBpin (0.18 mL, 1.2 mmol) was added and the reaction mixture kept under stirring at 55°C for 30 hours, The mixture was then diluted with dichloromethane (20 mL) and water (20 mL), stirred for one hour in an open vessel and, finally, the soluble components were extracted with water (3×50 mL). The organic phase was dried over magnesium sulfate, filtered off and evaporated to give the product **2** (130 mg, ca 0.19 mmol) as a honey-like liquid that was used in the next reaction without further purification (since a significant loss of boronic groups was observed at attempts for chromatographic purification). The compound **2** identity has been verified by mass spectroscopy (HRMS) and purity by NMR spectroscopy.
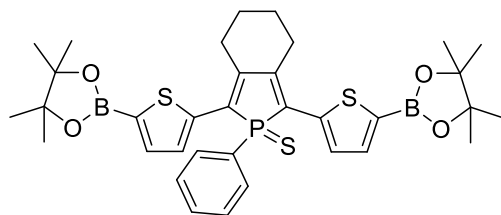
^{1}H NMR (400 MHz, CD$_2$Cl$_2$, δ/ppm): 7.87 (ddd, J(P,H) = 14.4 Hz, J(H,H) = 8.4 Hz, J(H,H) = 1.6 Hz 2 H, *o*-H Ph), 7.53 – 7.45 (m, 2H, *m*-H Ph), 7.43 (AB system, 4H, J_{AB}(H,H) =3.7 Hz, ν$_{AB}$ = 8.7 Hz, H$_{thienyl}$), 7.38 – 7.33 (m, 1H, *p*-H Ph), 2.98 (m, 4H, C=CC*H*$_2$CH$_2$), 1.90 (m, 4H, C=CCH$_2$C*H*$_2$), 1.24 (s, 24 H, CH$_3$).

^{31}P NMR (162 MHz, CD$_2$Cl$_2$, δ/ppm): +51.8 (s).

^{11}B NMR (128 MHz, CD$_2$Cl$_2$, δ/ppm): +22.4 (s).

^{13}C NMR (101 MHz, CD$_2$Cl$_2$, δ/ppm): 146.2 (d, J(P,C) = 21.0 Hz, PC=C), 135.3 (d, J(P,C) = 17.4 Hz, C$_{thienyl}$), 132.6 (d, J(P,C) = 3.2 Hz, C$_p$ Ph), 131.2 (d, J(P,C) = 11.8 Hz, C$_o$ Ph), 129.5 (d, J(P,C) = 75.4 Hz, PC=C), 129.4 (d, J(P,C) = 12.6 Hz, C$_m$ Ph), 128.9 (d, J(P,C) = 89.0 Hz, C$_i$ Ph), 128.5 (large s, B-C$_{thienyl}$), 127.7 (s, CH$_{thienyl}$), 127.4 (s, CH$_{thienyl}$), 83.6 (large s, *C*CH$_3$), 29.7 (d, J(P,H) = 12.4 Hz C=C*C*H$_2$CH$_2$), 24.9 (s, CH$_3$), 23.0 (s, C=CCH$_2$*C*H$_2$).

FT-IR (cm^{-1}): 3409 (s), 2979 (s), 2929(s), 2860(m), 2040(w), 1719(w), 1618 (m), 1571(w), 1514 (s), 1354(s), 1215(s), 1142(s), 983 (m), 957(m), 926(m), 852(s), 746 (m), 666(s), 613 (m), 578 (m), 517 (m), 448 (m), 419(m)

HRMS found m/z 685.1996 [M + Na$^+$], C$_{34}$H$_{41}$B$_2$O$_4$PS$_3$Na requires 685.1988

- Halogenation of central block

To a solution of 1-phenyl-2,5-bis(4-hexylthiophen-2-yl)thioxophosphole (0.345g; 0.6mmol) in DCM was dropwise added an acetonitrile solution of *N*-iodosuccinimide (0.284g; 1.25mmol) at –78°C. The reaction mixture was stirred for 15 min at –78°C and then while kept in darkness for next 18 hours at room temperature. All volatile materials were removed and red solid was dissolved in DCM and washed by saturated solution of Na$_2$S$_2$O$_3$ and water. Product was obtained as a red powder using column chromatography silica gel, heptane/DCM 4/1. Yield 0.339 g, 0.408 mmol, 68%.
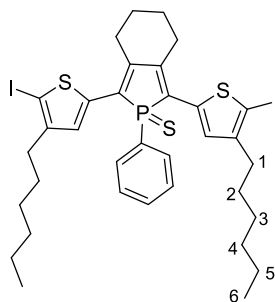
^{1}H NMR (400 MHz, CD$_2$Cl$_2$, δ/ppm): 7.84 (ddd, J = 14.1, 8.3, 1.4 Hz, 2H, σ$_{ph}$), 7.50 (td, J = 7.1, 1.8 Hz, 1H,p$_{ph}$), 7.42 (td, J = 7.5, 3.1 Hz, 2H, m$_{ph}$), 7.00 (s, 2H,th), 2.84 (tt, J = 5.9, 2.8 Hz, 4H, C-*CH$_2$*-CH$_2$), 2.44 (td, J = 7.4, 3.1 Hz, 4H, Hex1), 1.87 (dt, J = 6.9, 3.4 Hz, 4H,C-CH$_2$-*CH$_2$*), 1.43 (p, J = 7.4 Hz, 4H, Hex2), 1.33 – 1.17 (m, 12H, Hex3+Hex4+Hex5), 0.94 – 0.81 (m, 6H, Hex6).

^{31}P NMR (162 MHz, CD$_2$Cl$_2$, δ/ppm): 51.36

^{13}C NMR (101 MHz, CD$_2$Cl$_2$, δ/ppm): 148.14, 146.50 (d, J=20.70 Hz), 139.85 (d, J=17.48 Hz), 132.75 (d, J=3.18 Hz), 131.07 (d, J=11.13 Hz), 129.47 (d, J=12.70 Hz), 129.33 (d, J=74.70 Hz), 128.76 (d, J=5.60 Hz), 128.57 (d, J=83.50 Hz), 77.91, 32.51, 32.16, 30.24, 29.62 (d, J=13.51 Hz), 29.19, 23.14, 22.84, 14.43

FT-IR (cm^{-1}): 2948.14(s), 2924.52(s), 2865.70(m), 2852.68(s), 1464.19(w), 1451.65(w), 1438.64(m), 1412.12(m), 1298.34(m), 1101.15(s), 1016.30(w), 846.60(w), 835.99(w), 824.90(w), 748.73(m), 719.32(s), 691.84(w), 665.80(s), 602.65(w), 521.17(m)

HRMS found m/z [M + Na$^+$] 853.00896, C$_{34}$H$_{41}$I$_2$NaPS$_3$ requires 853.0095

4.3.2.3 Final coupling towards unimers

Connecting of the *tpy* end-groups or linkers capped with *tpy* end-groups to the functionalized central block were proceed either by Suzuki coupling between borylated central block and Br-*tpy* or by Sonogashira coupling of halogenated central block and acetylene linkers.

- Suzuki coupling towards **TPT** unimer

1-Phenyl-2,5-bis[5-(4,4,5,5-tetramethyl-1,3,2-dioxaboralene-2-yl)thiophen-2-yl]thioxophosphole) (0.13 g, 0.19 mmol), Br-tpy (0.12 g, 0.38 mmol), K$_2$CO$_3$ (80mg, 0.57 mmol) and Peppsi-IPr (13 mg, 0.10mol%), Aliquat 336 (cat.) were placed into a Schlenk flask and then evacuated and flushed with argon. Then toluene (5 mL) and water (5 mL) were added, and the reaction mixture was kept at 130°C for 18 hours. After cooling to room temperature the reaction mixture was diluted with dichloromethane (20 mL) and washed with water (3×20 mL), then dried with

magnesium sulfate, filtered off and evaporated. The crude product was purified by column chromatography (aluminum oxide, hexane/THF =3/2) giving **TPT** as a red powder (isolated yield: 24mg, 0.03 mmol, 15%). Purity and identity of **TPT** has been verified by NMR spectroscopy and mass spectrometry.
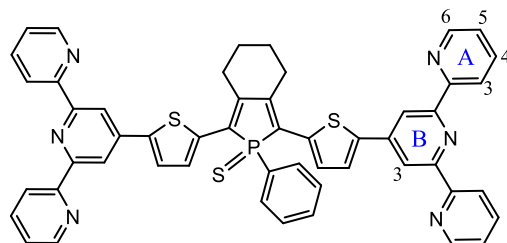
^{1}H NMR (300 MHz, CD_2Cl_2, δ/ppm): 8.73 (dd, $J(H,H)$ = 4.9 Hz, $J(H,H)$ = 1.0 Hz, 4H, $H_{pyridyl}$), 8.63 - 8.66 (m, 8 H, $H_{pyridyl}$), 7.98 (ddd, $J(P,H)$ = 14.3 Hz, $J(H,H)$ = 7.7 Hz, $J(H,H)$ = 1.0 Hz, 2H, o-H Ph), 7.89 ($J(H,H)$ = 7.5 and $J(H,H)$ = 2.00 Hz, 4H, $H_{pyridyl}$), 7.66 (d, $J(H,H)$ = 3.8 Hz, 2H, $H_{thienyl}$), 7.52 (d, $J(H,H)$ = 3.8 Hz, 2H, $H_{thienyl}$), 7.38 – 7.33 (m, 3H, p-H and m-H Ph), 7.35 - 7.40 (m, 4H, $H_{pyridyl}$), 3.11 (m, 4H, C=CCH_2,), 2.00 (m, 4H, C=CCH$_2$CH_2).

^{31}P NMR (121 MHz, CD_2Cl_2, δ/ppm): +52.0 (s).

^{13}C NMR (101 MHz, CD_2Cl_2, δ/ppm): 156.1 (s, $C_{pyridyl}$), 155.7 (s, $C_{pyridyl}$), 149.1 (s, $CH_{pyridyl}$) 146.8 (d, $^2J(P,C)$ = 23.2 Hz, PC=C), 142.8 (s, $C_{thienyl}$), 142.6 (s, $C_{pyridyl}$), 136.8 (s, $CH_{pyridyl}$) 136.5 (d, $^2J(P,C)$ = 17.9 Hz, $C_{thienyl}$), 132.3 (s, C_p Ph), 130.6 (d, $J(P,C)$ = 15.6 Hz, C_o Ph), 129.1 (s, $CH_{thienyl}$), 129.0 (d, $J(P,C)$ = 8.1 Hz, C_m Ph), 128.7 (d, $J(P,C)$ = 74.6 Hz, PC=C), 126.0 (s, $CH_{thienyl}$), 124.0 (s, $CH_{pyridyl}$), 121.1 (s, $CH_{pyridyl}$), 116.5 (s, $CH_{pyridyl}$), 29.5 (d, $J(P,H)$ = 13.0 Hz C=CCH_2CH$_2$), 22.3 (s, C=CCH$_2$CH_2). C_i Ph not observed.

FT-IR (cm^{-1}): 3432 (w), 3030 (w), 3051 (w), 3014 (w), 2946 (w), 2867(w), 1598(s), 1582(s), 1567 (s), 1547 (m), 1466 (m), 1449 (s), 1399(s), 1363(w), 1290(w), 1267 (w), 1224(w), 1145(w), 1097(m), 1075 (w), 1042 (w), 1011 (s), 990 (w). 878 (w), 850(w), 788(s), 775 (w), 745 (m), 731 (m), 718 (w) 691 (w), 678 (w), 665 (m), 635 (w), 623 (w), 608 (w), 555 (w), 533 (w), 499 (w), 468(w)

HRMS found m/z 873.2059 [M + H$^+$], $C_{52}H_{38}N_6PS_3$ requires 873.205773

- Sonogashira coupling towards E-type unimer

Several conditions were tested for the synthesis of E-type unimers. The unimer **E** was chosen as representative for other as it requires the most facile synthesis of precursors.

The conditions varied in used solvent, catalyst, base and temperature and are all summarized in Table 10. Synthetic strategy towards E-type unimers is described below.

Table 10: Conditions tested for synthesis of unimer **E** as model reaction

Solvent	Base	Catalyst	Temperature (°C)	Yield (%)
THF	diisopropylamine	$Pd(PPh_3)_4$	80	5
Toluene	diisopropylamine	$Pd(PPh_3)_4$	100	4
THF	DBU	$Pd(PPh_3)_4$	80	0
THF	diisopropylamine	$Pd(dba)_2$	80	0
THF	diisopropylamine	$Pd(PPh_3)_2Cl_2$, CuI	80	0
Toluene	diisopropylamine	PEPPSI™-IPr	100	4
THF	-	$Pd(PPh_3)_4$	80	0

The first conditions in Table 10 were used for synthesis of all E-unimers. General procedure of synthesis: Ethynyl(aryl)-terpyridine (2 eq) and 1-phenyl-2,5-bis(4-hexyl-5-iodothiophen-2-yl)thioxophosphole (1 eq) were placed into a Schlenk flask and dissolved in THF, then catalytic amounts of diisopropylamine and $Pd(PPh_3)_4$ were added and reaction mixture was stirred at 80 °C for 48 hours. Conversion of starting materials was monitored by TLC. Then all volatiles were evaporated, red solid was dissolved in DCM and washed with brine and water. The organic phase was dried with magnesium sulfate, filtered off and the crude product was purified by column chromatography (basic alumina, hexane/THF or toluene/acetone mobile phase). The isolated material was then washed with pentane and diethylether to remove phospholene species (which is formed in basic environment[142]) and catalyst residue. The purity of the product was checked by NMR spectroscopy. Product was dark red-violet powder in all cases.

- Characterization of E-unimers

Unimer E

Reactants: E-*tpy* (92 mg, 0.36 mmol), 1-phenyl-2,5-bis(4-hexyl-5-iodothiophen-2-yl)thioxophosphole (151 mg, 0.18 mmol), $Pd(PPh_3)_4$, diisopropylamine; solvent THF (10 mL); temperature 80°C; chromatography was performed using DCM and basic alumina. Product was obtained as dark red solid, in 11% yield (23mg, 0.02 mmol).
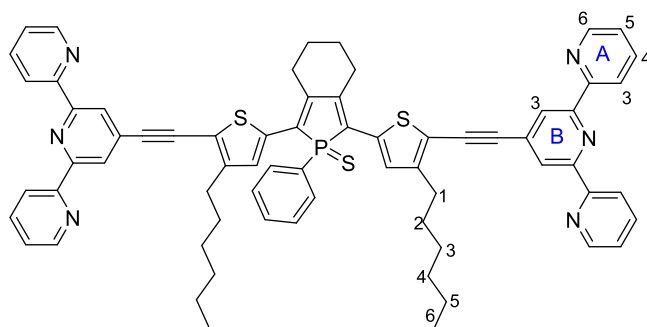
^{1}H NMR (400 MHz, CD$_2$Cl$_2$, δ/ppm): 8.70 (d, J=3.76 Hz, 4H,A6), 8.67 (d, J = 8.0 Hz, 4H, A3), 8.56 (s, 4H, B3), 8.01 – 7.89 (m, 6H, o-H Ph + A4), 7.64 – 7.48 (m, 3H, m-H Ph + p-H Ph), 7.41 (ddd, J = 7.6, 4.8, 1.3 Hz, 4H, A5), 7.32 (s, 2H, thiophene), 3.02 (s, 4H,C-CH$_2$-CH$_2$), 2.77 (t, J=7.53 Hz, 4H, Hex1), 1.98 (s, 4H,C-CH$_2$-CH$_2$), 1.63-1.53 (m, 10H, Hex2 + water), 1.33 - 1.26 (m, 12H, Hex 3-5), 0.98 – 0.82 (m, 6H, Hex6)

^{31}P NMR (121 MHz, CD$_2$Cl$_2$, δ/ppm): 51.28

^{13}C NMR (101 MHz CD$_2$Cl$_2$, δ/ppm): 156.22, 156.09, 150.15, 149.80, 147.60 (d, J=19.87Hz), 137.44, 136.82 (d, J=17.48Hz), 133.51 (d, J=3.00Hz), 132.88 (d, J=3.18 Hz), 131.25 (d, J=6.80 Hz), 131.16 (d, J=11.60 Hz), 129.58 (d, J=12.00 Hz), 129.20 (d, J=77.90 Hz), 128.98 (d, J=81.10 Hz), 124.65, 122.50, 121.55, 119.57, 96.67, 87.23, 32.18, 31.16, 30.58, 29.92 (d, J=11.10 Hz), 29.32, 23.18, 22.83, 14.46

FT-IR (cm^{-1}): 3057.58(w), 3010.82(w), 2950.07(w), 2926.45(m), 2857.02(w), 2193.15(m), 1598.22(m), 1581.82(s), 1566.40(s), 1540.85(w), 1465.64(m), 1431.89(w), 1390.91(m), 1265.07(w), 1115.62(w), 1103.08(w), 1092.96(w), 1069.34(w), 995.57(w), 986.41(w), 892.40(w), 792.60(s), 743.91(m), 720.28(w), 689.91(w), 661.46(m), 617.11(w), 523.10(w)

HRMS found m/z: 1089.3930 [M + H$^+$], C$_{68}$H$_{62}$N$_6$PS$_3$ requires 1089.3935

Unimer EPh

Reactants: EPh-*tpy* (0.1 g, 0.3 mmol), 1-phenyl-2,5-bis(4-hexyl-5-iodothiophen-2-yl)thioxophosphole (124 mg, 0.15 mmol), Pd(PPh$_3$)$_4$, diisopropylamine; solvent THF (10 mL); temperature 80°C Column chromatography was performed on basic alumina, using toluene/acetone (gradient 0-2%). Fractions corresponding to product was collected and evaporated, washed with diethylether and gained as dark red solid (12 mg, 6.5%).
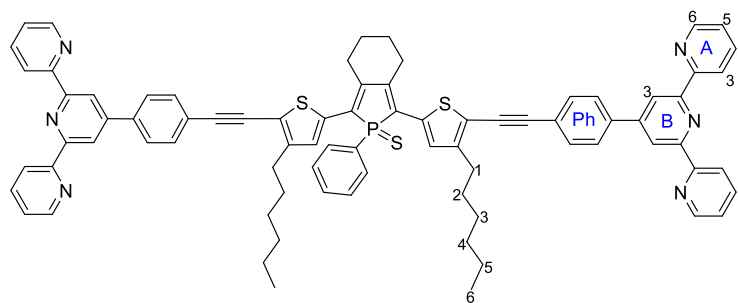
^{1}H NMR (300 MHz, CD$_2$Cl$_2$, δ/ppm): 8.80 (s, 4H, B3), 8.77 – 8.68 (m, 8H, A6+A3), 7.99 – 7.88 (m, 10H, A4+ *o*-H Ph + ph), 7.66 (d, *J* = 8.4 Hz, 4H,ph), 7.57 – 7.45 (m, 3H, *m*-H Ph + *p*-H Ph), 7.40 (ddd, *J* = 7.5, 4.8, 1.2 Hz, 4H, A5), 7.27 (s, 2H,thiophene), 2.98 (s, 4H, C-*CH$_2$*-CH$_2$), 2.70 (t, *J*= 7.5 Hz , 4 H, Hex1), 1.94 (s, 4H, C-CH$_2$-*CH$_2$*), 1.59 (m, 4H, Hex2), 1.31 (d, *J* = 3.9 Hz, 12H, Hex 3-5), 0.95 – 0.87 (m, 6H, Hex6)

^{31}P NMR (121 MHz, CD$_2$Cl$_2$, δ/ppm): 51.23

^{13}C NMR (151 MHz, CD$_2$Cl$_2$) δ 156.77, 156.62, 149.78, 149.76, 149.07, 147.18 (d, *J*=21.00 Hz), 138.95, 137.47, 135.83 (d, *J*=17.70 Hz), 132.82, 132.32, 131.21 (d, *J*=12.17 Hz), 129.64 (d, *J*=6.60 Hz), 129.57 (d, *J*=12.20 Hz), 129.52 (d, *J*=75.00 Hz), 129.13 (d, *J*=83.20 Hz), 127.88, 124.56, 124.48, 121.71, 120.38, 119.05, 98.11, 84.49, 32.20, 30.57, 29.90 (d, *J*=11.00 Hz), 29.35, 23.19, 22.92, 14.49

FT-IR (cm^{-1}): 3051.32(w), 2949.59(m), 2928.86(m), 2856.06(w), 2191.22(w), 1979.57(w), 1970.41(w), 1958.36(w), 1940.52(w), 1602.56(m), 1583.75(s), 1565.92(m), 1527.83(w), 1508.06(w), 1466.12(m), 1441.05(m), 1412.12(w), 1388.50(m), 1097.30(w), 1038.00(w), 989.79(w), 832.13(m), 791.64(s), 744.87(m), 737.16(w), 718.35(m), 691.84(w), 668.70(w), 660.98(w), 621.45(w), 520.69(w)

HRMS found m/z: 1241.4556 [M + H$^+$], C$_{80}$H$_{70}$N$_6$PS$_3$ requires 1241.4561

Unimer ET

Reactants: ET-*tpy* (81 mg, 0.24 mmol), 1-phenyl-2,5-bis(4-hexyl-5-iodothiophen-2-yl)thioxophosphole (100 mg, 0.12 mmol), Pd(PPh$_3$)$_4$, diisopropylamine; solvent THF (10 mL); temperature 80°C; two column chromatographies on basic alumina were used to purify the product. First one used gradient increasing polarity in hexane/THF system (from 4/1 to 1/1 by volume) and second one with DCM/1% methanol mobile phase. Product was obtained as red-violet solid in 3%yield (4mg, 0.004 mmol).
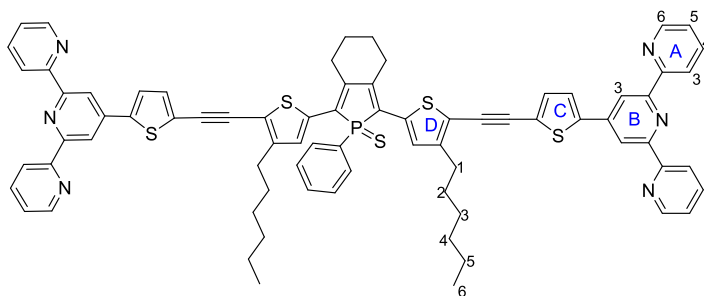
^{1}H NMR (600 MHz, CD$_2$Cl$_2$, δ/ppm): 8.73 (d, J=4.40 Hz, 4H, A6), 8.69 (s, 4 H, B3), 8.65 (d, J=8.10 Hz, 4 H, A3), 7.87 - 7.93 (m, 6H, A4+ o-H Ph), 7.71 (d, J = 3.9 Hz, 2H, C3), 7.50 - 7.54 (m, 2 H, m-H Ph), 7.44 - 7.48 (m, 1 H, p-H Ph), 7.40 (ddd, J = 7.5, 4.7, 1.2 Hz, 4H, A5), 7.33 (d, J = 3.9 Hz, 2H, C4), 7.27 (s, 2H, D3), 2.97 (br. s, 4H, C-CH_2-CH$_2$), 2.69 (t, J = 7.5 Hz, 4H, Hex1), 1.90 - 1.95 (m, 4H, C-CH$_2$-CH_2), 1.25 - 1.32 (m, 16 H, Hex2-5), 0.87 - 0.92 (m, 6 H, Hex6)

^{31}P NMR (121 MHz, CD$_2$Cl$_2$, δ/ppm): 51.22 (s, 1P)

^{13}C NMR (151 MHz, CD$_2$Cl$_2$, δ/ppm): 156.81, 156.22, 149.71, 149.45, 147.37 (d, J=19.90 Hz), 143.99, 143.06, 137.60, 136.28 (d, J=16.59 Hz), 133.70, 132.86 (d, J=3.00 Hz), 131.20 (d, J=11.06 Hz), 129.66 (d, J=5.53 Hz), 129.58 (d, J=13.10 Hz), 129.16 (d, J=84.20 Hz), 128.93 (d, J=75.20 Hz), 126.64, 125.12, 124.71, 121.75, 119.84, 117.43, 91.31, 88.54, 32.20, 30.52, 30.31, 29.93 (d, J=13.30 Hz), 29.34, 23.15, 22.88, 14.51

FT-IR (cm^{-1}): 3053.73(w), 2963.57(m), 2931.75(m), 2909.57(m), 2852.68(w), 2179.65(w), 1599.66(m), 1583.75(m), 1262.66(s), 1096.33(s), 1020.16(s), 864.92(m), 798.87(s), 743.42(m), 730.89(w), 717.87(m), 683.16(w), 666.29(m), 659.05(w), 621.45(w), 513.94(w)

HRMS found m/z 1253.3685 [M + H$^+$] C$_{76}$H$_{66}$N$_6$PS$_5$ requires 1253.3690

Unimer ET6

Reactants: ET6-*tpy* (60 mg, 0.14 mmol, 1-phenyl-2,5-bis(4-hexyl-5-iodothiophen-2-yl)thioxophosphole (58 mg, 0.07 mmol), Pd(PPh$_3$)$_4$, diisopropylamine; solvent THF (10 mL); temperature 80°C, column chromatography on basic alumina, using C6/THF (3/2 by volume) mixed mobile phase was used for purification of the product. Fractions corresponding to product was collected and evaporated, washed with diethylether/pentane (1/1, v/v mixture) and gained as dark violet solid (10 mg, 10%).
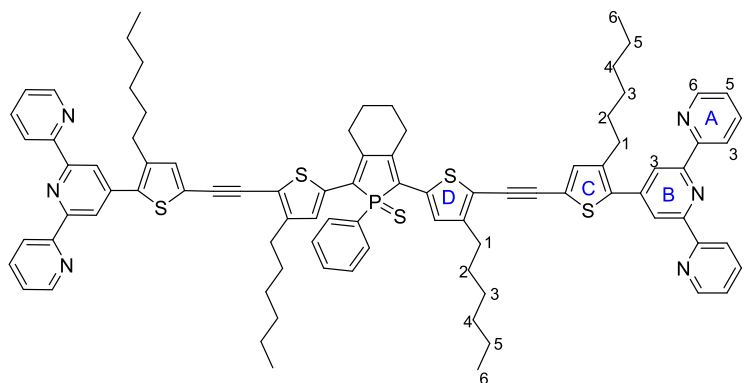
^{1}H NMR (600 MHz, CD$_2$Cl$_2$, δ/ppm): 8.71 (d, J= 4.04 Hz, 4H, A6), 8.67 (d, J =8.07 Hz, 4H, A3) 8.58 (s, 4 H, B3), 7.86 - 7.93 (m, 6 H, A4 + o-H Ph), 7.50 - 7.55 (m, 1 H, p-H Ph), 7.44 - 7.49 (m, 2 H, m-H Ph$_)$, 7.38 (ddd, J=6.69, 5.41, 1.10 Hz, 4 H, A5), 7.24 (s, 2 H, C4), 7.21 (s, 2 H, D3), 2.95 (br. s., 4 H, C-CH_2-CH$_2$), 2.81(t, J= 7.5 Hz, 4 H, C-Hex1), 2.66 (t, J=7.39 Hz, 4 H, D-Hex1), 1.92 (br. s., 4 H, C-CH$_2$-CH_2), 1.65 - 1.78 (m, 4 H, C-Hex2), 1.35 - 1.44 (m, 4 H,D-Hex2), 1.24 - 1.33 (m, 20 H, C-Hex3-5, D-Hex3-5), 0.80 - 0.93 (m, 12 H, C-Hex6, D-Hex6)

^{31}P NMR (121 MHz, CD$_2$Cl$_2$, δ/ppm): 51.20 (s, 1 P)

^{13}C NMR (151 MHz, CD$_2$Cl$_2$, δ/ppm): 156.49, 156.31, 149.81, 149.10, 147.20 (d, J=19.90 Hz), 143.91, 142.18, 138.18, 137.44, 135.98 (d, J=17.70 Hz), 135.56, 132.82 (d, J=3.30 Hz), 131.14 (d, J=11.10 Hz), 129.58, 129.52 (d, J=5.50 Hz), 129.39 (d, J=75.00 Hz), 129.04 (d, J=84.00 Hz), 124.57, 122.99, 121.61, 120.88, 120.03, 91.42, 87.64, 32.17, 31.36, 30.52, 30.26, 29.89, 29.89 (d, J=12.20 Hz), 29.62, 29.57, 29.29, 23.18, 23.16, 22.85, 14.48, 14.37

FT-IR (cm^{-1}): 3175.70(w), 3059.03(w), 3013.71(w), 2952.96(m), 2929.82(m), 2854.13(w), 2180.61(w), 1600.15(w), 1583.27(s), 1567.84(m), 1557.72(m), 1549.04(w), 1532.17(w), 1465.15(m), 1446.35(w), 1435.26(w), 1394.76(m), 1373.07(w), 1265.56(w), 1124.78(w), 1096.82(w), 1072.71(w), 1022.09(w), 989.30(w), 892.88(w), 887.10(w), 844.19(w), 838.88(w), 793.08(m), 743.42(m), 718.35(w), 687.50(w), 667.73(w), 659.54(w), 622.41(w), 616.15(w)

HRMS found m/z 1421.5563 [M + H$^+$] C$_{88}$H$_{90}$N$_6$PS$_5$ requires 1421.5568

4.3.3 Another synthetic approach to phosphole unimer

Another synthetic approach comprising Stille coupling of stannyl derivative of phosphole and Br-tpy was tested in order to obtain unimers in higher yields. 1-Phenyl-2,5-bis(trimethylstannyl)-thioxophosphole (later described as bis(stannyl)phosphole)

was synthesized from 1,8-bis(trimethylstannyl)octa-1,7-diyne[161] using Sato method.[104] Various conditions were tested (see Table 11) for bis(stannyl)phosphole (1 eq) and Br-*tpy* (2 eq).

Table 11: Tested conditions for Stille coupling of bis(stannyl)phoshole and Br-*tpy*

Set-up	solvent	Catalyst + co-catalyst	temperature
1	toluene	CuI, Pd(PPh$_3$)$_4$	130°C
2	toluene	CuO, Pd(PPh$_3$)$_4$	130°C
3	toluene	CuI, Pd(PPh$_3$)$_4$	90°C
4*	1,4-dioxane	P(tBu)$_3$, Pd$_2$(dba)$_3$, CsF, CuI	90°C

*conditions applied from reference[63]

4.4 COURSE OF COMPLEXATION

- Complexation of mono*tpy* ligands

Firstly complexation studies with E-*tpy* and Thio-*tpy* were performed using Zn^{2+} and Fe^{2+} as binding ions. Solutions of the exact concentration of ligands as well as metal salt were prepared by dissolving given amount of ligand or metal salt in acetonitrile. Set of samples with different metal to ligand ratio r ($r = n_M/n_L$) were prepared by mixing appropriate volume of prepared solutions. Then UV/vis, fluorescence and ^{1}H NMR spectroscopy was recorded for each sample. Stability constants were determined. For details reader is kindly asked to look into attached paper.[120]

- Assembly of unimers

Similar procedure was followed also for unimers. Unimers were dissolved in chloroform/acetonitrile (1/1, v/v) mixture, as they are not soluble just in acetonitrile, to give solution at exact concentration (0.02mM for UV/vis and fluorescence spectroscopy and 0.5mM for SEC measurements). Metal salts were dissolved in chloroform/acetonitrile (1/1 mixture) to give 100× more concentrated solution. Set of samples with different metal to ligand ratio r ($r = n_M/n_U$) were prepared by mixing appropriate volume of the prepared solution of unimer (V_U) and solution of metal salt (V_M) (Table 12). Addition of 100× times concentrated of metal salt slightly dilute the initial unimer concentration (c_U) in sample. This change was taken into account, where molar absorption coefficient was calculated. For intensity of fluorescence spectra the dilution was concerned as negligible. The solutions were allowed to equilibrate for

24 hours prior measuring their UV/vis and fluorescence spectra. Only several samples of certain ratio were prepared for SEC measurements, but similar protocol (with higher initial concentration) was applied.

Table 12: Protocol of preparation of samples; where V_U stands for volume of unimer solution, V_M volume of metal salt solution, r mole ratio M/U and c_U for unimer concentration in prepared sample

Sample	V_U (mL)	V_M (μL)	r	$c_U (10^{-5}M)$
0	2	0	0	2
1	2	2	0.1	1.998
2	2	4	0.2	1.996
3	2	6	0.3	1.994
4	2	8	0.4	1.992
5	2	10	0.5	1.990
6	2	12	0.6	1.988
7	2	16	0.8	1.984
8	2	20	1.00	1.980
9	2	25	1.25	1.975
10	2	30	1.5	1.970
11	2	40	2.00	1.961
12	2	60	3.00	1.942

Metallo-supramolecular polymers were obtained by mixing the solution of **U** and particular metal ion in the ratio r equal to 1.

- Thin films

The films for spectroscopic measurements were obtained by repeatedly casting a layer from solutions of **U** or MSPs directly on quartz glass support and subsequent solvent evaporation.

5 CONCLUSIONS

Novel synthetic procedures developed within this project represent a feasible path to the unimers comprising a phosphole unit in the central block and terpyridine end-groups. The route includes the first example of the C–H activation of phosphole species. Though the here prepared unimers contain the phosphole unit exclusively surrounded with two thiophene rings, the procedures developed can be potentially easily modified and thus exploited for preparation of others phosphole containing unimers. In total five novel unimers comprising phosphole unit in their central block and different conjugated linkers to *tpy* end-groups were prepared.

The comparison of the UV/vis and fluorescence spectra of the new phosphole comprising unimer **TPT** with the spectra of its α,ω-bis(*tpy*)-terthiophene and α,ω-bis(*tpy*)-quaterthiophene counterparts confirmed the idea that the replacement of the thiophene ring by a low-aromaticity phosphole ring in a unimer structure should increase the extent of the delocalization of electrons within the unimer molecules.

Assembling of all bis(*tpy*) unimers with various metal ions proceeds quite easily in dilute solutions, which is due to the high stability constants of bis(*tpy*) complexes with the ions (Zn^{2+}, Fe^{2+}, Co^{2+}, Ni^{2+} and Cu^{2+}). Nevertheless, the obtained results demonstrate that the complexes of nearly equal thermodynamic stability such as Zn^{2+}(Thio-*tpy*)$_2$ and Fe^{2+}(Thio-*tpy*)$_2$ substantially differ in their kinetic stability in solutions. This directly reflects in huge differences in the constitutional dynamics of corresponding MSPs: those with Fe^{2+} ion-couplers are so stable that their chains do not dissociate upon thousand fold dilution during analysis in SEC columns where the chains of Zn-MSPs totally decompose.

The prepared MSPs do not show luminescence, except for Zn-MSPs which show the fluorescence efficiency up to ca 7%. Fe-MSPs, on the other hand are only MSPs whose UV/vis spectra showed metal to ligand charge transfer (MLCT) band giving them typical purple/blue color..

6 REFERENCES

1   H. Shirakawa, J. Louis and A. G. Macdiarmid, *J. C. S. Chem. Comm.*, 1977, 578–580.

2   K. K. Kanazawa, a. F. Diaz, R. H. Geiss, W. D. Gill, J. F. Kwak, J. A. Logan, J. F. Rabolt and G. B. Street, *J. Chem. Soc. Chem. Commun.*, 1979, 854–855.

3   A. G. MacDiarmid, *Synth. Met.*, 2001, **125**, 11–22.

4   J. C. W. Chien, *Polyacetylene: Chemistry, Physics, and Material science*, Academic Press, INC., Orlando, Florida, 1984.

5   L. Olmedo, I. Chanteloube, A. Germain, M. Petit and E. M. Genies, *Synth. Met.*, 1989, **28**, 165–170.

6   A. G. Macdiarmid, J. C. Chiang, A. F. Richter and A. J. Epstein, *Synth. Met.*, 1987, **18**, 285–290.

7   J. Roncali, *Chem. Rev.*, 1992, **92**, 711–738.

8   R. D. McCullough, *Adv. Mater.*, 1998, **10**, 93–116.

9   D. R. Gagnon, J. D. Capistran, F. E. Karasz, R. W. Lenz and S. Antoun, *Polymer* , 1987, **28**, 567–573.

10   F. E. Karasz, J. D. Capistran, D. R. Gagnon and R. W. Lenz, *Mol. Cryst. Liq. Cryst.*, 1985, **118**, 327–332.

11   M. Fukuda, K. Sawada and K. Yoshino, *Jpn. J. Appl. Phys.*, 1989, **28**, 1433–1435.

12   M. Leclerc, *J. Polym. Sci. Part A Polym. Chem.*, 2001, **39**, 2867–2873.

13   A. Tsumura, H. Koezuka and T. Ando, *Appl. Phys. Lett.*, 1986, **49**, 1210.

14   T. W. Kelley, P. F. Baude, C. Gerlach, D. E. Ender, D. Muyres, M. A. Haase, D. E. Vogel and S. D. Theiss, *Chem. Mater.*, 2004, **16**, 4413–4422.

15   M. Ates, T. Karazehir and A. S. Sarac, *Curr. Phys. Chem.*, 2012, **2**, 224–240.

16   A. . MacDiarmid, L. . Yang, W. . Huang and B. . Humphrey, *Synth. Met.*, 1987, **18**, 393–398.

17   R. J. Tseng, J. Huang, J. Ouyang, R. B. Kaner and Y. Yang, *Nano Lett.*, 2005, **5**, 1077–80.

18   L.-Z. Fan, Y.-S. Hu, J. Maier, P. Adelhelm, B. Smarsly and M. Antonietti, *Adv. Funct. Mater.*, 2007, **17**, 3083–3087.

19   E. Bundgaard and F. Krebs, *Sol. Energy Mater. Sol. Cells*, 2007, **91**, 954–985.

20   J. Chen and Y. Cao, *Acc. Chem. Res.*, 2009, **42**, 1709–1718.

21   A. Chiolerio, S. Bocchini, F. Scaravaggi, S. Porro, D. Perrone, D. Beretta, M. Caironi and C. Fabrizio Pirri, *Semicond. Sci. Technol.*, 2015, **30**, 104001–104011.

22   D. T. McQuade, A. E. Pullen and T. M. Swager, *Chem. Rev.*, 2000, **100**, 2537–2574.

23   J. L. Brédas, B. Thémans, J. G. Fripiat, J. M. André and R. R. Chance, *Phys. Rev. B*, 1984, **29**, 6761–6773.

24   M. Barón, K.-H. Hellwich, M. Hess, K. Horie, A. D. Jenkins, R. G. Jones, J. Kahovec, P. Kratochvíl, W. V. Metanomski, W. Mormann, R. F. T. Stepto, J. Vohlídal and E. S. Wilks, *Pure Appl. Chem.*, 2009, **81**, 1131–1186.

25   M. Karahka and H. J. Kreuzer, *Polymers* , 2010, **3**, 51–64.

26   U. Salzner, J. B. Lagowski, P. G. Pickup and R. a. Poirier, *Synth. Met.*, 1998, **96**, 177–189.

27   J. Sedláček and J. Vohlídal, *Collect. Czechoslov. Chem. Commun.*, 2003, **68**, 1745–1790.

28   G. R. Whittell, M. D. Hager, U. S. Schubert and I. Manners, *Nat. Mater.*, 2011, **10**, 176–188.

29   A. Ciferri, *Macromol. Rapid Commun.*, 2002, **23**, 511–529.

30   L. Brunsveld, B. J. B. Folmer, E. W. Meijer and R. P. Sijbesma, *Chem. Rev.*, 2001, **101**, 4071–4097.

31   J. M. Lehn, *Prog. Polym. Sci*, 2005, **30**, 814–831.

32   R. Dobrawa and F. Würthner, *J. Polym. Sci. Part A Polym. Chem.*, 2005, **43**, 4981–4995.

33   F. J. M. Hoeben, P. Jonkheijm, E. W. Meijer and A. P. H. J. Schenning, *Chem. Rev.*, 2005, **105**, 1491–1546.

34   D.-C. Jeong, J. Lee, Y. Lee, C. Satheeshkumar and C. Song, *Macromolecules*, 2015, **48**, 1621–1626.

35   C.-L. Ho and W.-Y. Wong, *Coord. Chem. Rev.*, 2011, **255**, 2469–2502.

36   V. Duprez, M. Biancardo, H. Spanggaard and F. C. Krebs, *Macromolecules*, 2005, **38**, 10436–10448.

37   J. R. Kumpfer, Case Western Reserve University, Cleveland, Ohio, 2012.

38   H. Lodish, A. Berk, S. L. Zipursky, P. Matsudaira, D. Baltimore and J. Darnell, *Molecular Cell Biology*, W. H. Freeman, 2000.

39   J. W. Steed and J. L. Atwood, *Supramolecular Chemistry*, Wiley, 2nd editio., 2009.

40   B. Alberts, A. Johnson, J. Lewis, M. Raff, K. Roberts and P. Walter, *Molecular Biology of the Cell*, New York: Garland Science, 4th editio., 2002.

41   E. V. Anslyn and D. A. Dougherty, *Modern Physical Organic Chemistry*, University Science Books, Sausalito, California, 2006.

42   P. Muller, *Pure Appl. Chem.*, 1994, **66**, 1077–1184.

43   M. Zhang, P. Lu, Y. Ma and J. Shen, *J. Phys. Chem. B*, 2003, **107**, 6535–6538.

44   H. Irving and R. J. P. Williams, *J. Chem. Soc.*, 1953, 3192–3210.

45   R. Hogg and R. G. Wilkins, *J. Chem. Soc.*, 1962, 341–350.

46   F. Barigelletti, L. Flamigni, V. Balzani, J.-P. Collin, J.-P. Sauvage, A. Sour, E. C. Constable and A. M. W. C. Thompson, *J. Am. Chem. Soc.*, 1994, **116**, 7692–7699.

47   N. G. R. Schubert U. S, Hofmeier H., *Modern Terpyridine Chemistry*, Wiley-VCH, 2006.

48   M. Chiper, R. Hoogenboom and U. S. Schubert, *Macromol. Rapid Commun.*, 2009, **30**, 565–578.

49   P. R. Andres and U. S. Schubert, *Adv. Mater.*, 2004, **16**, 1043–1068.

50   H. Hofmeier and U. S. Schubert, *Chem. Soc. Rev.*, 2004, **33**, 373–399.

51   J. M. Hamilton, M. J. Anhorn, K. A. Oscarson, J. H. Reibenspies and R. D. Hancock, *Inorg. Chem.*, 2011, **50**, 2764–2770.

52   F. Tessore, D. Roberto, R. Ugo, M. Pizzotti, S. Quici, M. Cavazzini, S. Bruni and F. De Angelis, *Inorg. Chem.*, 2005, **44**, 8967–8978.

53   S. Kelch and M. Rehahn, *Chem. Commun.*, 1999, **3**, 1123–1124.

54   R. Siebert, A. Winter, U. S. Schubert, B. Dietzek and J. Popp, *Phys. Chem. Chem. Phys.*, 2011, **13**, 1606–1617.

55   J. P. Sauvage, J. P. Collin, J. C. Chambron, S. Guillerez, C. Coudret, V. Balzani, F. Barigelletti, L. De Cola and L. Flamigni, *Chem. Rev.*, 1994, **94**, 993–1019.

56   J. N. Demas and B. A. DeGraft, *Topics in Fluorescence Spectroscopy:Volume 4: Probe Design and Chemical Sensing*, 1994.

57   R. Englman and J. Jortner, *Mol. Phys.*, 1970, **18**, 145–164.

58   R. Siebert, A. Winter, M. Schmitt, J. Popp, U. S. Schubert and B. Dietzek, *Macromol. Rapid Commun.*, 2012, **33**, 481–497.

59   U. S. Schubert, C. Eschbaumer, P. Andres, H. Hofmeier, C. H. Weidl, E. Herdtweck, E. Dulkeith, A. Morteani, N. E. Hecker and J. Feldmann, *Synth. Met.*, 2001, **121**, 1249–1252.

60   M. Heller and U. S. Schubert, *Eur. J. Org. Chem.*, 2003, 947–961.

61   R.-A. Fallahpour, *Synthesis* , 2003, **2003**, 0155–0184.

62   A. C. Benniston, A. Harriman, D. J. Lawrie and A. Mayeux, *Phys. Chem. Chem. Phys.*, 2004, **6**, 51–57.

63   F. Odobel and H. Zabri, *Inorg. Chem.*, 2005, **44**, 5600–5611.

64   A. Wild, F. Schlütter, G. M. Pavlov, C. Friebe, G. Festag, A. Winter, M. D. Hager, V. Cimrová and U. S. Schubert, *Macromol. Rapid Commun.*, 2010, **31**, 868–874.

65   R. M. Lahn B., *Macromol. Symp.*, 2001, **163**, 157–176.

66   A. Wild, A. Teichler, C.-L. Ho, X.-Z. Wang, H. Zhan, F. Schlütter, A. Winter, M. D. Hager, W.-Y. Wong and U. S. Schubert, *J. Mater. Chem. C*, 2013, **1**, 1812–1822.

67   M. Chiper, M. a R. Meier, J. M. Kranenburg and U. S. Schubert, *Macromol. Chem. Phys.*, 2007, **208**, 679–689.

68   D. G. Kurth and M. Higuchi, *Soft Matter*, 2006, **2**, 915–927.

69   T. Sato, R. K. Pandey and M. Higuchi, *Dalton Trans.*, 2013, **42**, 16036–16042.

70   C.-Y. Hsu, J. Zhang, T. Sato, S. Moriyama and M. Higuchi, *ACS Appl. Mater. Interfaces*, 2015, **7**, 18266–18272.

71   G. Schwarz, T. K. Sievers, Y. Bodenthin, I. Hasslauer, T. Geue, J. Koetz and D. G. Kurth, *J. Mater. Chem.*, 2010, **20**, 4142–4148.

72   H. Padhy, M. Ramesh, D. Patra, R. Satapathy, M. K. Pola, H. C. Chu, C. W. Chu, K. H. Wei and H. C. Lin, *Macromol. Rapid Commun.*, 2012, **33**, 528–533.

73   S. Encinas, L. Flamigni, F. Barigelletti, E. C. Constable, C. E. Housecroft, E. R. Schofield, E. Figgemeier, D. Fenske, M. Neuburger, J. G. Vos and M. Zehnder, *Chem. - A Eur. J.*, 2002, **8**, 137–150.

74   Y. Kervella, E. Shilova, S. Latil, B. Jousselme and F. Silly, *Langmuir*, 2015, **31**, 13420–13425.

75   P. Štenclová, K. Šichová, I. Šloufová, J. Zedník, J. Svoboda, J. Vohlídal and J. Svoboda, *Dalton Trans.*, 2016, **45**, 1208–1224.

76   P. Bláhová, J. Zedník, I. Šloufová, J. Vohlídal and J. Svoboda, *Soft Mater.*, 2014, **12**, 214–229.

77   P. Štenclová-Bláhová, J. Svoboda, I. Šloufová and J. Vohlídal, *Phys. Chem. Chem. Phys.*, 2015, **17**, 13743–13756.

78   A. Wild, A. Winter, F. Schlütter and U. S. Schubert, *Chem. Soc. Rev.*, 2011, **40**, 1459–1511.

79   E. C. Constable, C. E. Housecroft, E. R. Schofield, S. Encinas, N. Armaroli, F. Barigelletti, L. Flamigni, E. Figgemeier and J. G. Vos, *Chem. Commun.*, 1999, 869–870.

80   A. Harriman, A. Mayeux, A. De Nicola and R. Ziessel, *Phys. Chem. Chem. Phys.*, 2002, **4**, 2229–2235.

81   F. S. Han, M. Higuchi and D. G. Kurth, *Tetrahedron*, 2008, **64**, 9108–9116.

82   Y.-Y. Chen and H.-C. Lin, *J. Polym. Sci. Part A Polym. Chem.*, 2007, **45**, 3243–3255.

83   S. H. Fu, M. Higuchi and D. G. Kurth, *J. Am. Chem. Soc.*, 2008, **130**, 2073–2081.

84   F. S. Han, M. Higuchi and D. G. Kurth, *Adv. Mater.*, 2007, **19**, 3928–3931.

85   G. Schwarz, I. Haßlauer and D. G. Kurth, *Adv. Colloid Interface Sci.*, 2014, **207**, 107–120.

86   D. G. Kurth, M. Schütte and J. Wen, *Colloids Surfaces A Physicochem. Eng. Asp.*, 2002, **198**–**200**, 633–643.

87   C.-W. Hu, T. Sato, J. Zhang, S. Moriyama and M. Higuchi, *J. Mater. Chem. C*, 2013, **1**, 3408–3413.

88   M. Higuchi, *Polym. J.*, 2009, **41**, 511–520.

89   J. Svoboda, P. Štenclová, F. Uhlík, J. Zedník and J. Vohlídal, *Tetrahedron*, 2011, **67**, 75–79.

90   P. Bláhová, J. Zedník, I. Šloufová, J. Vohlídal and J. Svoboda, *Soft Mater.*, 2014, **12**, 214–229.

91   W. Schafer, A. Schweig and F. Mathey, *J. Am. Chem. Soc.*, 1976, **98**, 407–414.

92   T. M. Krygowski and M. K. Cyranski, *Aromaticity in Heterocyclic Compounds*, Springer Science & Business Media, 2009.

93   C. Fave, M. Hissler, T. Kárpati, J. Rault-Berthelot, V. Deborde, L. Toupet, L. Nyulászi and R. Réau, *J. Am. Chem. Soc.*, 2004, **126**, 6058–6063.

94   M. Hissler, C. Lescop and R. Réau, *J. Organomet. Chem.*, 2005, **690**, 2482–2487.

95   Y. Matano and H. Imahori, *Org. Biomol. Chem.*, 2009, **7**, 1258–1271.

96   H.-C. Su, O. Fadhel, C.-J. Yang, T.-Y. Cho, C. Fave, M. Hissler, C.-C. Wu and R. Reau, *J. Am. Chem. Soc.*, 2006, **128**, 983–995.

97   O. Fadhel, M. Gras, N. Lemaitre, V. Deborde, M. Hissler, B. Geffroy and R. Réau, *Adv. Mater.*, 2009, **21**, 1261–1265.

98   M. G. Hobbs and T. Baumgartner, *Eur. J. Inorg. Chem.*, 2007, 3611–3628.

99   J. Casado, R. Réau and J. T. López Navarrete, *Chem. Eur. J.*, 2006, **12**, 3759–3767.

100   C. Hay, M. Hissler, C. Fischmeister, J. Rault-Berthelot, L. Toupet, L. Nyulászi and R. Réau, *Chem. Eur. J.*, 2001, **7**, 4222–4236.

101   S. A. Lee, S. Hotta and F. Nakanishi, *J. Phys. Chem. A*, 2000, **104**, 1827–1833.

102   C. Hay, C. Fischmeister, M. Hissler, L. Toupet and R. Réau, *Angew. Chem. Int. Ed.*, 2000, **39**, 1812–1815.

103   W. M. Sears, C. D. MacKinnon and T. M. Kraft, *Synth. Met.*, 2011, **161**, 1566–1574.

104   A. Saito, Y. Matano and H. Imahori, *Org. Lett.*, 2010, **12**, 2675–2677.

105   T. Izumi, S. Kobashi, K. Takimiya, Y. Aso and T. Otsubo, *J. Am. Chem. Soc.*, 2003, **125**, 5286–5287.

106   S. S. H. Mao and T. D. Tilley, *Macromolecules*, 1997, **30**, 5566–5569.

107   Y. Morisaki, Y. Aiki and Y. Chujo, *Macromolecules*, 2003, **36**, 2594–2597.

108   M. Sebastian, M. Hissler, C. Fave, J. Rault-Berthelot, C. Odin and R. Réau, *Angew. Chem. Int. Ed.*, 2006, **45**, 6152–6155.

109   Y. Dienes, M. Eggenstein, T. Neumann, U. Englert and T. Baumgartner, *Dalton Trans.*, 2006, 1424–1433.

110   M. Hissler, C. Lescop and R. Réau, *Comptes Rendus Chim.*, 2008, **11**, 628–640.

111   F. Leca, C. Lescop, L. Toupet and R. Reau, *Organometallics*, 2004, **23**, 6191–6201.

112   V. Vreshch, M. El Sayed Moussa, B. Nohra, M. Srebro, N. Vanthuyne, C. Roussel, J. Autschbach, J. Crassous, C. Lescop and R. Réau, *Angew. Chem. Int. Ed.*, 2013, **52**, 1968–1972.

113   D. R. Bai, C. Romero-Nieto and T. Baumgartner, *Dalton Trans.*, 2010, **39**, 1250–1260.

114   D. R. Bai and T. Baumgartner, *Organometallics*, 2010, **29**, 3289–3297.

115   F. Kröhnke and Z. W., *Angew. Chem. Int. Ed.*, 1962, **1**, 626–632.

116   V. Grosshenny, F. M. Romero and R. Ziessel, *J. Org. Chem.*, 1997, **62**, 1491–1500.

117   E. C. Constable, E. Figgemeier, C. E. Housecroft, S. L. Kokatam, E. A. Medlycott, M. Neuburger, S. Schaffner and J. A. Zampese, *Dalton Trans.*, 2008, 6752–6762.

118   M. Beley, D. Delabouglise, G. Houppy, J. Husson and J. P. Petit, *Inorganica Chim. Acta*, 2005, **358**, 3075–3083.

119   R. H. Holyer, C. D. Hubbard, S. F. a Kettle and R. G. Wilkins, *Inorg. Chem.*, 1966, **5**, 622–625.

120   T. Vitvarová, J. Zedník, M. Bláha, J. Vohlídal and J. Svoboda, *Eur. J. Inorg. Chem.*, 2012, 3866–3874.

121   W. Goodall and J. a Williams, *Chem. Commun. (Camb).*, 2001, 2514–2515.

122   P. S. Braterman, R. D. Peacock and J.-I. Song, *Inorg. Chem.*, 1992, **31**, 555–559.

123   F. Grimm, N. Ulm, F. Gröhn, J. Düring and A. Hirsch, *Chem. - A Eur. J.*, 2011, **17**, 9478–88.

124   A. Winter, C. Friebe, M. Chiper, M. D. Hager and U. S. Schubert, *J. Polym. Sci. Part A Polym. Chem.*, 2009, **47**, 4083–4098.

125   P. Gans, A. Sabatini and A. Vacca, *Talanta*, 1996, **43**, 1739–1753.

126   A. C. Benniston, A. Harriman, D. J. Lawrie, A. Mayeux, K. Rafferty and O. D. Russell, *Dalton Trans.*, 2003, 4762–4769.

127   A. Harriman, J. P. Rostron, M. Cesario, G. Ulrich and R. Ziessel, *J. Phys. Chem. A*, 2006, **110**, 7994–8002.

128   R. Dobrawa and F. Würthner, *Chem. Commun.*, 2002, 1878–1879.

129   W. Delaunay, Université de Rennes 1, France, 2013.

130   F. Schlütter, A. Wild, A. Winter, M. D. Hager, A. Baumgaertel, C. Friebe and U. S. Schubert, *Macromolecules*, 2010, **43**, 2759–2771.

131   A. Winter and U. S. Schubert, *Chem. Soc. Rev.*, 2016, **45**, 5311–5357.

132   A. Wild, A. Teichler, C. Von Der Ehe, A. Winter, M. D. Hager, B. Yao, B. Zhang, Z. Xie, W. Wong, U. S. Schubert and F. Jena, *Macromol. Chem. Phys.*, 2013, **214**, 1072–1080.

133   Q. Chu and Y. Pang, *J. Polym. Sci. Part A-Polymer Chem.*, 2006, **44**, 2338–2345.

134   J. Crassous and R. Réau, *Dalton Trans.*, 2008, 6865–6876.

135   J. Crassous, C. Lescop and R. Reau, *Phosphorus Compounds*, Springer Netherlands, Dordrecht, 2011, vol. 37.

136   T. Baumgartner and R. Reau, *Chem. Rev.*, 2006, **106**, 4681–4727.

137   P. J. Fagan, W. a. Nugent and J. C. Calabrese, *J. Am. Chem. Soc.*, 1994, **116**, 1880–1889.

138   P. J. Fagan and W. a. Nuget, *J. Am. Chem. Soc.*, 1988, **110**, 2310–2312.

139   K. Harada, H. Urabe and F. Sato, *Tetrahedron Lett.*, 1995, **36**, 3203–3206.

140   S. Yamaguchi and R. Jin, *J. Org. Chem.*, 1998, **63**, 10060–10062.

141   G. A. Chotana, V. A. Kallepalli, R. E. Maleczka and M. R. Smith, *Tetrahedron*, 2008,

64, 6103–6114.

142   L. Nyulászi, O. Hollóczki, C. Lescop, M. Hissler and R. Réau, *Org. Biomol. Chem.*, 2006, **4**, 996–998.

143   M. J. Frisch, G. W. Trucks, H. B. Schlegel, G. E. Scuseria, M. A. Robb, J. R. Cheeseman, G. Scalmani, V. Barone, B. Mennucci, G. A. Petersson, H. Nakatsuji, M. Caricato, X. Li, H. P. Hratchian, A. F. Izmaylov, J. Bloino, G. Zheng, J. L. Sonnenberg, M. Hada, M. Ehara, K. Toyota, R. Fukuda, J. Hasegawa, M. Ishida, T. Nakajima, Y. Honda, O. Kitao, H. Nakai, T. Vreven, J. A. Montgomery, J. E. Peralta, F. Ogliaro, M. Bearpark, J. J. Heyd, E. Brothers, K. N. Kudin, V. N. Staroverov, R. Kobayashi, J. Normand, K. Raghavachari, A. Rendell, J. C. Burant, S. S. Iyengar, J. Tomasi, M. Cossi, N. Rega, J. M. Millam, M. Klene, J. E. Knox, J. B. Cross, V. Bakken, C. Adamo, J. Jaramillo, R. Gomperts, R. E. Stratmann, O. Yazyev, A. J. Austin, R. Cammi, C. Pomelli, J. W. Ochterski, R. L. Martin, K. Morokuma, V. G. Zakrzewski, G. A. Voth, P. Salvador, J. J. Dannenberg, S. Dapprich, A. D. Daniels, Ö. Farkas, J. B. Foresman, J. V. Ortiz, J. Cioslowski and D. J. Fox, 2009.

144   C. Ringenbach, A. De Nicola and R. Ziessel, *J. Org. Chem.*, 2003, **68**, 4708–4719.

145   P. Štenclová, Charles University in Prague, Czech Republic, 2016.

146   T. Vitvarová, J. Svoboda, M. Hissler and J. Vohlídal, *Organometallics*, 2017, **36**, 777–786.

147   T. E. Janini, J. L. Fattore and D. L. Mohler, *J. Organomet. Chem.*, 1999, **578**, 260–263.

148   A. Barbieri, B. Ventura, F. Barigelletti, A. De Nicola, M. Quesada and R. Ziessel, *Inorg. Chem.*, 2004, **43**, 7359–7368.

149   A. Harriman, M. Hissler, A. Khatyr and R. Ziessel, *Eur. J. Inorg. Chem.*, 2003, 955–959.

150   A. P. Yang, M. Kuroda, Y. Shiraishi and T. Kobayashi, *J. Chem. Phys.*, 1998, **109**, 8442–8450.

151   M. Sauer, J. Hofkens and J. Enderlein, *Basic Principles of Fluorescence Spectroscopy*, Wiley-VCH., 2011.

152   M. E. Gallina, G. Bergamini, S. Di Motta, J. Sakamoto, F. Negri and P. Ceroni, *Photochem. Photobiol. Sci.*, 2014, **13**, 997–1004.

153   V. Stepanenko, M. Stocker, P. Müller, M. Büchner and F. Würthner, *J. Mater. Chem.*, 2009, **19**, 6816–6826.

154   R. Dobrawa, M. Lysetska, P. Ballester, M. Grüne and F. Würthner, *Macromolecules*, 2005, **38**, 1315–1325.

155   M. A. R. Meier, B. G. G. Lohmeijer and U. S. Schubert, *Macromol. Rapid Commun.*, 2003, **24**, 852–857.

156   M. A. R. Meier, H. Hofmeier, C. H. Abeln, C. Tziatzios, M. Rasa, D. Schubert and U. S. Schubert, *e-Polym.*, 2006, **6**, 209–215.

157   B. G. G. Lohmeijer and U. S. Schubert, *Angew. Chem. Int. Ed.* , 2002, **41**, 3825–3829.

158   D. Rais, M. Menšík, P. Štenclová-Bláhová, J. Svoboda, J. Vohlídal and J. Pfleger, *J. Phys. Chem. A*, 2015, **119**, 6203–14.

159   A. Hinke and W. Kuchen, *Phosphorus Sulfur Relat. Elem.*, 2006, **15**, 93–98.

160   J. Linshoeft, E. J. Baum, A. Hussain, P. J. Gates, C. Näther and A. Staubitz, *Angew. Chemie Int. Ed.*, 2014, **53**, 12916–12920.

161   K. Oouchi, M. Mitani, M. Hayakawa, T. Yamada and T. Mukaiyama, *J. Organomet. Chem.*, 1996, **516**, 111–114.

7   LIST OF PUBLICATIONS

1) <u>T. Vitvarová</u>, J. Zedník, M. Bláha, J. Vohlídal and J. Svoboda: Effect of ethynyl and 2-thienyl substituents on the complexation of 4'-substituted 2,2':6',2″-terpyridines with Zn^{2+} and Fe^{2+} ions, and the spectroscopic properties of the ligands and formed complex species; *Eur. J. Inorg. Chem.*, 2012, 3866–3874.

2) <u>T. Vitvarová</u>, J. Svoboda, M. Hissler and J. Vohlídal: Conjugated metallo-supramolecular polymers containing a phosphole unit; *Organometallics*, 2017, 36, 777-786.

3) J. Křížková, <u>T. Vitvarová</u>: 20 let Úmluvy o zákazu chemických zbraní; *Chemické listy*, 2017, accepted for april issue.

8   ATTACHMENTS

A) <u>T. Vitvarová</u>, J. Zedník, M. Bláha, J. Vohlídal and J. Svoboda: Effect of ethynyl and 2-thienyl substituents on the complexation of 4'-substituted 2,2':6',2″-terpyridines with Zn^{2+} and Fe^{2+} ions, and the spectroscopic properties of the ligands and formed complex species; *Eur. J. Inorg. Chem.*, 2012, 3866–3874.

B) <u>T. Vitvarová</u>, J. Svoboda, M. Hissler and J. Vohlídal: Conjugated metallo-supramolecular polymers containing a phosphole unit; *Organometallics*, 2017, 36, 777-786.

ATTACHMENT A

T. Vitvarová, J. Zedník, M. Bláha, J. Vohlídal and J. Svoboda: Effect of ethynyl and 2-thienyl substituents on the complexation of 4'-substituted 2,2':6',2″-terpyridines with Zn^{2+} and Fe^{2+} ions, and the spectroscopic properties of the ligands and formed complex species; *Eur. J. Inorg. Chem.*, 2012, 3866–3874.

ATTACHMENT B

T. Vitvarová, J. Svoboda, M. Hissler and J. Vohlídal: Conjugated metallo-supramolecular polymers containing a phosphole unit; *Organometallics*, 2017, 36, 777-786

VU :   VU :

Le Directeur de Thèse   **Le Responsable de l'École**
Doctorale
        (Nom et Prénom)

                    VU pour autorisation de soutenance

                    Rennes, le

Le Président de l'Université de Rennes 1

        David ALIS

    VU après soutenance pour autorisation de publication :

                    Le Président de Jury,
                                (Nom et Prénom)